

Separation of Enantiomers by a Process Combination of Chromatography and Crystallisation

Dissertation

zur Erlangung des akademischen Grades

Doktoringenieur

(Dr.-Ing.)

von: Dipl.-Ing. Malte Kaspereit

geboren am: 31. Juli 1973

in: Merseburg

genehmigt durch die Fakultät für Verfahrens- und Systemtechnik
der Otto-von-Guericke Universität Magdeburg.

Gutachter: Prof. Dr.-Ing. habil. Andreas Seidel-Morgenstern
Prof. Dr.-Ing. habil. Henner Schmidt-Traub

eingereicht am: 28. Oktober 2005

Promotionskolloquium am 10. März 2006.

Forschungsberichte aus dem Max-Planck-Institut
für Dynamik komplexer technischer Systeme

Band 14

Malte Kaspereit

**Separation of Enantiomers by a Process Combination
of Chromatography and Crystallisation**

Shaker Verlag
Aachen 2006

Bibliographic information published by Die Deutsche Bibliothek

Die Deutsche Bibliothek lists this publication in the Deutsche Nationalbibliografie; detailed bibliographic data is available in the internet at <http://dnb.ddb.de>.

Zugl.: Magdeburg, Univ., Diss., 2006

Copyright Shaker Verlag 2006

All rights reserved. No part of this publication may be reproduced, stored in a retrieval system, or transmitted, in any form or by any means, electronic, mechanical, photocopying, recording or otherwise, without the prior permission of the publishers.

Printed in Germany.

ISBN-10: 3-8322-5130-8

ISBN-13: 978-3-8322-5130-7

ISSN 1439-4804

Shaker Verlag GmbH • P.O. BOX 101818 • D-52018 Aachen

Phone: 0049/2407/9596-0 • Telefax: 0049/2407/9596-9

Internet: www.shaker.de • eMail: info@shaker.de

Acknowledgements

This thesis evolved from research I performed at the Max Planck Institute for Dynamics of Complex Technical Systems in Magdeburg, Germany.

First and foremost I am deeply grateful to Prof. Andreas Seidel-Morgenstern, who enabled me to work at the MPI and allowed me great latitude in performing my research. Without his patient but encouraging guidance, his many ideas and deliberate advices the preparation of this work would have been impossible.

I am very thankful to Prof. Henner Schmidt-Traub who acted as a referee for this thesis.

For his complaisant support I am indebted to Prof. Achim Kienle, who gave me financial funding while I was largely busy with writing up.

Scientific work certainly requires a stimulating and productive atmosphere, which is what I found at the MPI. Decent technical facilities and, much more important, numerous discussions with and collaborative support by my colleagues were utmost valuable. In this respect I am particularly grateful to the group for Physical and Chemical Fundamentals of Process Engineering. Here special thanks go to Knut Gedicke and, furthermore, to Dorota Antos, Jacqueline Kaufmann, Alan Mahoney, Dragomir Sapoundjiev, Patrick Sheehan, Volker Zahn, and Grzegorz Ziomek.

Life was made much easier by many friends I found at the MPI, in particular by the "veterans" from the institute's early years. I'll never forget the daily routine of a dozen or more colleagues squeezing into a ridiculously small tea kitchen, while performing an incredible and unachieved mixture of in-depth discussions and hilarious jokes. The accumulation of so many perceptive and nice people within one institute is certainly one of the most enjoyable aspects of science. There are too many people I'd have to mention here – so just many thanks to all of you.

Finally, I want to thank my family and, especially, my girlfriend Anke, who provided a calm asylum and endured all the little crises I brought home with me – while managing her own successful research and dissertation in an admirable fashion.

Contents

| | |
|--|-----------|
| Introduction | 1 |
| 1 Concept of a Process Combination for Enantioseparations | 3 |
| 1.1 Background | 3 |
| 1.1.1 Fundamentals of Stereochemistry | 3 |
| 1.1.2 Biological and Economical Relevance | 5 |
| 1.1.3 Production Methods for Pure Enantiomers | 7 |
| 1.2 Concept of the Process Combination | 13 |
| 1.2.1 Some Remarks on Process Intensification | 13 |
| 1.2.2 Basic Concept | 15 |
| 1.2.3 Possible Synergisms | 16 |
| 1.2.4 State of Research | 18 |
| 2 Theoretical Foundations of Individual Unit Operations | 21 |
| 2.1 Continuous Chromatography | 21 |
| 2.1.1 Principle | 21 |
| 2.1.2 Adsorption Equilibria | 24 |
| 2.1.3 Fundamental Relations | 26 |
| 2.1.4 Modelling of Batch Chromatography | 28 |
| 2.1.5 Modelling of TMB Chromatography | 30 |
| 2.1.6 Modelling of SMB Chromatography | 31 |
| 2.1.7 Design Aspects | 32 |
| 2.2 Enantioselective Crystallisation | 32 |
| 2.2.1 Principle | 32 |
| 2.2.2 Solid-Liquid Equilibria in Enantiomeric Systems | 33 |
| 2.2.3 Enantioselective Cooling Crystallisation from Solution | 36 |

| | | |
|----------|---|-----------|
| 2.2.4 | Modelling | 37 |
| 2.2.5 | Design Aspects | 38 |
| 3 | Model Systems | 39 |
| 3.1 | System I – Mandelic Acid | 39 |
| 3.1.1 | Chromatographic Separation | 40 |
| 3.1.2 | Ternary Solubility Equilibria | 42 |
| 3.2 | System II – Threonine | 44 |
| 3.2.1 | Chromatographic Separation | 44 |
| 3.2.2 | Solubility Equilibrium | 46 |
| 3.3 | System III – Pharmaceutical Intermediate PDE | 47 |
| 3.3.1 | Chromatographic Separation | 47 |
| 3.3.2 | Solubility Equilibrium | 48 |
| 3.4 | Chemicals and Equipment Used | 48 |
| 4 | Impact of Adsorption Isotherms on SMB Processes | 51 |
| 4.1 | Background | 51 |
| 4.2 | Theoretical Fundamentals | 52 |
| 4.2.1 | Performance Parameters | 52 |
| 4.2.2 | Isotherm Model | 52 |
| 4.2.3 | Equilibrium Design of SMB processes | 52 |
| 4.2.4 | Determination of Productivities from Equilibrium Design | 55 |
| 4.3 | Analysis for Pure Products Based on Equilibrium Design | 56 |
| 4.3.1 | Parameter Specifications | 56 |
| 4.3.2 | Definition of Reference Isotherms | 56 |
| 4.3.3 | Results for the Model Systems | 57 |
| 4.3.4 | Parametric Study Based on a Reference Isotherm | 58 |
| 4.4 | Analysis for Variable Purity Based on Numerical Simulations | 60 |
| 4.4.1 | Parameter Specifications | 60 |
| 4.4.2 | Separation Regions for Varying Outlet Purity | 60 |
| 4.4.3 | Productivity as Function of Feed Concentration and Purity | 62 |
| 4.5 | Conclusions | 64 |

| | | |
|----------|--|-----------|
| 5 | Design of SMB Processes for Predefined Purity | 65 |
| 5.1 | Background | 65 |
| 5.2 | Model and Parameters | 66 |
| 5.2.1 | Generic Example System | 67 |
| 5.3 | Influence of the Regeneration Zones | 68 |
| 5.3.1 | Internal Concentration Profiles | 68 |
| 5.3.2 | Separation Regions | 69 |
| 5.4 | Optimisation of Restrictive and Non-restrictive Designs | 70 |
| 5.4.1 | Process Performance | 70 |
| 5.4.2 | Internal Concentration Profiles | 72 |
| 5.4.3 | Process Robustness | 72 |
| 5.5 | Conclusions | 74 |
| 6 | Impact of Solubility Equilibria on Enantioselective Crystallisation | 77 |
| 6.1 | Modelling of Ternary Solid-Liquid Equilibria | 77 |
| 6.1.1 | Thermodynamic Models | 77 |
| 6.1.2 | SLE Model based on Solubility Approximation | 79 |
| 6.2 | Equilibrium Design of Enantioselective Crystallisation | 82 |
| 6.2.1 | Mass Balances and General Relations | 83 |
| 6.2.2 | Determination of Compositions | 84 |
| 6.2.3 | Determination of Temperatures | 85 |
| 6.3 | Performance of Crystallisation for the Model Systems | 86 |
| 6.3.1 | Theoretical Yield | 86 |
| 6.3.2 | Operating Temperatures | 86 |
| 6.3.3 | Yield Limitation and Stepwise Crystallisation | 87 |
| 6.3.4 | Considerations on Solution Density and Concentrations | 89 |
| 6.3.5 | Specific Solvent Removal in a Process Combination | 90 |
| 6.3.6 | Supersaturation | 91 |
| 6.3.7 | Summary of Performance for the Model Systems | 92 |
| 6.4 | Conclusions | 93 |

| | | |
|----------|--|------------|
| 7 | Evaluation and Design of the Process Combination | 95 |
| 7.1 | Detailed Concept of the Process Combination | 95 |
| 7.2 | Mass Balancing Approach for Separator Networks | 97 |
| 7.2.1 | Nonsharp Binary Separators | 97 |
| 7.2.2 | Networks of Nonsharp Separators with Recycles | 99 |
| 7.3 | Shortcut Approach for Evaluation of the Process Combination | 101 |
| 7.3.1 | Basic Concept | 102 |
| 7.3.2 | Derivation of Process Parameters for the Process Combination | 102 |
| 7.3.3 | Determination of Characteristics for SMB Processes | 105 |
| 7.3.4 | Illustrative Example | 106 |
| 7.4 | Evaluation and Design of the Process Combination | 107 |
| 7.4.1 | Detailed Procedure | 107 |
| 7.4.2 | Evaluation for Different Process Configurations | 108 |
| 7.4.3 | Evaluation for Different Model Systems | 113 |
| 7.4.4 | Remarks and Limitations of the Approach | 115 |
| 7.5 | Further Aspects of Process Engineering | 116 |
| 7.6 | Conclusions | 118 |
| | Summary and Conclusions | 119 |
| | A SMB and TMB Models | 121 |
| A.1 | Numerical Solution of Equilibrium-Dispersive Model | 121 |
| A.2 | Steady-State Optimisation of SMB Processes | 122 |
| A.3 | SMB Performance under Reduced Purity Requirements | 123 |
| A.4 | Determination of Flow Rates and Bed Lengths | 124 |
| | B Data and Parameters for SLE Models | 125 |
| B.1 | Experimental Data for Ternary SLEs | 125 |
| B.2 | Coefficients for SLE Models | 127 |
| B.3 | Determination of Adsorption Isotherms from Perturbations | 127 |
| B.4 | Densities of Chromatographic Solvents | 128 |
| | C Dynamic Model for the Process Combination | 129 |
| | Bibliography | 131 |

LIST OF SYMBOLS

Latin symbols

| | |
|------------------|---|
| A | coefficient in VAN DEEMTER equation [cm] |
| A_c | column cross-sectional area [cm ²] |
| $a_{i,j}$ | coefficient for solubility approximations (species i at composition j) |
| B | nucleation rate [1/m ³ /s] |
| b_i | parameter of LANGMUIR adsorption isotherm of component i [l/g] |
| C | coefficient in VAN DEEMTER equation [min] |
| $c_{p,i}$ | specific heat [kJ/kg/K] |
| c_i | liquid phase concentration of component i [g/l] |
| D_{ax} | axial dispersion coefficient [m ² /s/kg] |
| D_a | apparent dispersion coefficient [m ² /s/kg] |
| d_p | particle diameter [μ m] |
| F | phase ratio |
| G | particle growth rate [m/s] |
| H_i | HENRY coefficient of component i |
| $HETP$ | height-equivalent of a theoretical plate [cm] |
| $\Delta h_{m,i}$ | heat of fusion of component i [J/mol] |
| k_0 | coefficient in pressure drop correlation [bar/min/cm ²] |
| k_b | coefficient in growth law [m/g/s] |
| k_g | coefficient for nucleation rate [m ⁴ /(g · s)] |
| L_c | column length [cm] |
| L | load of SMB unit |
| m | mass [g] |
| M_i | i th moment of a particle size distribution |
| NTP | number of theoretical plates |
| P | purity |
| P_{max}^F | maximum feed purity for one-step crystallisation |
| Δp | pressure drop [bar] |
| PR | specific productivity [g/d/ml] |
| Q | volumetric flow rate (liquid) [ml/min] |
| q_i | solid phase loading [g/l] |
| Q_S | volumetric flow rate (solid) [ml/min] |
| q_S | saturation capacity in LANGMUIR adsorption isotherm [g/l] |
| R | universal gas constant, 8.314472 J/mol/K |

| | |
|-------------|---|
| S_i^j | sensitivity of state i with respect to parameter j |
| SC | specific solvent consumption [l/g] |
| SR | specific solvent removal [l/g] |
| t | time [min] |
| T | temperature [°C] |
| $T_{m,i}$ | melting temperature [°C] |
| t_0 | dead time [min] |
| t_S | switching time [min] |
| u | superficial velocity [cm/min] |
| u_0 | interstitial velocity [cm/min] |
| V_c | column volume [cm ³] |
| x_i | mass fraction of component i |
| Y | yield |
| $y_i^{j,k}$ | segregation factor (species i at node j of unit k) |
| z | space coordinate [cm] |

Greek symbols

| | |
|------------|--|
| α | separation factor |
| β^j | safety margin for flow rate in zone j of a TMB or SMB unit |
| ϵ | total porosity |
| γ^j | dimensionless flow rate in zone j of a TMB or SMB unit |
| γ_i | activity coefficient of component i |
| ν^k | recycle ratio of flux originating from unit k |
| ψ | linearisation factor for SLE model |
| ρ | density [g/l] |
| τ | residence time [s] |

Subscripts

| | |
|------------|---------------------------|
| I, ..., IV | zones in TMB or SMB units |
| e | eutectic composition |
| r | racemic composition |
| p | pure enantiomer |

Superscripts

| | |
|-----------------|---|
| A, B, F | in- and outlet nodes of nonsharp separators (together with I, II, III, ...) |
| I, II, III, ... | units in separator networks (together with A, B, F) |
| D, E, F, R | desorbent, extract, feed, raffinate of an SMB or TMB unit |
| C, F, L | crystal phase, feed, mother liquor in crystallisation |

INTRODUCTION

Separation technology plays a vital role in most chemical and biotechnological productions. In particular this holds true in the manufacturing of high-value products like fine chemicals and pharmaceuticals. Processes in this field are usually characterised by the demand for a very high product purity and the simultaneous need to realise rather complex separation tasks. Examples for this are separations of isomers and stereoisomers, or the isolation of a single specific protein from a fermentation broth. Expenses for separations in such processes often dominate overall production costs.

A class of compounds where the above is notably true are enantiomers. Essentially, enantiomers are molecules that are structured like non-superimposable mirror images of each other. Such substances are of particular importance in the production of pharmaceuticals, since biological systems exhibit a distinct ability to discriminate between the two enantiomers of a compound. As a consequence, usually only one enantiomer exhibits the desired physiological effect. In the best case, the other promotes the efficacy of the drug. However, more often it is ineffective – and in the worst case even harmful. This explains why both the number of drugs sold in enantiopure form and the economical revenues from these pharmaceuticals rise vigorously.

The direct synthesis of a single enantiomer requires a long and cost-intensive development of a suitable catalyst. In contrast to this it is much easier to produce a 1:1 mixture of two enantiomers via classical chemistry. Subsequently this mixture can be separated to obtain the favoured enantiomer. However, due to their structural similarity enantiomers have practically identical physical and chemical properties, which makes such separations complicated and expensive.

The development of improved separation processes for enantiomers therefore appears desirable. One possible approach, which will be investigated here, is to apply a combination of two complementary separation processes in order to purposefully create cost-reducing synergisms.

In this work, such a process combination that incorporates continuous Simulated Moving Bed (SMB) chromatography and enantioselective crystallisation from solution will be investigated in order to contribute to economically and ecologically more efficient processes for enantioseparations. The first process considered, SMB chromatography, is a rather complex and expensive unit operation, which is well-established in enantioseparations. The second process, enantioselective crystallisation, might be regarded as simpler and less expensive, yet it requires a certain enrichment with respect to the desired enantiomer prior to application. In a combination of the two processes, the typically high purity demands on SMB chromatography (that limit the performance of this process) could be reduced, since only the mentioned enrichment necessary for crystallisation has to be provided.

It will be investigated whether this reduction of purity requirements on SMB processes in combination with a crystallisation step entails a potential with respect to the improvement of process performance. The analysis of such processes that include a complex unit operation like SMB chromatography and that (as will be demonstrated later) contain recycles, is not possible on the basis of intuition only. In this connection, the main goals of this thesis are to reveal the origins of synergisms and limitations that arise from coupling the two units, to contribute to the understanding of the behaviour of the individual unit operations and the process combination as a whole, and to develop methods for the conceptual design and the evaluation of the performance of this process combination.

The above goals cannot be achieved by determining an optimal design for a particular enantiomeric system only. Rather than this, in order to establish general conclusions with regard to feasibility and important design aspects of the process combination, in this work model-based investigations of the two individual unit operations as well as of their combination will be performed. Different enantiomeric model systems will be considered in these examinations.

The fundamental concept of the process combination and the expected synergisms from its application will be introduced in the first chapter. This will be preceded by a brief survey on chirality and its biological and economical consequences in order to familiarise the reader with this field. State-of-the-art technologies for the preparative manufacturing of pure enantiomers will be also reviewed.

In Chapter 2 the theoretical fundamentals of the two unit operations, SMB chromatography and enantioselective crystallisation from solution, will be explained in the degree of detail that is required to follow the argumentations in later chapters. Subsequently, in Chapter 3 all necessary parameters will be summarised for the different experimental model systems to be studied. A brief explanation of applied experimental methods will be included.

A fundamental study of a process combination requires a thorough understanding of the incorporated individual processes. Of particular importance in this connection are the impact of the involved thermodynamic equilibria, and the specific design requirements that result from combining the two processes. In Chapter 4 the influence of the adsorption isotherms on SMB chromatography will be examined using parameters of different model systems. A design approach for SMB processes under reduced purity requirements will be suggested in Chapter 5. Analogously, in Chapter 6 the effects of the solid-liquid equilibrium and the design of enantioselective crystallisation will be demonstrated, again using several model systems.

In Chapter 7 the process combination as a whole will be investigated. Applying the results from preceding chapters, a shortcut method will be suggested that simplifies the design of the combined processes and allows for the straightforward evaluation of its performance. A comparison of different process configurations will be performed. The results for different model systems will demonstrate the significant potential that arises from combining chromatography and crystallisation for the separation of enantiomers. The chapter concludes with a short summary of engineering aspects that deserve consideration in further investigations.

CONCEPT OF A PROCESS COMBINATION FOR ENANTIOSEPARATIONS

Enantioseparations are becoming increasingly important in drug manufacture and life science applications. Engineers dealing with this subject have to face the complex field of stereochemistry and a sometimes confusing special terminology. Therefore, the first part of this chapter is devoted to the most important definitions of stereochemistry and the significance of enantiopure drugs. Subsequently, a survey will be given on preparative production methods for pure enantiomers.

In the second part of this chapter the basic concept of a process combination for enantioseparation will be introduced. Possible synergisms that are expected from the approach will be discussed, followed by an overview on state of research and scope of this work.

1.1 Background

1.1.1 Fundamentals of Stereochemistry

Objects lacking inverse symmetry, *viz.* objects that cannot be superimposed on their mirror image, are called chiral. The term originates from the Greek word for hand, *cheir* ($\chi\epsilon\iota\rho$), because the left and the right hand represent non-superimposable mirror images of each other. Other examples of chiral objects from everyday life are screws, winding staircases, and keys.

In chemistry, the concept of molecular chirality is associated with stereo-isomerism. Stereoisomers have identical constitutions. That is, such molecules consist of the same type and number of functional groups which are attached to the same atoms (identical connectivity). The difference between stereoisomers lies in the arrangement of these substituents in space. Although this distinction might appear subtle, it can have dramatic consequences, as will be explained below.

Enantiomers and Diastereomers

Enantiomers are stereoisomers that are non-superimposable mirror images of each other. This property is understood best when looking at the molecular origin of this coexistence of symmetry and asymmetry.

As stated independently by VAN'T HOFF [1] and LE BEL [2], a tetrahedral arrangement results if a central carbon atom (stereogenic or chiral centre) is saturated with four different functional groups (Figure 1.1). Because of the different spatial arrangement of the groups, it is impossible to superimpose the two molecules shown in the figure by any means of rotation or translation, *viz.* the two molecules are *chiral*. Besides chiral centres, other origins of molecular chirality are chiral axes, chiral planes, or chiral helices.

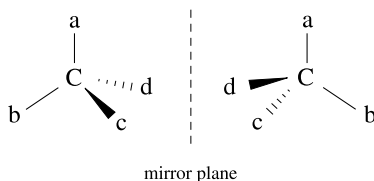


Figure 1.1. Example for the source of chirality – a tetrahedral arrangement of four substituents at a central carbon atom.

It can be seen from Fig. 1.1 that enantiomers have – except for the spatial orientation of one or more functional groups – identical structures. Due to this structural similarity, in an achiral environment (*i.e.*, a milieu lacking any other chiral compound) enantiomers have identical physical and chemical properties. The only measurable differences are related to properties that change sign, but not magnitude, upon reflection. Thus, enantiomers differ in their chiroptical properties, such as optical rotation, circular dichroism, and optical rotatory dispersion [3].

On the basis of their opposite specific optical rotation, a classification into (+)- and (–)-enantiomers is possible. While the former rotates polarised light in positive direction, the latter changes the rotation angle by the same value in negative direction. Another classification, common for amino acids and sugars, is the discrimination between *D*- and *L*-enantiomers. This system was introduced by FISCHER [4]. A newer and more powerful notation is the CIP system (named after the authors CAHN, INGOLD, and PRELOG [5]). Based on the sequence of substituents at a chiral centre, it distinguishes between (*R*)- and (*S*)-enantiomers. For details see, for example, [3, 6].

Diastereomers are stereoisomers with a spatial difference not related to mirror reflection. They are molecules with two or more chiral centres in which not all stereogenic centres have opposite configuration. Figure 1.2 shows the stereoisomers (enantiomers and diastereomers) of tartaric acid. The number of chiral centres, n , determines the number of possible stereoisomers. Tartaric acid has two chiral centres. There are $2^n = 4$ different stereoisomers. However, in the case of tartaric acid, two of these diastereomers are identical (see Fig. 1.2).

In contrast to enantiomers, diastereomers have different physical and chemical properties. Consequently, one of the most common techniques in enantioseparations is the crystallisation of diastereomeric salts that are derived from the respective enantiomers (see section 1.1.3).

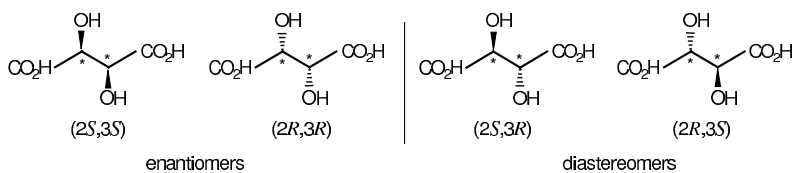


Figure 1.2. Stereoisomers of tartaric acid. The asterisk denotes chiral centres. Note, that the two diastereomers on the right are actually identical.

Racemates

An important term related to mixtures of enantiomers is the *racemate*, which denotes a 1:1 mixture of two enantiomers. Classical chemical syntheses of chiral compounds usually lead to racemic mixtures, necessitating the subsequent application of a suitable separation technique to obtain pure enantiomers.

An important aspect for this work is the existence of different types of solid racemates, because the type of racemate determines whether it is possible to perform an enantioselective crystallisation in a given system. This not only holds true for crystallisation from the melt, but also for crystallisations from solutions. The three main types – the conglomerate, the racemic compound, and solid solutions – can be distinguished based on their binary melting diagrams (see section 2.2.2) [7]. Only the former two types allow for the crystallisation of pure enantiomers.

It is estimated that about 10% of all enantiomeric systems form conglomerates, while the majority form racemic compounds [7]. Solid solutions are found only scarcely. It should be noted that for certain systems the type of racemate changes as a function of external conditions like temperature. While this polymorphism is usually undesired in process design, it can also be used to induce a favourable crystallisation behaviour (*e.g.*, by derivatisation). Often, salts of enantiomers develop conglomerates, while the underderivatised systems reveal formation of racemic compounds [3].

The crystallisation behaviour of some systems is not covered by the categories above (*e.g.*, systems with racemic compound formation and simultaneous solid solution at high optical purity; anomalous racemates; polymorphism not related to change of racemate type) [7, 8]. Although such systems are out of scope in this work, their existence emphasises the necessity of accurate experimental investigations of the solid-liquid equilibria for the design of enantioselective crystallisation processes.

1.1.2 Biological and Economical Relevance

Biological Relevance

Molecular chirality is not only inherent, but essential to living systems. Although the probability for the formation of two enantiomers is identical, in nature actually a breakage of this symmetry can be observed. For example, the monomer blocks of proteins (the 18 optically active protein

amino acids), are all *L*-enantiomers. In contrast, DNA, RNA, and most carbohydrates commonly appearing are of the *D*-type. As a result, essential physiological processes utilise exclusively only one of the possible stereoisomers of each compound involved. While the origin of this biomolecular homochirality is not yet clarified and subject to both experimental research and numerous speculations [3], it is widely accepted that chiral homogeneity is essential for the existence of life [9].

An important consequence of the above is that biological systems show a distinct ability of chiral discrimination with respect to exogenous compounds. It is well known that the two enantiomers of a substance can have very different effects on a living cell. Numerous examples cover differences in odour, taste, and more important, pharmacological effects of enantiomers (see, *e.g.*, [3], pp. 132). While one enantiomer has the desired physiological effect, the other might be either inactive, have some (lower) positive effect, have the opposite effect, or some different activity [10, 11]. Several tragic examples related to the prescription of drugs in racemic form clarify this fact. One of the enantiomers of thalidomide, a mild sedative, is presumed to have caused thousands of severe birth defects in the 1960s. The use of racemic perhexiline, a treatment for heart rhythm problems, in the 1980s lead to several fatalities. The slow human metabolism for one of its enantiomers lead to its unrecognised accumulation [12]. The recognition of such phenomena had – and still has – major implications on the production of pharmaceuticals (see below).

Economical Relevance

Enantiopure substances have a significant economical impact. Primarily this is due to the sales volumes of pharmaceuticals. To circumvent undesired side effects or unnecessary physiological ballast resulting from the different medical actions of enantiomers, since the 1990s a growing fraction of active pharmaceutical agents is produced as single enantiomers. More rigorous regulations on the approval of new drugs amplified this trend. Manufacturers are required to evaluate the pharmacological and toxicological effects of both enantiomers of a racemic drug, and to include data on the conversion of the active enantiomer (the eutomer) into its counterpart (the distomer) [13].

Table 1.1 demonstrates that both the total market for pharmaceuticals as well as the market share of enantiopure drugs are growing. This trend is expected to continue, because most pharmaceuticals in the pipeline today are single enantiomers [14].

Table 1.1. Development of sales (in billion US\$) and market share of single enantiomeric drugs. Data from [15, 16].

| year | total market | single enantiomers | market share |
|------|--------------|--------------------|--------------|
| 1999 | 360 | 115.9 | 32.2% |
| 2000 | 390 | 132.5 | 34.0% |
| 2001 | 410 | 146.1 | 35.6% |
| 2002 | 429 | 159.1 | 37.1% |

Another driving force for the increasing manufacture of enantiopure pharmaceuticals is the possibility to re-patent the single enantiomers of a racemic drug (*chiral switch*). Patents on drug agents are usually valid for 20 years (E.U. and U.S.), afterwards the genuine substance usually is replaced by less expensive generic drugs. The chiral switch thus prolongs the time span for commercialisation of a substance [12, 14].

The fine chemistry is a second important commercial field of pure enantiomers. The market volume of 6.3 Billion US\$ in 2000 will grow to 16 Billion US\$ in 2007 [15]. This is mostly due to products for the pharmaceutical industry, for example chiral building blocks like non-natural amino acids, chiral auxiliaries, and intermediates. Related to this are so-called chiral technologies, *viz.* the supply of material related to synthesis and separation of enantiomers. Here, revenues are expected to grow with an annual rate of approx. 12% from 4.8 (1999) up to 14.9 billion US\$ in 2009 [16]. This trend is driven by the increasing interest in production methods like enantioselective synthesis and biocatalysis (see section 1.1.3). Further enantiopure fine chemicals are agrochemicals, agents for electronics, flavours, and fragrances.

The trends listed above were made possible by significant advances in manufacturing methods for pure enantiomers. Both synthetic methods like (bio-)catalysis, as well as separation processes like chiral chromatography (here in particular the development of new chiral stationary phases and the acceptance of sophisticated process schemes like the Simulated Moving Bed (SMB) process) are becoming standard tools in the manufacturing of pure enantiomers (see section 1.1.3).

1.1.3 Production Methods for Pure Enantiomers

Classification of Methods

Essentially all approaches towards enantiomerically pure substances have in common the generation of a chiral milieu to provide for enantioselective interactions. Consequently, since there are many ways to establish such interactions, numerous different approaches exist to obtain pure enantiomers, in particular at lab-scale. However, a limited number of techniques dominates in preparative applications. These will be reviewed in the following.

Preparative production methods can be classified into two categories. The first route is to attempt a selective synthesis of the desired enantiomer (or of an asymmetrical mixture of both enantiomers). The second is based on the production of the racemate and its subsequent resolution. Figure 1.3 gives a rough classification of the most important preparative techniques. This classification should not be considered complete, because additional methods are available; many of them representing a combination of two or more different techniques.

Common methods of the first category – enantioselective syntheses – include chemical and biological catalysis, the generation of desired molecules from pure chiral building blocks that are already available (*chiral pool*), and the use of chiral auxiliaries to create some asymmetry during synthesis (*chiral handle*). Although these approaches can be considered as straightforward, there are some limitations important for practical realisation. The development of catalysts with high

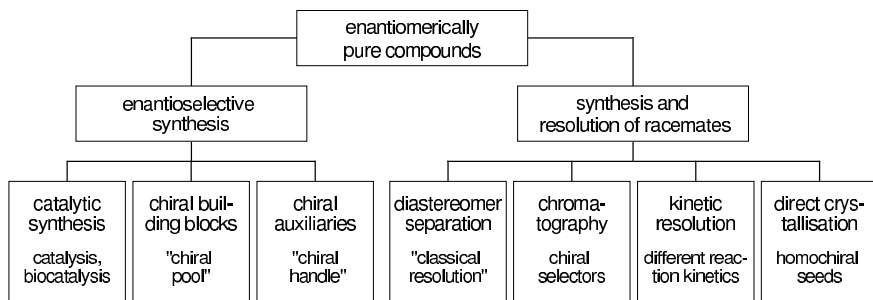


Figure 1.3. Classification of preparative production methods for enantiopure products.

enantioselectivity is time consuming and expensive, and process scale-up might be difficult. The same holds true for the determination, modification, and production of suitable enzymes. Another problem is the (yet) limited availability of chiral building blocks. Despite these restrictions, industry shows increasing interest in synthetic methods [16].

In contrast, the advantage of the second category – the racemic approach – is that racemates are generally easier obtained from classical chemistry. Frequently, the main challenge here is to find an economically competitive method for the resolution of the racemic mixture. Like in enantioselective syntheses, methods for resolution of racemates require a chiral milieu to provide for enantioselective interactions. Most important preparative techniques are the formation and separation of diastereomers (*classical resolution*) and, with a growing acceptance, enantioselective chromatography.

Currently, the resolution of racemates and chiral pool-related techniques contribute about 55% to the market, chemical and biological methods account for about 30% and 10%, respectively. At the same time, the importance of the synthetic methods (biocatalysis, catalysis, chiral pool) is expected to increase, while revenues from racemic approaches (separation of diastereomers, chromatography) will decrease. However, the dominance of the latter is expected to hold on through 2009, in particular due to the application of sophisticated chromatographic techniques like the SMB process (see section 2.1) [16].

Production from Enantioselective Syntheses

The different approaches in enantioselective synthesis (catalysis, biocatalysis, chiral building blocks, chiral auxiliaries; see below) are also referred to as "asymmetric synthesis", because they often deliver enantioenriched – rather than enantiopure – products.

Catalytic Syntheses. There are two approaches in enantioselective catalysis – classical chemical catalysis and biocatalysis.

Currently, the field of enantioselective *chemical catalysis* experiences a remarkable development. Important reaction types are hydrogenation, hydroformylation, oxidation, epoxidation, and cycloaddition [17]. Both homogeneous and heterogeneous catalysts are in use, most importantly

complexes involving rhodium phosphine, ruthenium, and transition metals [18, 19]. Significant research efforts aim at the development of new techniques and catalysts. Comprehensive reviews on this topic can be found in [17, 18, 20]. Important preparative applications of catalytic methods are the productions of carboxylic acids, (–)-menthol, (*R*)- and (*S*)-glycidol, and naproxen. More examples are listed in [21, 22].

Advantages of classical chemical catalysis are the straightforward approach and, on a more philosophical level, the elegant chemistry. However, it also suffers from some drawbacks. For example, often large amounts of additional chemicals are needed while the achievable optical purity is usually only moderate, still requiring additional resolution techniques [23].

Biocatalysis, as the second class of catalytic methods, is attracting more and more interest. This is reflected by extensive research in the development of new enzymes and their adaptation to organic solvents (see, *e.g.*, [24–26]). (Semi-)synthetic or naturally occurring enzymes provide for stereoselective catalytic action. Examples are lipases, hydrolases, and acylases [27]. Enzymes are used either *in-vivo* (whole cell biocatalysis) or as free proteins in solution. Examples for preparative processes involving biocatalysis are the manufacture of natural and unnatural amino acids, aspartame, and carnitine [21, 22]. It is expected that enzymatic methods in future will play a major role amongst the production methods for pure enantiomers [24].

Enzymes have several advantages in comparison to conventional catalysis. They provide for remarkable acceleration of reaction rates, are environmentally friendly, and – because they usually require similar reaction regimes – different enzymes can be combined in one-pot syntheses. Their major drawbacks are the limited stability and the narrow application ranges due to their distinct specificity [26]. Similar to conventional catalysts, significant efforts are necessary for identification, development and production of an enzyme. Furthermore, the enzyme has to be adapted to process conditions (*e.g.*, to the presence of organic solvents).

Syntheses from Chiral Building Blocks (“*Chiral Pool*”). Methods in this class utilise enantiomerically pure compounds as starting material for a synthesis. Such building blocks are either occurring naturally (“*natural pool*”) or produced synthetically (“*new pool*”). Common building blocks are, for example, amino acids, carbohydrates, terpenes, and alkaloids. There are several examples of preparative syntheses using chiral building blocks. A compilation was given by CROSBY [19]. It can be expected that the importance of chiral pool syntheses will increase with the number of building blocks available.

The major advantage of chiral pool syntheses is the large and constantly growing number of enantiopure compounds available. Many of these substances are rather inexpensive bulk chemicals. A disadvantage can be the necessity to recycle large amounts of product if diastereomers are formed during synthesis.

Syntheses Using Chiral Auxiliaries. The chiral milieu necessary for a stereo-selective synthesis can be achieved by temporarily binding a chiral auxiliary to one of the reactants. This “*chiral handle*” is removed after the reaction and separated from the mixture. The necessary step-wise procedure is the main difference to catalytic methods (see above), where binding, reaction, and release occur

spontaneously [17, 18].

Using an auxiliary allows to control the stereochemistry of the reaction. However, practical concerns of using chiral auxiliaries are related to the step-wise mechanism described above. In particular, the binding, removal, and subsequent separation of the auxiliary can be a challenge.

Production from Syntheses and Resolutions of Racemates

Formation and Separation of Diastereomers. The underlying principle of the separation of diastereomeric derivatives (also called "classical resolution"), is that the association of a racemate with a pure enantiomer (resolving agent) leads to the formation of diastereomers. These diastereomers, usually salts or esters, have different properties, facilitating a physical separation. The latter usually is carried out by exploiting solubility differences (crystallisation). Also chromatography is used frequently since the separability is significantly higher for diastereomers than for enantiomers. After separation the resolving agent is released and recycled. A schematic example is shown in Fig. 1.4.

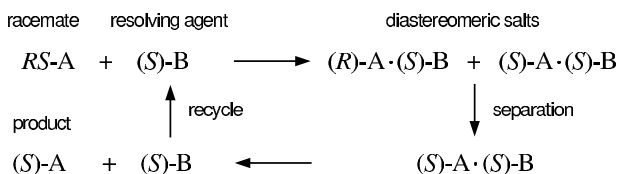


Figure 1.4. Classical resolution of diastereomers. The racemic mixture $RS\text{-}A$ is converted into two diastereomeric salts using the homochiral resolving agent $(S)\text{-}B$. The diastereomers are separated, and pure enantiomer, $(S)\text{-}A$, is released. The resolving agent is recycled.

The two main design aspects of a classical resolution are the choice of a suitable resolving agent out of numerous agents available, and the choice of an appropriate solvent for separation. The latter determines the separability of the diastereomers (both in crystallisation or in chromatography). Unfortunately, no methods exist for the *a priori* selection of a resolving agent and a corresponding suitable solvent.

As for the chemistry involved, classical resolutions might be seen as lacking elegance in comparison to asymmetric synthesis. However, they represent the most important resolution technique in terms of the total number of preparative separations carried out [16, 28]. Examples of industrial productions are the antibiotics ethambutol (with resolving agent (R, R) -tartaric acid) and chloramphenicol (with 1- (S) -(+)-camphor-10-sulfonic acid), or the anti-inflammatory naproxen (with cinchonidine) [29].

Despite their industrial importance, classical resolutions suffer from some drawbacks, especially at larger scales. Mainly the requirements on process equipment (multiple reactors, tanks, etc.) and the costly recovery of the resolving agent can make it a rather expensive process. Often, process economy depends on the possibility to racemise the undesired enantiomer [29].

Enantioselective Chromatography. Chromatographic separations are based on different distributions of the compounds to be separated between a mobile phase and a stationary phase. The main feature of enantioselective chromatography (frequently referred to as "chiral" chromatography) is the use of a stationary phase that has chiral selectors attached to its surface (chiral stationary phase, CSP). The selector provides for the chiral milieu necessary for enantioselective interactions. Different types of CSPs are in use, for example phases based on cyclodextrines, proteins, or polysaccharides. The development of new CSPs is topic of ongoing research efforts. For an overview on techniques and CSPs the author refers to [27, 30]. Section 2.1 summarises the fundamentals of chromatographic processes.

While enantioselective chromatography is the method of choice for analytical determination of optical purity, it also has become one of the most important techniques for preparative purposes up to scales of several hundred tons per year. There are several reasons for the growing number of applications, for example fast performance and low development times, rather simple scale-up, and the availability of a larger number of different CSPs for many separation problems. Notably, the implementation of the Simulated Moving Bed (SMB) technology proved to reduce separation costs. Compared to batch-wise elution chromatography, the SMB process facilitates significant improvements in terms of productivity and solvent consumption. Because SMB units essentially are binary fractionators, this technology is especially suited for separating racemic mixtures.

However, preparative enantioselective chromatography also has some drawbacks; for example, the high costs and the limited capacity and stability of the stationary phase. Comprehensive reviews on the topic are given in [27] and [31].

Kinetic Resolutions. Kinetic resolutions are based on different reaction kinetics of two enantiomers with an enantiopure reagent, which can be either a chemical reactant or an enzyme. Ideally, the rate of conversion is zero for one enantiomer, while the other is readily converted to the target product. Although very high selectivity can be achieved, in practice usually a compromise has to be made between conversion and enantiomeric purity [6]. It should be noted, that enzymatic reagents often deliver higher optical purities [19]. Recent research results emphasise the future potential of enzymatic methods [24].

As for all methods based on the resolution of racemates, the further use of the second enantiomer, or its racemisation, is of economical interest. Thus, an important aspect of kinetic resolutions is that enantiomeric excess can be obtained both in the product and in the residual substrate [19].

Several preparative resolutions are carried out using kinetic resolution, for example syntheses of naproxen and pyrethroid acid [19]. Further examples are compiled in [3].

Direct Crystallisation. The prerequisite to enantioseparations by direct crystallisation is that the racemate of the respective substance forms a conglomerate (see section 1.1.1). It is estimated that about 10% of the enantiomeric systems form conglomerates [7]. It should be mentioned, that for some components that crystallise as racemic compounds, the formation of the conglomerate can be achieved through a change of temperature, or by converting it into a derivative [3].

A self-evident method to perform a separation by direct crystallisation is to crystallise out the

conglomerate. This so-called spontaneous resolution delivers both enantiomers as a mixture of the two enantiopure crystals. Obviously, the problem then is to identify and separate the different crystals. In fact, the first enantioseparation was performed by PASTEUR [32], who could visually distinguish between the enantiopure crystals of sodium ammonium tartrate and manually sorted them. However, for obvious reasons this method is rather inappropriate for preparative purposes.

A variant feasible for preparative applications is preferential crystallisation, where homochiral seeds (*i.e.*, pure crystals of one of the enantiomers) are added to a solution of dissolved racemate. The respective enantiomer preferably deposits on the surface of these seeds. A process option of preferential crystallisation is the so-called crystallisation by entrainment. Here, the seeds are added to initially enriched solutions. Crystallisation kinetics lead to the depletion of the remaining mother liquor beyond the thermodynamic equilibrium (*i.e.*, the racemic composition). After stopping crystallisation, removal of the crystals, and addition of fresh racemate, the process is restarted in the opposite direction by addition of seeds of the second enantiomer [33].

As a further option, the use of chiral additives should be mentioned. While in achiral environments the solid-liquid equilibria of enantiomers are strictly symmetrical, the addition of a chiral compound leads to asymmetry facilitating selective crystallisation by cooling or evaporation [34].

There are several preparative applications of preferential crystallisation, for example in the production of diltiazem [23]. However, it should be noted that preferential crystallisation processes are non-equilibrium operations. Thus, conditions have to be adjusted very carefully in order to prevent spontaneous nucleation of the unseeded enantiomer. In particular, the possible accumulation of impurities is of major concern in preparative applications, necessitating the use of extremely pure starting material [19].

In order to apply direct crystallisation methods, the knowledge of the system's solid-liquid equilibrium (SLE) is mandatory. Fundamentals concerning SLE of enantiomers and enantioselective crystallisation from solution are given in section 2.2.

Other Techniques

The compilation of methods given above cannot be exhaustive. For example, process schemes should be mentioned that include classical engineering techniques like *distillation* (*e.g.*, [35]) or *liquid-liquid-extraction* [27, 36]. In addition, there is a number of methods of more or less practical importance and possible future relevance for preparative applications, respectively.

Most productions are multi-step processes. Thus, *process combinations* of two or more of the above techniques are common, for example biological and chemical catalysis [37].

Membrane technologies are considered as having a high potential for future applications [27]. Membranes allow for continuous operation and are readily applicable to large-scale processes [36]. They offer interesting perspectives for process integration; for example, in connection with biocatalysis [38] or in combination with other separations. Considerable research efforts are devoted to the development of new enantioselective membranes. The design of tailor-made membranes

and chiral stationary phases by *molecular imprinting* [39] appears very promising. However, despite their potential, chiral membranes are industrially not yet relevant, because their enantioselectivity is usually rather low [31, 36].

Another important aspect in preparative applications is the possibility to include *racemisations*. Obviously, this is of special interest in approaches where a racemate is resolved. Unresolved mixtures with an excess of the undesired enantiomer can be racemised and recycled, thus theoretically allowing yields of 100%. Racemisations can be performed by thermal means, or using catalysts or enzymes.

Recent results suggest that *ionic liquids* might be of interest in catalytic processes for the stabilisation of heterogeneous or the recycling of homogeneous catalysts. They also could serve as promoters of chiral discrimination or as the source of chirality itself [40].

Feasibility was shown for enantioselective extraction using supercritical fluids, and for gas chromatography SMB processes [41, 42]. However, the interest in these processes yet appears to be restricted to academia. Other processes like capillary electrophoresis will probably remain restricted to analytical applications.

1.2 Concept of the Process Combination

The previous section summarised the various methods in preparative enantioseparations. Among them, chromatography is gaining more and more interest due to its relatively short development times and the capability of accomplishing even difficult enantioseparations. However, chiral chromatography is an expensive technology. Thus, there is a strong motivation for the development of more efficient chromatographic processes.

A well known fact in engineering is that separation costs rise with increasing purity requirements. Purity requirements on chromatography might be reduced by the introduction of a second, complementary unit operation. This section presents the concept of a process combination for enantioseparations that complements continuous chromatography with enantioselective crystallisation from solution in order to create cost-reducing synergisms.

1.2.1 Some Remarks on Process Intensification

Before introducing the concept of the process combination and explaining the benefits expected from this, a few general remarks should help to classify the approach.

Most generally, process combinations like the one to be investigated in this work belong into the framework of *process intensification*. This collective term subsumes different innovative measures that offer drastic improvements with respect to some goal function in chemical processing. Such

goals can be very different: for example, reduction of costs for equipment, energy, auxiliaries, raw materials, or solvents; minimisation of emissions, effluents, and waste; or enhancement of process stability and safety. There are well known examples of process intensification, such as reactive separations (*e.g.*, reactive distillation, membrane reactors, and chromatographic reactors), heat exchanger networks, and micro-reaction devices. Specific examples can be found, for instance, in [43–47].

Unfortunately, in some cases the literature about process intensification does not provide a consistent terminology. To avoid possible misconceptions, below a classification of different methods in process intensification is suggested (Figure 1.5). The scheme reflects the author’s view on the topic and was derived on the basis of a classification for reactive separations published by STANKIEWICZ [43].

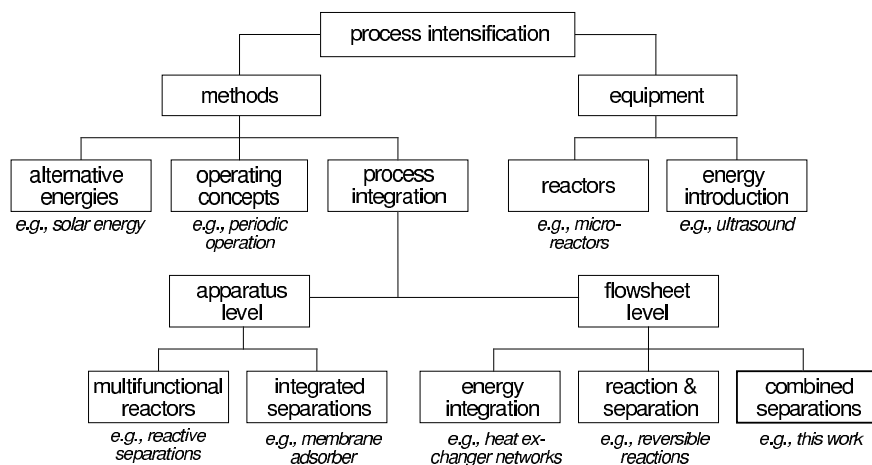


Figure 1.5. Suggestion for a classification of measures for process intensification.

According to the figure, measures can be divided into methodological and equipment-related attempts.¹ An important example of equipment for process intensification are micro-reaction devices. These can provide for improved mass and heat transfer while they are safer to operate than large-scale processes. Among methods, the development of new operating concepts should be mentioned (*e.g.*, the periodic pressure-swing adsorption process). Another methodological approach is *process integration*, which in this work will denote any systematic combination of unit operations. Integrated processes can be established both on the level of apparatuses (*e.g.*, multifunctional reactors, reactive distillation, or membrane adsorbers; see [48] for more examples) as well as on the level of flowsheets (*e.g.*, heat exchanger networks, reactor-separator combinations) [49]. Process integration on the flowsheet level in the following will be referred to as *process com-*

¹ Some approaches will not clearly fit into a classification into equipment and methods, because new methods often require new types of equipment and vice versa. However, the scheme above should provide a fair introductory basis.

binations. These are usually characterised by the purposeful establishment of heat and/or mass recycles between different unit operations. The process investigated in this work belongs into this category.

Another important term that is often used in different notions is the *hybrid process*. In chemical engineering this is often used as a synonym for an integrated process. However, in this work the system-theoretical definition for hybrid is applied; *viz.* a hybrid process will refer to a system that contains both continuous and discrete components.

1.2.2 Basic Concept

Synthesis and subsequent resolution of racemates will remain a method of choice in preparative productions of pure enantiomers – despite the advances in synthetic approaches. The reason for this is that it is generally easier to produce a racemate than to develop a synthesis for a pure enantiomer. The economically limiting factor in a racemate-based process is usually the separation of the enantiomers. In this context, chromatographic methods, in particular continuous SMB chromatography, are becoming increasingly important, because they offer a number of advantages over other separation methods (see section 1.1.3).

However, chiral chromatographic separations have to be considered as expensive processes. The main reasons for this are *i)* high investment costs for CSPs, *ii)* limited capacity, selectivity, and life time of CSPs, *iii)* significant consumption of highly purified solvents, and *iv)* the high purity requirements that are typical in productions of fine chemicals and pharmaceuticals.

It is a well known fact in engineering that costs of a separation decrease if purity requirements are lowered. Concerning enantioseparations by chromatography, cost-reducing synergism might be created by introducing a second, complementary process that allows to reduce the purity requirements on the chromatographic process. This work investigates whether enantioselective crystallisation from solution can be used as such a complementary unit operation. Crystallisation can deliver a pure enantiomer in the form of solid crystals, provided that the feed of the crystalliser possesses a certain minimum purity with respect to this enantiomer (see Chapter 2 for details).

According to the above, here a process combination of continuous chromatography and crystallisation is suggested, where chromatography is used to only partially resolve a (racemic) mixture. A subsequent crystallisation produces the pure solid enantiomer from the mixture delivered by chromatography. Figure 1.6 contains a schematic representation of a possible process configuration. A racemic feed solution of (*R*)- and (*S*)-enantiomers is enriched by chromatography. The stream that contains an excess of the desired enantiomer, here (*R*), is sent to a crystalliser, where cooling or evaporation is applied to achieve supersaturation and to crystallise out this component. While the enantiopure solid product (*R*) is withdrawn from crystallisation, the remaining mother liquor can be recycled. The second stream from chromatography contains mostly the undesired (*S*)-enantiomer. It either represents waste or can be processed further.

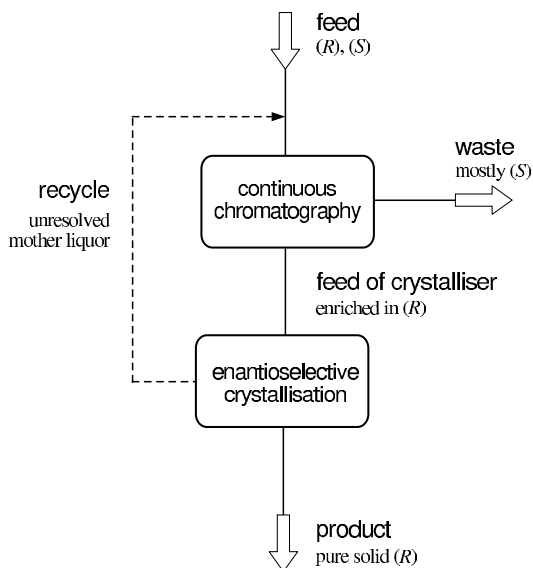


Figure 1.6. Basic concept of the process combination of chromatography and enantioselective crystallisation. A mixture of the (*R*)- and (*S*)-enantiomers of a compound is separated. The (*R*)-enantiomer is the desired product.

It should be mentioned that in order to perform an enantioselective crystallisation, certain conditions have to be met with respect to the solid-liquid equilibrium. Most notably, the enantiomeric system must either form a conglomerate or a racemic compound. For the latter, the transition purity (*i.e.*, the purity of the stream entering crystallisation) must exceed the eutectic composition of the system. These issues are discussed in detail in section 2.2.

According to Fig. 1.5, the process combination above represents a *separator combination* (*i.e.*, two separation units that are integrated on the flowsheet level in order to create certain synergisms). Because of the discrete events occurring in the involved SMB process, it simultaneously is a hybrid process. To the author's best knowledge, there have been no general systematic studies on the optimal design of such process combinations.

1.2.3 Possible Synergisms

An optimised process combination of chiral chromatography and enantioselective crystallisation might be economically advantageous in comparison to producing an enantiomerically pure solution by stand-alone chromatography.

In the case of chromatography, the following benefits can be expected from lowering purity requirements:

1. Higher specific productivity (*i.e.*, a higher ratio of throughput and amount of stationary phase). This in turn will allow to reduce the investment costs for chiral stationary phase, that can be responsible for more than 50% of the overall costs [50].
2. Lower solvent consumption (*i.e.*, a lower volume of solvent used per mass of product obtained). This will reduce operational costs for purchase, make-up, and recycling of chromatography-grade solvents.
3. Higher outlet concentrations, thus reducing operational costs for obtaining concentrated solutions or solid products (usually carried out by evaporation).

In addition to these main benefits, some further aspects favour an integrated process design of chromatography and crystallisation:

4. Most enantiomers are marketed as solids [50, 51]. The process combination readily delivers the solid product. Furthermore, the crystal structure or morphology determines physical and – sometimes – chemical properties of pharmaceuticals, thus it influences key drug properties such as dissolution rate, stability, and their processing [51]. By choosing appropriate crystallisation conditions, the integrated scheme might also deliver the desired polymorph and product quality.
5. Because crystallisation is commonly applied as a final polishing step for a product (see above), manufacturers normally possess both equipment and expertise for crystallisation. Thus, investment costs for crystallisers usually can be neglected.
6. The incorporation of crystallisation delivers not only the desired enantiomer, but also can facilitate the simultaneous removal of impurities [50].
7. In cases where a chiral switch is considered (see section 1.1.2), production methods for the racemates are already established, and the single enantiomer must be produced at comparable costs. The integrated scheme might allow for such cost minimisation.

Figure 1.7 contains – schematically – the expected costs as a function of required product purity for a stand-alone separation by chromatography and by the process combination, respectively.

The first situation depicted (solid line) corresponds to a stand-alone separation by chromatography. The corresponding cost-characteristic increases monotonously with increasing purity and has typically a steep slope for purities approaching 100%. The second cost-function (dashed lines) corresponds to an optimal process combination. Since it requires less stationary phase, the investment-offset is lower. On the other hand, the lower amount of stationary phase somewhat decreases the performance the unit and leads to a somewhat steeper slope of this function. At a certain transition purity above the eutectic composition of the system, the output of chromatography is transferred to crystallisation. This necessitates some additional investment (denoted by a step increase of costs at the transition purity). The cost-characteristic of crystallisation has a lower slope, since here

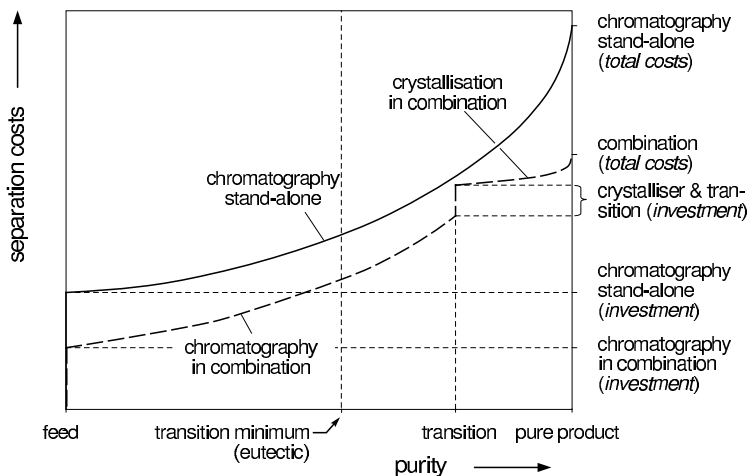


Figure 1.7. Schematic comparison of separation costs for stand-alone chromatography (solid line) and a combination of chromatography and crystallisation (dashed). Favourable investment and operational costs for crystallisation compensate for unfavourable performance of chromatography at high purity.

operation costs are less dominated by purity. Only at very high purity the slope increases due to additional efforts for filtering and washing of the solid.

The figure shows a hypothetical situation where an overall benefit results (*i.e.*, the total separation costs of the process combination are lower than those in stand-alone chromatography). The identification of conditions that lead to such overall benefit is one of the subjects of this work.

In order for the process combination to be more profitable than stand-alone chromatography, the benefits listed above must counterbalance additional efforts necessary for coupling the two units. The main issues to be considered are:

- Efforts for process development and data generation for crystallisation (for example, the measurement of solid-liquid equilibria, see section 2.2).
- Integrated schemes with internal recycles (like the process in Fig. 1.6) are usually more difficult to operate.
- Expenses for additional equipment (if not already available), such as the crystalliser itself, valves, and piping. An additional enrichment device has to be implemented if chromatography delivers product concentrations that are too low to perform crystallisation.

1.2.4 State of Research

The concept explained above is currently subject to research activities of several groups. However, so far only few publications on the topic exist.

LIM *et al.* [52] suggested the use of enantioselective crystallisation to separate racemic mixtures of praziquantel enantiomers (an anthelmintic) that were partially resolved by SMB chromatography. However, they did not intend to exploit the benefits of reduced purity requirements in chromatography, but tried to experimentally maximise the purity of the SMB separation. Since the involved solid-liquid equilibrium revealed some complexity, focus was set on development of a step-wise crystallisation procedure for the desired (-)-praziquantel [53].

In sugar industry, crystallisation is frequently applied to mixtures delivered by chromatography (see, *e.g.*, [54, 55]). However, here the unit operations are considered as purification steps only. A purposeful creation of synergisms has not been reported.

BLEHAUT and NICLOUD [50] were the first to recognise most of the potential benefits listed in section 1.2.3. They discussed the process combination in the framework of industrial aspects of SMB chromatography and predicted that an integrated design of chromatography and crystallisation can lead to cost-reduction and improved global process robustness. A simulation study of the SMB separation of a chiral ester was performed. It was concluded that there are different optimal operating conditions with respect to solvent consumption and productivity, respectively.

The first comprehensive survey on the concept was given in [56], where in particular the principles of enantioselective crystallisation were discussed in more detail using the solid-liquid equilibrium of mandelic acid in water. A model-based study of the SMB process was performed and a significant improvement of the productivity was predicted.

In this context, the author of this work investigated systematically the impact of adsorption isotherm parameters on the performance of SMB processes [57, 58]. For different experimental isotherms the productivity enhancement as a function of required purity was determined from numerical simulations. Chapter 4 will present the corresponding results in detail.

STRÖHLEIN *et al.* [59] performed a theoretical study of the process combination from an industrial perspective and tried to develop a design procedure for the process. They investigated an industrially relevant compound and the above-mentioned mandelic acid system. However, the approach presented suffers from some shortcomings to be discussed in Chapter 7.

GEDICKE *et al.* [60] also performed a model-based evaluation for the separation of two diastereomers. The importance of recycling mother liquor from crystallisation back to chromatography (see Fig. 1.6) was stressed. Their industrially relevant example revealed some problems related to an impurity and a certain minimum purity of the mother liquor. Due to this, the process combination was found to be somewhat less economic than a separation by SMB chromatography only.

The author published a shortcut-method for design and performance evaluation of the process combination [61]. The method requires only few information and experimental efforts. Its application to the separation of mandelic acid enantiomers revealed a significant potential in terms of productivity and investment costs. The according results will be included in Chapter 7.

Before investigating the integrated process as a whole, in the next chapter the theoretical fundamentals of the two involved unit operations, SMB chromatography and enantioselective crystallisation, will be summarised.

THEORETICAL FOUNDATIONS OF INDIVIDUAL UNIT OPERATIONS

When deliberating the question, whether the purposeful combination of two separation processes can improve overall process performance, a thorough understanding of the individual unit operations is indispensable. This is particularly true for the process combination to be investigated in this work. Experience teaches that one of the processes involved, SMB chromatography, is rather difficult to understand, to model, and to design. Although the other technique, enantioselective crystallisation, is much easier to understand, it is yet scarcely used in industrial practice and, therefore, also deserves special consideration.

This chapter compiles the fundamentals of both unit operations in the degree of detail that is required to follow the argumentations in later chapters.

2.1 Continuous Chromatography

2.1.1 Principle

An outstanding feature of chromatography is its ability to realise even extremely difficult separations, both on analytical as well as on preparative scale. Chromatographic processes exploit differences in the distribution equilibria of compounds between a stationary phase, the adsorbent, and a mobile phase, the eluent or solvent, respectively. The potential of chromatography arises from the possibility to design stationary phases that offer highly specific interactions, and to adjust the strength and ratio of these interactions by changing the properties of the mobile phase.

There are several types of chromatographic methods that differ with respect to the type of mobile and stationary phase used, and interactions exploited. Comprehensive reviews on the different methods in preparative chromatography are given, for example, in [62–66]. In this work, only adsorption chromatography using liquid mobile phases is considered, which is the most common technique in preparative chromatography. Below the fundamentals of liquid chromatography will be explained.

The adsorbent (usually small particles, sometimes also monoliths) is densely packed into columns. The eluent is transported through the void volumes of the column by application of a pressure gradient (*i.e.*, by pumping). The compounds dissolved in the eluent have different affinities towards the solid phase. Consequently, they distribute differently between the two phases. A strong adsorbing compound (*i.e.*, a substance with a high affinity towards the solid) migrates slower through the column than a less-adsorbing component. This difference in migration velocity represents the separation mechanism in chromatographic processes.

Single Column (Batch) Chromatography

In the simplest operation mode of chromatography, batch or elution chromatography, a limited amount of a mixture to be separated is injected into a continuous stream of mobile phase that enters a single column. Because of their different migration velocities, the components get separated on their way through the packing and – if the column has sufficient efficiency and length – can be collected consecutively at different characteristic times (*retention times*) at the column outlet.

The concentration-time profiles of the components leaving the column (*peaks*) exhibit more or less strong deformations in comparison to the profile of the injection (which typically corresponds approximately to a rectangular pulse). This band broadening is caused by dispersive effects (like axial dispersion or mass transfer resistances) and by the nonlinearity of the adsorption equilibrium.

Continuous Chromatography – The TMB Concept

In analogy to rectification processes, in chromatography a countercurrent between two phases (here: solid and liquid phase) allows for continuous separation. The True Moving Bed (TMB) process is the straightforward realisation of this concept. As shown in Fig. 2.1, in a single column the two phases are transported in opposite directions. The in- and outlet ports divide the unit into four different zones. A continuous feed stream that contains the components to be separated (1, 2) is introduced between zones *II* and *III*, respectively. Provided that a proper relative velocity of the two phases is adjusted, the less adsorbing component 1 preferably travels in the direction of the liquid phase and can be collected at the raffinate port, while the stronger adsorbing component 2 is transported by the solid phase downwards. The recycled liquid that enters in zone *I*, together with the pure eluent (desorbent) introduced at this position, make up a relatively high flow rate in this zone. Due to this, component 2 is desorbed from the solids' surface and is withdrawn at the extract port. After a certain time of operation, the process reaches a steady state (*i.e.*, stationary concentration waves establish within the unit).

The individual zones fulfil different tasks. The separation is performed in zones *II* and *III*, while zones *I* and *IV* are responsible for regeneration of the liquid and solid phases. In a process designed for complete separation of the two solutes, the detailed tasks of the zones are:

- Zone *I*: regeneration of the solid phase. The flows of liquid and solid are adjusted such, that all remaining traces of the two components are desorbed.

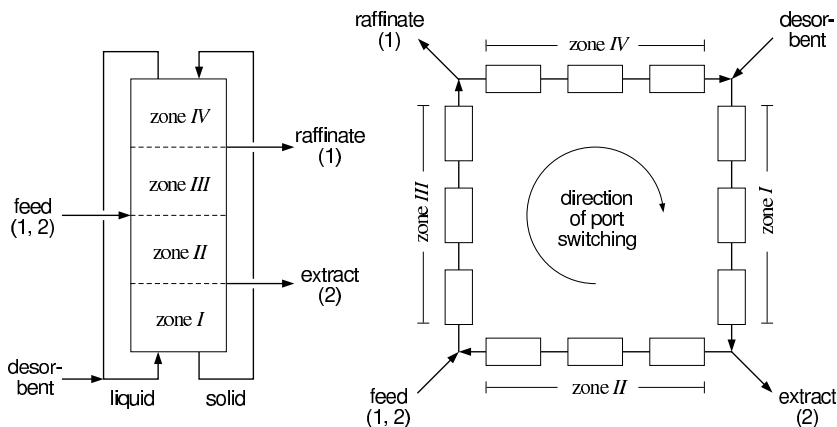


Figure 2.1. Continuous chromatographic separation of a binary mixture of components 1 and 2. Schemes of True Moving Bed concept (left) and Simulated Moving Bed process (right).

- Zone II: separation of the less adsorbing solute 1 from the stronger adsorbing 2. The concentration wave of 2 should stand here.
- Zone III: separation of the stronger adsorbing solute 2 from the less adsorbing 1. The concentration wave of 1 should stand here.
- Zone IV: regeneration of the liquid phase. The flows are adjusted such, that both solutes are adsorbed while the (non-adsorbing) eluent migrates further.

Practical implementations of the TMB concept suffer from significant problems related to the transport of the solid phase (*e.g.*, back-mixing and abrasion of particles) [65, 67]. Nonetheless, the realisation of continuous countercurrent adsorption processes remains appealing; for example, FRANZEN *et al.* recently reported investigations of a stage-wise countercurrent liquid-solid fluidised bed [68].

Usually, the TMB process serves as a tool for conceivability and modelling of countercurrent chromatographic separations. Models for TMB processes have comparatively low computational requirements (see section 2.1.5), which simplifies the development of new process concepts and control strategies for continuous chromatography. The application of equilibrium theory to the TMB concept also simplifies the design of SMB processes (see Chapter 4).

Continuous Chromatography – The SMB Process

The Simulated Moving Bed (SMB) concept was introduced in 1961 [67] and represents the feasible realisation of the TMB concept. SMB processes originally were used for large-scale processing of components with more or less linear adsorption isotherms, for example for separations of

o-xylene / p-xylene and sugars like fructose, glucose, and sucrose. Since then, several technological advances facilitated the use of SMB in more difficult processes that involve nonlinear equilibria. This was promoted by an improved process understanding through mathematical modelling (see 2.1.4), by the development of highly efficient, stable and selective stationary phases, and by the development of design procedures (see 2.1.7). Today the SMB technology is increasingly applied in productions of fine chemicals, pharmaceuticals (*e.g.*, enantiomers), and biotechnological compounds (*e.g.*, proteins and monoclonal antibodies). More examples of preparative applications are reviewed, for example, in [50, 65, 66, 69, 70]. In many of them the SMB process was shown to outperform conventional batch chromatography. In particular, the pronounced concentration profiles within the unit and the recycling of solvent usually lead to higher adsorbent usage and lower solvent consumption [71].

Figure 2.1 (right) contains a schematic illustration of an SMB unit. In this process, the problems of solid handling, that are inherent to the TMB concept, are circumvented by packing the solid phase into several single columns and arranging them in a closed series connection. In this way the continuous bed of the TMB process is discretised into single sections. Ports located between the individual columns allow for the connection of inlet and outlet streams that divide the unit into different zones. The four zones fulfil the same tasks as in a TMB process. The countercurrent between the solid and liquid phases is achieved by periodically switching all ports by one position in the direction of the liquid phase flow. This corresponds to moving each column by one position backwards, *viz.* in opposite direction to the liquid flow. The time period between two of these events is called switching time. This cyclic repositioning of the solid phase is referred to as “simulating” the counter current movement, hence the name Simulated Moving Bed.

In contrast to the TMB process explained above, the SMB process does not reach a steady state. Rather than this, after a certain start-up period, a periodically repetitive state establishes which is usually referred to as periodic or cyclic steady state. Characteristic for this state are the periodic changes of the product concentrations at the two outlets. The more columns an SMB equipped with, the shorter the switching periods and the closer its behaviour approaches that of a TMB unit.

The hybrid nature of the SMB process constitutes a fundamental difference in comparison to the TMB concept. However, the time axis in such dynamic regenerative processes represents an additional degree of freedom [44], which is utilised in new operating concepts. Current research projects focus on the improvement of process performance by a superposition of additional periodic boundary conditions. Successful examples are periodic modulations of feed concentration (*ModiCon*) [72, 73], zone length (*VariCol*) [74, 75], and flow rates (*PowerFeed*) [76–80]. Another important research field is the development of SMB reactors (see, for example, [48, 66]).

2.1.2 Adsorption Equilibria

Chromatographic processes rely on differences between the distribution equilibria of the compounds to be separated. Moreover, the equilibrium has a dominant impact on the shape of the

concentration fronts migrating inside a column and, thus, significantly influences process performance. Therefore, the quantification of the adsorption equilibria is an essential prerequisite for the design of any preparative chromatographic process [81, 82].

In general, the adsorption equilibrium of a component i depends on the concentrations of all species contained in a mixture. It is described by a functional relation of the form

$$q_i = q_i(c_1, \dots, c_N, T) \quad (i = 1, \dots, N) \quad (2.1)$$

where c is the concentration in the liquid phase and q the concentration on the surface of the solid (*i.e.*, the loading). N is the total number of components. Since this relation usually is determined for a constant temperature, T , it is referred to as adsorption isotherm.

For very low concentrations it can be assumed that there is an excess of adsorption sites on the solid's surface and that there is no competition for these sites between the molecules of the individual compounds. This ideal equilibrium is described by a linear isotherm:

$$q_i = H_i c_i, \quad (i = 1, \dots, N) \quad (2.2)$$

In analogy to gas absorption, the coefficient H_i is often called HENRY's constant. Note that in the case of linear isotherms, the equilibria of the individual components are independent from each other. The separation capability of a system can be quantified by defining a separation factor, $\alpha \geq 1$, according to

$$\alpha = \frac{H_2}{H_1} \quad (2.3)$$

There are only few preparative processes where the adsorption isotherms are basically linear (*e.g.*, adsorption of sugars and proteins on ion-exchange resins). In preparative applications, concentrations are usually very high in order to maximise throughput and productivity. Often competition of the components for adsorption sites and saturation of these sites occurs, which leads to nonlinear adsorption behaviour. The most common nonlinear adsorption isotherm model is the LANGMUIR isotherm

$$q_i = q_{s,i} \frac{b_i c_i}{1 + \sum_{j=1}^N b_j c_j}, \quad (i = 1, \dots, N) \quad (2.4)$$

In Eq. (2.4) the saturation capacity, $q_{s,i}$, is a measure for how many molecules of a compound can be adsorbed until all adsorption sites are occupied. The energetical parameter b_i describes the binding strength. For very low concentrations, Eq. (2.4) reduces to the linear isotherm (Eq. 2.2). The separation factor, α , is then given by

$$\alpha = \frac{q_{s,2} b_2}{q_{s,1} b_1} = \frac{H_2}{H_1} \quad (2.5)$$

The LANGMUIR model assumes a mono-layer occupation of energetically equivalent adsorption sites and that there are no interactions between adsorbed molecules. Note, that identical values for

the saturation capacities are required for thermodynamic consistency [83]. However, for modelling purposes often individual values for $q_{s,i}$ are used.

If a solid phase offers more than one type of adsorption site, the LANGMUIR approach above can be extended. The following isotherm contains two energetic sites of the above type (denoted by I and II , respectively).

$$q_i = q_{s,i}^I \frac{b_i^I c_i}{1 + \sum_{j=1}^N b_j^I c_j} + q_{s,i}^{II} \frac{b_i^{II} c_i}{1 + \sum_{j=1}^N b_j^{II} c_j}, \quad (i = 1, \dots, N) \quad (2.6)$$

This so-called bi-LANGMUIR isotherm offers good modelling results for different systems [63] and is often appropriate to describe the adsorption of enantiomers on chiral stationary phases (CSPs) [84]. In this work, only adsorption isotherms of the linear, the LANGMUIR, and the bi-LANGMUIR types are used. However, there are numerous other isotherm models (*e.g.*, the IAS and RAS models; the FREUNDLICH, REDLICH-KWONG, HILL, BRUNAUER-EMMETT-TELLER isotherm models). Reviews on this topic can be found in [63, 81, 85–90].

Generally, parameters of adsorption isotherms are not predictable and must be determined experimentally. Different methods are available to perform such measurements. These can be classified into static methods, where a certain amount of stationary phase is equilibrated with different amounts and compositions of adsorbate, and dynamic methods, which are applied directly to packed columns. More details can be found in the sources cited above.

2.1.3 Fundamental Relations

Before introducing mathematical models that allow for a quantitative description of chromatographic processes, some fundamental relations will be introduced. The explanations refer to batch chromatographic processes, but they are also useful for the understanding of continuous chromatography.

Obviously, the migration velocity of a component must depend on the relative amounts of liquid and stationary phases inside a chromatographic column. These are described by the total porosity, ϵ , which is the ratio between the liquid hold-up of a column, V_l , and its total volume, V_c :

$$\epsilon = \frac{V_l}{V_c} \quad (2.7)$$

A further differentiation is possible between external porosity (related to the interstitial volume between particles) and intra-particle porosity (liquid inside the pores of the particles). However, in this work it will be assumed that no concentration gradients exist between interstitial and intra-particle liquids, thus Eq. (2.7) is sufficient to describe the phase proportions. Alternatively, the phase ratio, F , can be used. It is defined as the ratio of the volumes of solid and liquid:

$$F = \frac{1 - \epsilon}{\epsilon} \quad (2.8)$$

The interstitial velocity (*i.e.*, the velocity at which a non-adsorbing component travels through a column), u , is given by

$$u = \frac{Q}{\epsilon A_c} \quad (2.9)$$

Here, Q is the volumetric flow rate applied by the pump and A_c is the column cross-sectional area. For the retention time of non-adsorbing species (“dead time”), t_0 , holds

$$t_0 = \frac{\epsilon A_c L_c}{Q} = \frac{L_c}{u} \quad (2.10)$$

where L_c denotes the column length.

The migration behaviour of adsorbing species is influenced by the adsorption isotherms (see above). From mass balance considerations the following relation can be established for the retention time, t_R , of solutes with linear adsorption isotherms

$$t_R = t_0(1 + FH) \quad (2.11)$$

where H is again the HENRY coefficient, see Eq. (2.2). The retention time is a fundamental characteristic of a chromatographic process.

For nonlinear adsorption, the migration velocity depends on the curvature of the isotherm. A mass balance for a single component in a differential volume reads [89]:

$$\frac{\partial c}{\partial t} = D_{ax} \frac{\partial^2 c}{\partial z^2} - F \frac{\partial q}{\partial t} - u \frac{\partial c}{\partial z} \quad (2.12)$$

Here, D_{ax} is the axial dispersion coefficient. Neglecting all dispersive effects, the balance equation can be simplified to

$$\frac{\partial c}{\partial t} + \frac{u}{1 + F \frac{dq}{dc}} \frac{\partial c}{\partial z} = 0 \quad (2.13)$$

From this wave equation it follows for the migration velocity, u_c , of the concentration level of a solute

$$u_c(c) = \frac{u}{1 + F \frac{dq}{dc} \Big|_c} \quad (2.14)$$

Correspondingly, the retention time related to this concentration level is

$$t_R(c) = t_0 \left(1 + F \frac{dq}{dc} \Big|_c \right) \quad (2.15)$$

This is a fundamental and helpful equation, for example for the determination of isotherm parameters (if the assumptions of local equilibrium and negligible dispersion are valid). The total derivative in this equation must be evaluated from the adsorption isotherm (see section 2.1.2). It can be seen that for a linear isotherm, Eq. (2.15) reduces to Eq. (2.11).

Besides the influence of thermodynamic equilibrium on migration speed, for a quantitative description also dispersive effects, like mass transfer resistances and axial diffusion, have to be taken into account. A convenient measure for quantification is the number of theoretical plates of a column, NTP , which can be evaluated from a chromatographic peak by [63]

$$NTP = \frac{\mu^2}{\sigma^2} \quad (2.16)$$

In this equation, μ is the first absolute moment (*i.e.*, the retention time), and the variance σ^2 is the second central moment of the peak. For linear adsorption the peaks correspond to GAUSSian distributions. The value for NTP can then be estimated from the correlation

$$NTP = 5.54 \left(\frac{t_R}{w_{1/2}} \right)^2 \quad (2.17)$$

where $w_{1/2}$ the width of the peak at half of its height.

Generally, NTP is a function of the linear flow rate, u . This dependence is often described using the well known VAN DEEMTER equation [91]

$$HETP(u) = A + \frac{B}{u} + Cu \quad (2.18)$$

where $HETP = L/NTP$ is the height-equivalent of a theoretical plate. A , B , and C are constants that describe different physical contributions to peak-broadening. A is a measure for the different paths molecules can use in the porous packing material, B is related to molecular diffusion, and C depends on mass transfer kinetics.

2.1.4 Modelling of Batch Chromatography

A mathematical model of a chromatographic process should consider all significant transport phenomena occurring in the chromatographic column. Depending on process conditions and the nature of the involved solutes, one or more of the following effects will dominate process performance:

- adsorption equilibrium,
- axial dispersion (usually considered as an effect combining axial diffusion, eddy diffusion, and tortuosity/restriction of channels between particles [65]),
- mass transfer resistances in and around particles that determine the rate at which equilibrium is established,
- diffusion inside the pores of the particles,
- diffusion of solutes on the particle's surface.

The list above is not complete. For example, a model for gas chromatography often requires the use of an energy balance and the consideration of density effects due to adsorption.

Mathematical models of chromatographic processes usually consist of the equations for mass conservation and transport for the individual components, which leads to a system of partial differential equations. Different models are in use, depending on modelling purpose and dominating physical effects of the actual system. Comprehensive reviews on this topic were given, for example, by GUIOCHON *et al.* [63, 65] and SEIDEL-MORGENSTERN [89].

Equilibrium Dispersive Model

A model which attempts to take into account all non-ideal effects mentioned above (a "general rate model") is computationally very expensive and, thus, inappropriate for systematic parameter studies and optimisations. Therefore, in this work mostly the simpler equilibrium dispersive model will be used. This is a reduced kinetic model (*i.e.*, kinetic and diffusive effects are combined into a single parameter). The following main assumptions apply: *i*) adsorption equilibrium is always established at any position in the column, *ii*) all dispersive effects in axial direction can be aggregated into a single parameter, *iii*) there are no radial concentration gradients, and *iv*) isothermal operation.

The mass balance equations for the equilibrium-dispersive model are

$$\frac{\partial c_i}{\partial t} = D_{a,i} \frac{\partial^2 c_i}{\partial z^2} - F \frac{\partial q_i(c_1, \dots, N)}{\partial t} - u \frac{\partial c_i}{\partial z}, \quad (i = 1, \dots, N) \quad (2.19)$$

where z is the space coordinate and $D_{a,i}$ is the apparent axial dispersion coefficient. If the values for $D_{a,i}$ are rather small, they can be evaluated from the following correlation [63]:

$$D_{a,i} = \frac{u}{2} \frac{L_c}{NTP}, \quad (i = 1, \dots, N) \quad (2.20)$$

To solve Eqs. (2.19), initial and boundary conditions have to be specified. The initial conditions are

$$c_i(t = 0, z) = c_{i,0}(z) \quad (2.21)$$

For an initially unloaded column holds $c_{i,0}(z) = 0$. Typical boundary conditions are:¹

$$u c_{i,in} = u c_i(t, z = 0) - D_{a,i} \left. \frac{\partial c_i}{\partial z} \right|_{z=0} \quad \text{for} \quad 0 < t \leq t_{inj}, \quad (2.22a)$$

$$0 = u c_i(t, z = 0) - D_{a,i} \left. \frac{\partial c_i}{\partial z} \right|_{z=0} \quad \text{for} \quad t > t_{inj} \quad (2.22b)$$

$$0 = \left. \frac{\partial c_i}{\partial z} \right|_{z=L_c} \quad (2.22c)$$

¹ Different formulations of boundary conditions can be used in chromatographic models. Above the "closed-closed" or DANCKWERTS conditions are given for a finite column. For discussions on this see [63, 89, 92].

The above model equations were solved numerically using the approach developed by GODUNOV [93] and ROUCHON [94]. In this method, the dispersion term in Eqs. (2.19) is neglected and the resulting equilibrium model is used. The numerical dispersion is purposefully exploited to "match" the physical dispersion. Since this is computationally very efficient, the method is well-suited for extensive parameter studies [89]. Details about the algorithm can be found in [63, 89, 94, 95]. A short overview is given in Appendix A.

It should be noted, that the ROUCHON algorithm prevents the use of above boundary conditions. However, the effects of this simplification are negligible for batch chromatography using highly efficient columns.

2.1.5 Modelling of TMB Chromatography

Equilibrium Dispersive Model

In order to derive a model for the TMB process in Fig. 2.1, the equilibrium dispersive model given by Eqs. (2.19) can be extended by a convective term for the solid phase:

$$\frac{\partial c_i}{\partial t} + F \frac{\partial q_i}{\partial t} = D_{a,i} \frac{\partial^2 c_i}{\partial z^2} - u \frac{\partial c_i}{\partial z} + u_s F \frac{\partial q_i}{\partial z} \quad (i = 1, \dots, N) \quad (2.23)$$

where u_s denotes the solid phase velocity. DANCKWERTS boundary conditions were used for each zone of the TMB. At the liquid inlet (solid outlet, $z = 0$):

$$u c_{i,in} = u c_i(z = 0) - D_{a,i} \left. \frac{\partial c_i}{\partial z} \right|_{z=0} \quad (2.24)$$

and at the liquid outlet (solid inlet, $z = L$):

$$u_s F q_{i,in} = u_s F q_i(z = L) - D_{a,i} \left. \frac{\partial c_i}{\partial z} \right|_{z=L} \quad (2.25)$$

The partial differential equations were discretised by a method of lines approach to yield ordinary differential equation. The complete model consists of these ODEs, expressions for the adsorption isotherms, and the transition conditions for the flows between the individual zones. The model was implemented in the simulation environment DIVA [96]. An comprehensive explanation of the model and its numerical solution can be found in [97].

Equilibrium Stage Model

An alternative to the equilibrium dispersive model is to conceive the TMB unit as a series connection of well mixed cells (stages) which are passed through by countercurrent streams of solid and liquid phase, respectively. Figure 2.2 contains a representation of such an equilibrium cell.

Assuming equilibrium, the mass balances for a component i in a single stage k of zone j of the TMB are

$$\epsilon V \frac{\partial c_i}{\partial t} = Q_S [q_{i,k+1}(\bar{c}_{k+1}) - q_{i,k}(\bar{c}_k)] + Q_{k-1}^{(j)} c_{i,k-1} - Q_k^{(j)} c_{i,k} \pm Q_e c_{i,e} \quad (2.26)$$

$(i = 1, \dots, N; j = I, \dots, IV; k = 1, \dots, N_s)$

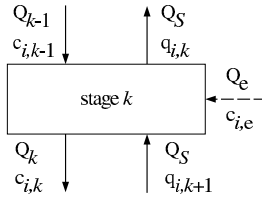


Figure 2.2. Equilibrium stage of a TMB process. The stage is passed by countercurrent streams of solid and liquid. External streams (denoted by Q_e) apply only to the four ports feed, raffinate, extract, and desorbent.

In this equation, V is the volume of a stage. $Q_{k-1}^{(j)}$ and $Q_k^{(j)}$ are the volumetric liquid flow rates that enter and leave the stage, respectively, while Q_S denotes the solid flow rate (which is identical in all four zones).

The model was implemented in the simulation environment PROMOT/DIVA [96, 98].

For highly efficient columns, the stage model is almost equivalent to the equilibrium dispersive model. The main difference is that boundary conditions cannot be included. However, comparison of selected simulation results proved an excellent agreement between the two approaches.

2.1.6 Modelling of SMB Chromatography

In order to model the SMB process, the lumped equilibrium dispersive model (section 2.1.4) is used to calculate the internal concentration profiles in the individual columns. Besides this, the switching of the columns has to be considered by periodically changing the boundary conditions. Thus, a hybrid model results which is explained in detail elsewhere [95]. At this point only the fundamental concept will be reviewed.

The model equations are solved on a constant time grid specified using the procedure described in Appendix A. In order to provide for a numerically efficient solution, in each zone of the unit different space increments are adjusted as a function of the zone flow rate [95]. This raises some limitations concerning applicable initial and boundary conditions. After each switching of the columns, the initial concentrations are calculated by a linearisation of the previous concentration profile of this column. Boundary conditions like Eq. (2.22) cannot be used; instead the first volume elements of each column are considered as CSTRs which perform a mixing of the previous concentration and the incoming stream.

After specification of the initial and boundary conditions, the concentration profiles are calculated along the columns (starting from the first element of each column) from the explicit equation A.2. The solid phase loadings, q_i , follow from the adsorption isotherms. If the determination of the profiles is complete, the next time increment is increased. If the end of the switching interval is reached, the initial conditions are updated (see above). The simulation is stopped if the state at the

end of an switching interval corresponds to the periodic state at the end of the previous switching interval. This is determined from the criterion suggested by Kniep [95].

2.1.7 Design Aspects

The optimal design of continuous chromatographic separations is a rather complex task, since numerous parameters influence the performance of the process, for example:

- adsorption isotherms (see section 2.1.2),
- column efficiency (affected by particle size, mass transfer kinetics, dispersion, etc.),
- number of columns and column arrangement within the plant (zone configuration),
- hydrodynamics and pump positioning (pressure drop and dead volumes).

For a complete design that takes into account all of the above, the optimisation of a mathematical model is indispensable. Examples of this approach can be found in the literature (*e.g.*, [82, 99, 100]). However, it should be recognised that this is still a tedious procedure which is most useful for the final design of a specific separation problem.

Other available design procedures neglect most of these parameters. Instead, they rely on the TMB concept and consider the (nonlinear) thermodynamic equilibrium as the most important factor for design. Examples are the MCCABE-THIELE analysis [88] and the “triangle theory” (see below). Alternatively, the “standing wave analysis” offers algebraic relations for the design of systems with significant mass transfer resistances [101, 102]. It should be mentioned that the latter two approaches apply for the design of separations with pure products only.

Design methods for pure products are not applicable to specify operating conditions for lowered SMB purity requirements, as it is the case in the process combination studied here. However, since they can serve as a valuable basis for comparison, in this work, the popular “triangle theory” [103] will be used frequently. The method is based on an equilibrium model of the TMB process and delivers explicit expressions for optimal flow rates (provided that the adsorption isotherms are known). Chapter 4 will explain details of the approach.

2.2 Enantioselective Crystallisation

2.2.1 Principle

Crystallisation from solution is the process of solidifying a species dissolved in a liquid solvent. Since the majority of chemicals is marketed as solids, it is a common process for final “product

polishing”. Also, it is widely used for purification purposes, since highly purified products can be obtained from relatively impure solutions [104].

The basis of crystallisation processes is that the solubility of a compound in a solvent is limited and usually decreases with decreasing temperature. Exceeding the solubility limit, the solution becomes supersaturated. This can be achieved, for example, by evaporating the solvent (evaporative crystallisation) or by cooling the solution (cooling crystallisation). In a supersaturated solution, the component forms solid crystals by nucleation or, alternatively, already existing crystals will grow. These processes stop if equilibrium is reached again. If several dissolved compounds have different solubilities, the least soluble component can be obtained in pure form by selective (fractional) crystallisation. This is the basis for enantioselective crystallisation.

The driving force for crystallisation of a compound i is quantified by the supersaturation, σ_i , which is a measure for the deviation from the solid-liquid equilibrium. Decisive factors like nucleation and crystal growth rate depend directly on the supersaturation. In this work, the following definition for σ_i will be applied

$$\sigma_i = \frac{c_i}{c_i^*(T, c_{1,\dots,N})} - 1 \quad i = (1, \dots, N) \quad (2.27)$$

where c_i and c_i^* denote the concentration of i in the mother liquor and at equilibrium, respectively, and N is the number of components. Note, that since in this work multi-component systems will be studied, c_i^* depends not only on temperature, but also on composition.

The knowledge of the ternary SLE (*i.e.*, the solubility of mixtures of two enantiomers in a solvent for different temperatures) is a mandatory pre-requisite for the quantitative examination of enantioselective crystallisation processes. The next section gives an introduction to this topic. The impact of ternary SLE on crystallisation performance will be discussed in more detail in Chapter 6.

2.2.2 Solid-Liquid Equilibria in Enantiomeric Systems

Binary Melting Equilibria

The type of racemate determines whether crystallisation of a pure enantiomer is possible from a given mixture (see section 1.1.1). It is useful to consider first the binary melting diagrams of enantiomeric systems, since they anticipate important properties of the corresponding ternary SLE. Figure 2.3 contains the binary SLE for the three main types of racemates (conglomerate, racemic compound, solid solution).

The first type of solid racemate, the conglomerate, is an equimolar mixture of pure crystalline enantiomers. If the two crystals are distinguishable, they might be separated mechanically (*e.g.*, by PASTEUR’s [32] manual picking of the different crystals). The binary melting diagram (Fig. 2.3, left) is symmetric (which is a general characteristic of enantiomeric systems). The lowest melting temperature is found at racemic composition ($x_r = 0.5$). For conglomerates, the racemic composition corresponds to a eutectic point (denoted by E), thus $x_e = x_r$. In the areas left and right of the

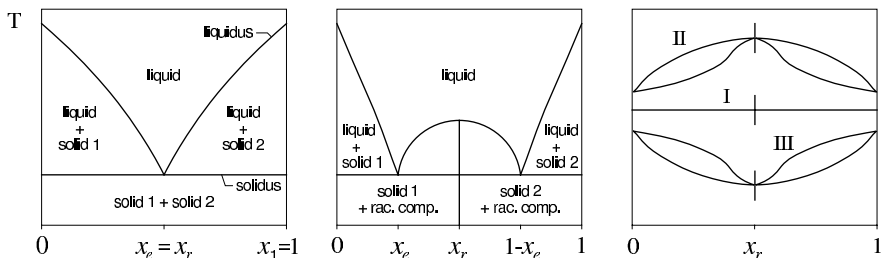


Figure 2.3. Schematic melting diagrams for systems with different types of solid racemates. Conglomerates (left) and racemic compounds (middle) allow for the crystallisation of pure enantiomers, in contrast to solid solutions (right) [7].

eutectic, between the liquidus and solidus lines, liquid melt is in equilibrium with pure crystalline enantiomers. Thus, in these regions, the separation of liquid and solid phase provides for a simple enantioseparation. It is estimated, that about 10% of all enantiomeric systems belong into the group of conglomerates [7].

The second type, also facilitating crystallisation of pure enantiomers, corresponds to the formation of a racemic compound (Fig. 2.3, middle). The racemic compound is a crystal structure that contains both enantiomers in its lattice. The system reveals two eutectic points at x_e and $(1 - x_e)$, respectively. Again, there are two regions above and below the eutectic compositions where pure enantiomers are in equilibrium with liquid melt. This type of behaviour accounts for the majority of systems. The eutectic composition in a compound forming systems is of significant importance for the application of the process studied in this work (see Chapters 6 and 7).

The last type of SLE, solid solutions (Fig. 2.3, right), will not be considered in this work since this type does not allow to obtain pure enantiomers by crystallisation. There are three different subtypes - the ideal solid solution (type *I*), systems where the racemate has the highest melting temperature (type *II*), and systems with a minimum melting temperature (type *III*) [105, 106]. It was reported that solid solutions are rare [7]; however, recent studies indicate that they might occur more frequently than expected [107]. It should be noted, that solid solutions might be of future interest with respect to process combinations, since types *II* and *III* might allow to achieve a certain enantiomeric enrichment.

Ternary Solubility Equilibria

The ternary solubility equilibrium of an enantiomeric system reflects the properties of its binary melting diagram. This becomes perceptible when plotting mass or molar fractions of the equilibrium compositions in the ternary GIBBS diagram. Figure 2.4 contains isothermal cuts of the ternary SLE for a conglomerate and a compound-forming system, respectively. Since the boundaries of the triangles represent the binary equilibria, the eutectic points shown in Fig. 2.3 are located at the lower boundaries of the ternary diagrams in Fig. 2.4.

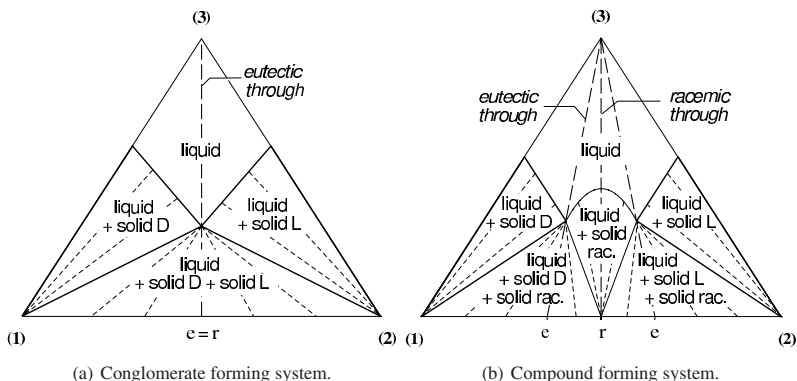


Figure 2.4. Ternary solubility diagrams of two enantiomers (1, 2) in a solvent (3) for constant temperature. Left – conglomerate system. Right – system forming a racemic compound.

The diagram of each system contains distinct regions where different numbers and types of solid phases are in equilibrium with the liquid solution. In the case of the conglomerate system there are four regions: the liquid phase (top), two two-phase regions where pure enantiomers crystals and the liquid coexist (left and right), and a three-phase region between the former two, where crystals of both enantiomers are in equilibrium with the solution (middle). Tie lines (dashed) connect equilibrium points of liquid solution and solid products. From these tie lines it can be seen that enantiopure crystals are obtained only when operating within the two two-phase regions (thick lines).

The ternary SLE of the compound forming system contains six regions: the liquid phase without crystals (top), two two-phase regions where pure enantiomers are in equilibrium with the liquid (left and right), one regions where the liquid is in equilibrium with the racemic compound (middle), and two three-phase regions with liquid, pure solid enantiomer, and solid racemic compound.

Further detailed information about SLE of enantiomeric systems can be found in the monograph by JACQUES *et al.* [7] or in [8, 107].

The lines connecting the solvent and the eutectics in the above diagrams are obviously of major importance with respect to process design. According to [108], in this work such line will be denoted as *eutectic through*. Analogously, the straight line from the solvent to the racemate will be called *racemic through* (which for conglomerate-forming systems corresponds to a eutectic through).

Remark on Analogies with Respect to Vapour-Liquid Equilibria

For readers experienced in distillation, the analogy of the above SLE to vapour-liquid equilibria (VLEs) will be striking. A classification in this sense possibly imparts engineering understanding of enantioselective crystallisation.

Obviously, the eutectic points in the SLE above correspond to azeotropes in VLEs. Applying the corresponding terminology (see, *e.g.*, [109, 110]) to enantiomeric systems, the binary equilibria in the diagrams above form a number of stable and unstable nodes, which result in several manifolds that in turn divide the triangle into the different regions explained above. When considering the residue curves of the mother liquor with decreasing temperature (*i.e.*, during crystallisation), the pure enantiomer is an unstable node, since the residues (or crystallisation paths) will move away from it. In contrast, the pure solvent represents a stable node, since it attracts these residues. Finally, the eutectics correspond to saddle points, since in the binary SLE they attract such paths and in the ternary diagram they move away from them. The above-mentioned eutectic throughs are the stable manifolds of these saddle points and correspond to the so-called separatrixes in VLEs.

2.2.3 Enantioselective Cooling Crystallisation from Solution

An equilibrium-controlled crystallisation process that should deliver pure enantiomer crystals must start in one of the above-mentioned two-phase regions (see Fig. 2.4). If the educt has racemic composition, an initial enrichment process is necessary to reach such a region. In this work, chromatography will be considered for this task.

The upper boundaries of the regions (*i.e.*, the solubility lines) depend on the temperature of the system. Usually solubility decreases with decreasing temperature and the solubility lines move towards pure solvent if temperatures are lowered. Figure 2.5 illustrates this situation for cooling crystallisation processes for a conglomerate-forming and a compound-forming system, respectively.

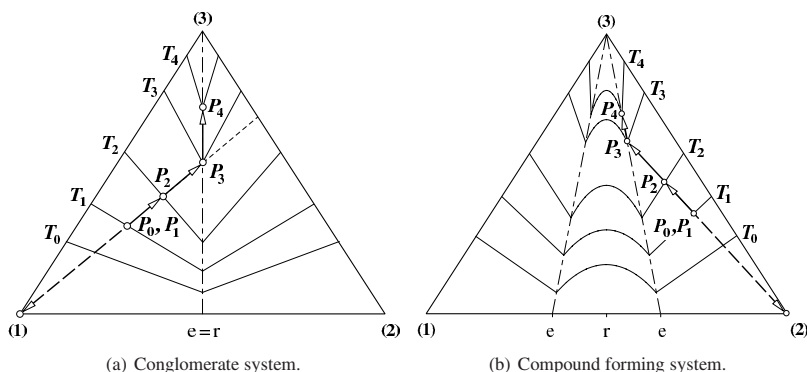


Figure 2.5. Enantioselective cooling crystallisation. (a) Crystallisation of enantiomer 1 for a conglomerate system, (b) crystallisation of enantiomer 2 for a system with racemic compound formation.

In the example of the conglomerate-system (Fig. 2.5 a) a process starts at temperature $T = T_0$ with a solution initially enriched in enantiomer 1 (point P_0). The solution is then cooled and reaches

the solubility limit at $T = T_1$ (i.e., the solution is saturated). Further cooling to $T = T_2$ leads to supersaturation, which causes nucleation and growth of crystals. These crystals contain only enantiomer 1. The remaining mother liquor changes its composition along a straight line away from this enantiomer. The solution reaches equilibrium at the solubility line that corresponds to T_2 (point P_2). Cooling can be continued until $T = T_3$, where the solution reaches the eutectic (racemic) through (point P_3). If the solution is further cooled down (from $T = T_3$ to $T = T_4$), equal amounts of the desired enantiomer 1 and the undesired enantiomer 2 will crystallise, while the composition of the mother liquor will change along the eutectic through.

As a second example, a similar process for a system with compound formation is shown in Fig. 2.5 b. Note, that here the enantiomer 2 is the target product. Crystallisation starts at $T = T_1$. The mother liquor reaches equilibrium at the eutectic through in point P_3 for the minimum temperature T_3 . Cooling below $T = T_3$ will lead to the additional formation crystals of the racemic compound (and, thus, to an impure solid product). The purity of the mother liquor will remain constant, since its composition will change only along the eutectic through.

In the two examples above, the temperature $T = T_3$ represents the minimum temperature tolerable to guarantee for enantiomerically pure crystals from a solution with initial composition P_0 . Knowledge of this temperature obviously is very important for process design. A method for its determination is introduced in Chapter 6. The amount of crystals formed in a crystallisation process depends on the operating conditions (temperature and purity of the feed). A detailed discussion of this aspect is also included in Chapter 6.

2.2.4 Modelling

Modelling approaches of different complexity are in use for crystallisation processes (as is the case in chromatography, see section 2.1.4). A complete model would have to consider numerous parameters; for example, the SLE, operating temperatures and cooling profiles, kinetics of growth and nucleation, stirring rate and hydrodynamics, and particle size distribution (PSD) [111].

In particular one should distinguish between models that treat the solid as a pseudo-homogeneous phase and models that include a description of the PSD. Detailed modelling of the dynamic development of a PSD is a complex task and leads to numerically challenging models. As a simplification, moment methods might be used to simplify the treatment of the PSD. An introduction is given in [112]. Further comprehensive treatments of modelling and design of crystallisation processes were given, for example, by MERSMANN [111] and RANDOLPH and LARSON [113].

For the conceptual design and an *a priori* evaluation of the process combination of chromatography and crystallisation the above-mentioned detailed modelling approaches are not required. Here, an equilibrium model for crystallisation will be used to study the impact of the SLE on process performance. The model is based on an appropriate description of the solid-liquid equilibrium and treats the crystals as a pseudo-homogeneous phase. It is presented in detail in Chapter 6.

2.2.5 Design Aspects

There are different factors that influence performance and product quality in selective cooling crystallisation processes. The most important are

- the solid-liquid equilibrium (determines feasibility and yield in selective crystallisations),
- the operating temperature,
- the supersaturation,
- the metastable zone width (characterising the “readiness” of the system to form nuclei),
- kinetics of mass transfer (influences the necessary residence time in continuous crystallisers),
- the crystal structure or morphology (which is closely related to the SLE),
- particle phenomena like nucleation, growth, and breakage (these influence the PSD and, therefore, also subsequent process steps like filtering and washing),
- the mode of operation (continuous/discontinuous).

For the design of a specific separation by crystallisation, many of the above aspects have to be investigated experimentally. Numerous publications exist on parameter determination and design of crystallisation processes. Reviews on the topic can be found, for example in [111, 113].

In this work, special emphasis is put on the equilibrium design of crystallisation processes. Therefore, the first two points of the list above are of particular importance and will be treated in detail in Chapter 6.

MODEL SYSTEMS

Model-based studies of chemical processes require a reliable basis of experimental data. In this work, the process combination of continuous chromatography and enantioselective crystallisation will be investigated considering three different experimental systems: mandelic acid (system I), threonine (system II), and a substance denoted as PDE (system III). The most important parameters are related to the thermodynamic equilibria involved (*i.e.*, the adsorption isotherms and the ternary solid-liquid equilibria).

This chapter summarises the corresponding parameters that were either obtained experimentally or extracted from literature sources.

3.1 System I – Mandelic Acid

Mandelic acid is the most intensely studied compound in this work. It is a cyclic carboxylic acid with the sum formula $C_6H_5-CH(OH)-COOH$ (molar weight 152.15). Figure 3.1 shows the structures of the two enantiomers. The asymmetric centre (the α -carbon atom next to the carboxyl group) has attached to it a hydroxyl group and a single hydrogen atom. Mandelic acid is a strong acid with a pK_a -value of about 3.4. Its enantiomers have rather high specific optical rotatory powers of $[\alpha]_D^{20} \approx \pm 156^\circ$. [114]

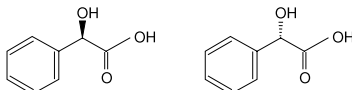


Figure 3.1. System I. *R*-(-)-mandelic acid (left) and *S*-(+)-mandelic acid (right).

Industrially, mandelic acid is produced by hydrolysis of mandelic acid nitrile (which in turn is obtained from the conversion of benzaldehyde and hydrogen cyanide) or, alternatively, by hydrolysis of α, α -dichloroacetophenone [115]. The compound is of some therapeutic importance because of its analgesic, spasmolytic, and anti-rheumatic effects. Furthermore, mandelic acid is frequently used in chiral syntheses, for example as a chiral building block or resolving agent [115]. Thus, as regards enantiomers, mandelic acid is a rather well-studied substance.

3.1.1 Chromatographic Separation

Chromatographic Systems

Six different chromatographic systems are considered for the separation of mandelic acid enantiomers. They are summarised in Tab. 3.1.

Table 3.1. Chromatographic systems for mandelic acid separation. The last column indicates the availability of ternary solubility data for the system (denoted by \circ ; see next section for corresponding SLE).

| No. | T [°C] | CSP | Mobile phase ¹ | Ref. | SLE |
|-----|--------|-----|--|-----------|---------|
| I.a | 40 | 1 | EtOH:H ₂ O (1:1 v/v), unbuffered | [57, 116] | – |
| I.b | 40 | 1 | MeOH:0.3M TEAAc (20:80 v/v), pH=4.02 | [57, 116] | \circ |
| I.c | 40 | 1 | EtOH:0.36M TEAAc (1:1 v/v), pH=6.56 | [57, 116] | \circ |
| I.d | 40 | 1 | MeOH:MeCN:TEAAc:HOAc (54.5:45:0.25:0.25 v/v) | [57, 116] | – |
| I.e | 20 | 2 | MeCN:HOAc:0.05M AAc (4.5:9.1:86.4 v/v), pH=3.0 | [57] | \circ |
| I.f | 23 | 3 | MeOH:0.3M TEAAc (20:80 v/v), pH=4.1 | [61] | \circ |

Three different CSPs were used. CSP1 is an analytical column Chirobiotic T column. “T” stands for the chiral selector Teicoplanin (an antibiotic) that is covalently bound to a silica support. The column’s dimensions are 150×4.6 mm, with a particle diameter of $d_p = 5\mu\text{m}$, and a porosity of $\epsilon = 0.683$. CSP2 is an analytical Nucleodex β -OH column (200×4 mm, $d_p = 5\mu\text{m}$, $\epsilon = 0.798$). The chiral selector here is β -cyclodextrine. CSP3 is a semi-preparative Chirobiotic T column. Thus, in comparison to the other CSPs it has larger dimensions and particle size (150×10 mm, $d_p = 16\mu\text{m}$, $\epsilon = 0.775$).

Adsorption Isotherms

Adsorption isotherms of mandelic acid enantiomers were measured for all chromatographic systems listed in Tab. 3.1. The first four systems (I.a through I.d) were examined by JANDERA and co-workers, who performed frontal analysis experiments [116]. Isotherms for systems I.e and I.f were determined by the author of this work. For system I.e also frontal analysis was used [57], while a perturbation method was applied to system I.f [61]. The retention times measured for this system are listed in Tab. B.7. For further details on experimental techniques and parameter estimation see the references given. More information on methods for adsorption isotherm determination can be found in the literature; see, for example, [63, 81, 117].

Table 3.2 contains the obtained multi-component adsorption isotherm parameters. For systems I.a through I.e isotherms were described by the LANGMUIR model, see Eq. (2.4). For system I.f a bi-LANGMUIR isotherm is given (Eq. (2.6)). The third column contains the upper concentration limit for each isotherm. Please note, that these are not related to the solubility, but to the experimental separability of the enantiomers (*i.e.*, at high concentrations the resolution of binary breakthrough

¹ Abbreviations: AAc – ammonium acetate, EtOH – ethanol, MeCN – acetonitrile, MeOH – methanol, HOAc – acetic acid, TEAAc – triethylammonium acetate.

curves and of perturbation responses vanishes). The last column lists the separation factors at infinite dilution according to Eq. (2.5).

Table 3.2. Adsorption isotherms of mandelic acid enantiomers for the systems listed in Tab. 3.1.

| System | Enantiomer | c_i^{\max} [g/l] | $q_{s,i}^I$ [g/l] | b_i^I [l/g] | $q_{s,i}^{II}$ [g/l] | b_i^{II} [l/g] | α [-] |
|--------|------------|-----------------------|----------------------|------------------|-------------------------|---------------------|-------------------|
| I.a | R(-) | 15.2 | 1.27 | 0.6336 | – | – | 4.33 |
| | S(+) | 15.2 | 3.28 | 0.0567 | – | – | |
| I.b | R(-) | 15.2 | 77.8 | 0.0207 | – | – | 1.40 |
| | S(+) | 15.2 | 261.2 | 0.0044 | – | – | |
| I.c | R(-) | 54.8 | 181.3 | 0.0064 | – | – | 1.14 |
| | S(+) | 54.8 | 168.9 | 0.0060 | – | – | |
| I.d | R(-) | 38.0 | 155.1 | 0.0086 | – | – | 1.24 |
| | S(+) | 38.0 | 276.4 | 0.0039 | – | – | |
| I.e | R(-) | 5.0 | 70.6 | 0.1222 | – | – | 1.07 |
| | S(+) | 5.0 | 72.5 | 0.1111 | – | – | |
| I.f | R(-) | 7.5 | 142.0 | 0.0073 | 3.19 | 0.7041 | 2.87 |
| | S(+) | 7.5 | 142.0 | 0.0073 | 3.19 | 0.0273 | |

Figure 3.2 contains the single-component isotherms corresponding to the parameters given in the table above. Significant differences exist between the individual systems concerning separation factor, linearity, and concentration range. While, for example, the isotherms of system I.e have a steep slope, but a low separation factor at very limited concentrations, system I.c reveals a higher separation factor even at comparatively high concentrations. For system I.a, even a selectivity reversal at $c_i \approx 9$ g/l is predicted.

It can be expected that the performance of a chromatographic separation process will be very different for each of these systems. This is studied in detail for SMB processes in Chapter 4 for systems I.a through I.e. Furthermore, in Chapter 7 system I.f together with systems II and III (see following sections) are used to investigate the performance of the process combination of chromatography and crystallisation. For this evaluation, relations for pressure drop and column efficiency are necessary, which are specified in the following.

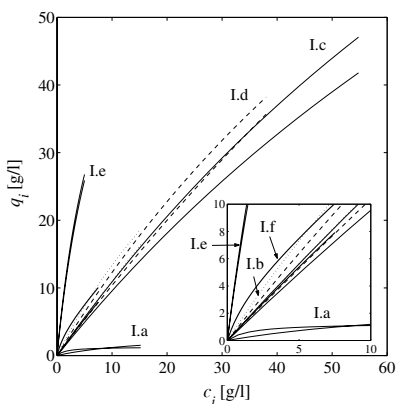


Figure 3.2. Single component adsorption isotherms for R(-)- and S(+)-mandelic acid corresponding to the parameters given in Tab. 3.1.

Inset: magnification for low concentrations.

Pressure drop and column efficiency

For system I.f the dependence of pressure drop and theoretical plate height on flow rate was determined experimentally in the range of 0.5...10.0 ml/min. From analytical pulse injections of the two enantiomers, a mean value of the plate heights was determined from Eq. (2.17). A linear dependency was found in this range. Thus, the VAN-DEEMTER equation (2.18) reduces to:

$$HETP = A + Cu \quad (3.1)$$

The following values were determined: $A = 0.0082$ cm and $C = 0.0023$ min.

For the semi-preparative Chirobiotic T column used, the pressure drop over column length depends linearly on the superficial velocity:

$$\frac{\Delta p}{L_c} = k_0 u_0 \quad (3.2)$$

This equation is similar to DARCY'S law (see, e.g., [63]); L_c denotes the column length and k_0 a proportionality parameter. For system I.f a value of $k_0 = 0.2232$ bar min/cm² was determined.

3.1.2 Ternary Solubility Equilibria

Solubility data for mixtures of mandelic acid enantiomers are available for three of the chromatographic systems in Tab. 3.1, namely for systems I.b, I.e, and I.f [118, 119]. (Note that the composition of system I.b basically corresponds to that of system I.f.) The corresponding ternary SLE are shown in Figs. 3.3 (I.b and I.f) and 3.4 (I.e).

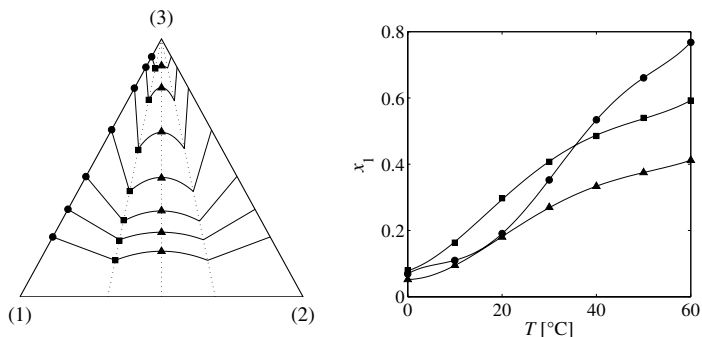


Figure 3.3. Left – Ternary SLE for mandelic acid enantiomers in methanol:water 20:80 (systems I.b and I.f) between 0 and 60 °C. 1, 2, and 3 denote (+)-enantiomer, (–)-enantiomer, and solvent, respectively. Right – corresponding solubility of the single enantiomer 1 at different purities. Symbols – experimental data from [119] (see Tab. B.1): ● – pure enantiomer, ■ – eutectic through, ▲ – racemic through. Solid lines – obtained from the SLE model derived in Chapter 6.

The left side of each diagram contains the ternary representation of the SLE. The right side shows the solubility of the single enantiomer 1, x_1 , at different enantiomeric purities (*i.e.*, x_1 for pure enantiomer, x_1 at racemic composition, and x_1 along the eutectic through). Symbols represent experimental data, while solid lines are calculated from an SLE model which is derived in section 6.1.2. For a fundamental explanation of SLE for enantiomeric systems see section 2.2.

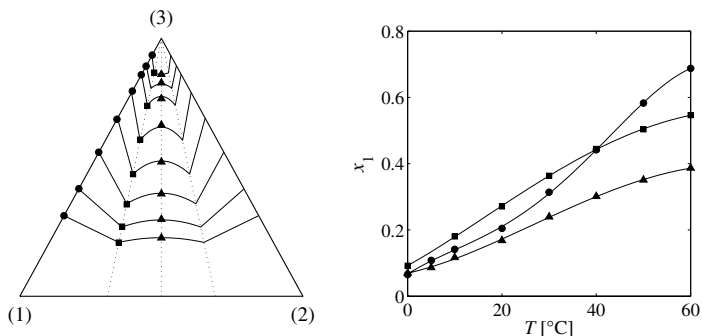


Figure 3.4. Solubility of mandelic acid enantiomers between 0 and 60 °C in acetonitrile/water 4.5/95 (system I.e in Tab. 3.1). Data points from [118]; see Tab. B.2. For notation see Fig. 3.3.

Figure 3.5 contains a third solubility equilibrium (mandelic acid in water) that was taken from [120]. This SLE will be applied as a surrogate for systems where the actual SLE is not available (*i.e.*, for systems I.c and I.d, respectively). This rather well-examined system is also used to derive the SLE model in section 6.1.2.

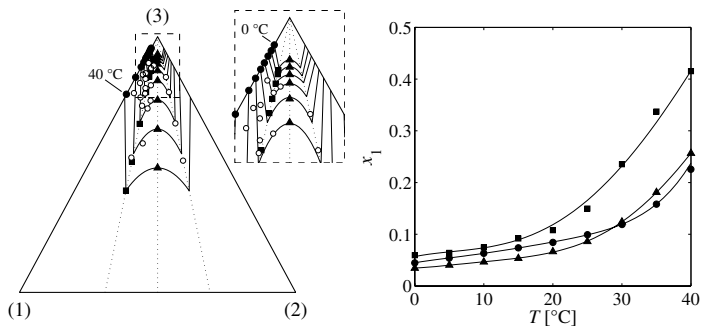


Figure 3.5. Solubility of mandelic acid enantiomers between 0 and 40 °C in water (surrogate system). Data points from [118]; see Tab. B.3. For notation see Fig. 3.3.

3.2 System II – Threonine

Threonine is a natural amino acid that contains two chiral centres. Therefore, four diastereomers of the compound are possible. Subject of this work are the two enantiomers *L*-threonine or (2*S*,3*R*)-2-amino-3-hydroxy butanoic acid and *D*-threonine or (2*R*,3*S*)-2-amino-3-hydroxy butanoic acid. Figure 3.6 shows the structure of the two enantiomers. The *L*-form corresponds to the (–)-enantiomer.

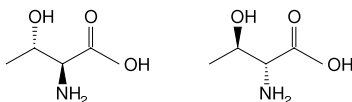


Figure 3.6. System II. *L*-threonine (left) and *D*-threonine (right).

Threonine is an amphoteric compound (*i.e.*, it has acidic and basic properties). The two pK -values are $pK_1 = 2.2$ (COOH) and $pK_2 = 9.1$ (NH_3^+). The sum formula of threonine is $\text{C}_4\text{H}_9\text{NO}_3$ (molar weight 119.1 g/mol). [114] Commercially interesting is mostly the essential amino acid *L*-threonine, which is produced by fermentation [121].

3.2.1 Chromatographic Separation

Adsorption isotherms for *D*- and *L*-threonine were determined for the semi-preparative Chirobiotic T column that was also used for mandelic acid (system I.f, CSP3, see p. 40). The results of this study were not previously published, therefore a brief overview will be given below.

A 60:40 (v/v) ethanol:water mixture was used as eluent. The porosity of the column was determined to $\epsilon = 0.753$ from injections of small amounts of methanol. Experiments were carried out at ambient temperature (23 °C) using the perturbation method. This technique is based on the application of a small disturbance (perturbation) to a column that is pre-equilibrated with a mixture of the compounds to be separated. A number of responses result equal to the number of adsorbed species (here: two). Perturbations were repeatedly applied at different levels of equilibration concentrations. Using Eq. (2.15) the retention times of the responses can be fitted to the local derivatives of the adsorption isotherms. For more details about the perturbation method see, for example, [117].

Perturbations were applied by injecting 20 μl of either pure eluent or mixtures of different enantiomeric purity at different flow rates (1, 2, and 2.5 ml/min). Measured retention times and corresponding conditions are listed in Tab. B.8. It is noteworthy, that injections of pure eluent did not allow to detect separated responses at concentration levels higher than $c_i = 2.5$ g/l. With increasing concentrations, the second response began to vanish and also tended to fall together with the first response. However, injections of asymmetrical mixtures of the enantiomers led to detectable responses up to $c_i = 5$ g/l. This approach was suggested by FORSSÉN *et al.*, who published

a very interesting paper on the problem of vanishing peaks in perturbation experiments for chiral systems [122]. Here, it was found convenient to use injection concentrations that were slightly lower than the equilibrium level for the less adsorbing enantiomer and slightly higher than this for the stronger adsorbing enantiomer, respectively. One positive and one negative response resulted that could be distinguished easily.

The bi-LANGMUIR equation, Eq. (2.6), was used to model the adsorption behaviour. The number of free parameters in this equation (initially: eight) was reduced using the following arguments. *i*) Thermodynamically consistent behaviour was assumed, therefore $q_{s,1}^I = q_{s,2}^I = q_s^I$ and $q_{s,1}^{II} = q_{s,2}^{II} = q_s^{II}$. *ii*) There is one non-selective adsorption site (I) and one enantioselective site (II), respectively. Thus, $b_1^I = b_2^I = b^I$. This behaviour is often found for enantiomeric systems [116]. *iii*) The initial slope of the isotherms is given by the HENRY coefficients, which were determined separately from analytical injections. This leads to $H_i = q_s^I b^I + q_s^{II} b_i^{II}$, $i = (1, 2)$. These five relations reduce the number of free parameters to three; namely q_s^I , q_s^{II} , and b^I . A least-squares method was used for fitting calculated and measured retention times.

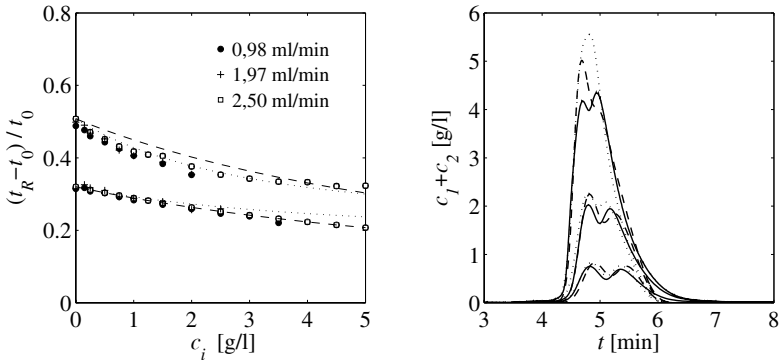


Figure 3.7. Determination of adsorption isotherms for system II. Left – dimensionless measured perturbations (symbols); t_0 calculated from Eq. (2.10). Fits from perturbation method (dotted lines) and peak-fitting procedure (dashed lines). Right – series of overloaded injections (thick lines; $V^{\text{inj}} = 1000\mu\text{l}$, $c_i^{\text{inj}} = 1, 2,$ and 5 g/l , respectively). Line styles correspond to left panel.

A satisfactory fit of the retention times resulted from the above procedure, which is shown as dotted lines in Fig. 3.7 (left). However, numerical simulations of a series of overloaded injections (using the equilibrium-dispersive model, section 2.1.4) lead to a rather unsatisfactory agreement (dotted lines in Fig. 3.7, right). In particular, there are deviations under strongly overloaded conditions. To improve the agreement, these adsorption isotherms were used as starting values in a peak-fitting procedure. A LEVENBERG-MARQUARDT procedure available in MATLAB (`fmincon`) was used to minimise the sum of squares of the differences between all three experimental and simulated chromatograms, respectively. The results are shown as dashed lines in Fig. 3.7. While the fit of the retention times somewhat worsened, the chromatograms are now described with reasonable

accuracy. The most noticeable deviation remaining is found at the dispersive front of the stronger adsorbing *D*-enantiomer. The retention times of this front apparently increase with increasing injection concentrations. However, this is in conflict with the decreasing retention times of the perturbations. Therefore, it is concluded that this behaviour is not caused by equilibrium but must be attributed to higher dispersion, which is typically found in chiral chromatography for stronger retained components.

The following adsorption isotherm parameters resulted (in brackets: initial values from perturbation method): $q_s^I = 1486 \text{ g/l}$ (3165), $q_s^{II} = 29.8 \text{ g/l}$ (7.82), $b^I = 3.16 \cdot 10^{-5} \text{ l/g}$ ($1.74 \cdot 10^{-4}$). Obviously, the peak fitting procedure predicted a lower capacity and almost linear behaviour for the non-selective site I, while for site II a higher capacity and a lower nonlinearity was obtained. The complete adsorption isotherms corresponding to these results read (units omitted; c_i, q_i in [g/l]):

$$q_i = 1486 \cdot \frac{3.16 \cdot 10^{-5} c_1}{1 + 7.32 \cdot 10^{-5} (c_1 + c_2)} + 29.8 \cdot \frac{0.0312c_1}{1 + 0.0312c_1 + 0.0504c_2} \quad (3.3a)$$

$$q_i = 1486 \cdot \frac{3.16 \cdot 10^{-5} c_2}{1 + 7.32 \cdot 10^{-5} (c_1 + c_2)} + 29.8 \cdot \frac{0.0504c_2}{1 + 0.0312c_1 + 0.0504c_2} \quad (3.3b)$$

In the above, indices 1 and 2 denote the less adsorbing *L*-enantiomer and the stronger adsorbing *D*-enantiomer, respectively. These adsorption isotherms result in a separation factor at infinite dilution of $\alpha = 1.59$. They are valid up to concentrations of $c_i = 5 \text{ g/l}$.

Pressure drop and column efficiency

The dependency of column efficiency and pressure drop for system II was determined using the same procedure as described for system I.f (see page 42). The resulting parameters for the *HETP*-correlation Eq. (3.1) are $A = 0.0011 \text{ cm}$ and $C = 0.0041 \text{ min}$, respectively. For the constant in the pressure-drop correlation Eq. (3.2), a value of $k_0 = 0.2804 \text{ bar min/cm}^2$ was determined.

3.2.2 Solubility Equilibrium

Solubility data for threonine enantiomers in the chromatographic solvent (60:40 ethanol:water) were taken from [118] and are shown in Fig. 3.8. Raw data are compiled in Tab. B.4. Obviously, the solubilities of the threonine enantiomers are very low in comparison to the mandelic acid SLE above.

From the figure it can be seen that there are only few SLE data points available. Thus the course of the solubility interpolations (Fig. 3.8, right) cannot be ensured. Predictions from the SLE model should therefore be handled with care. However, the model is expected to correctly predict the general trends.

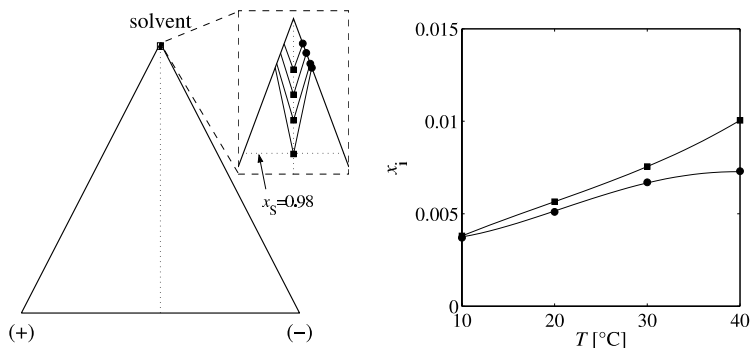


Figure 3.8. Ternary solubility equilibrium threonine enantiomers in ethanol:water 60:40 (v/v) between 10 and 40 °C. Data points from [118]; see Tab. B.4 . The inset shows the ternary solubility above a solvent content of 98%. For notation see Fig. 3.3.

3.3 System III – Pharmaceutical Intermediate PDE

The third system that is studied is an industrial pharmaceutical intermediate, which will be denoted as PDE. The *R*-form corresponds to the (–)-enantiomer. No further specific properties about this compound are available. However, some studies about the chromatographic separation and the solubility of the two enantiomers are available in the literature [118, 123]. The author previously published a study on the productivity of SMB processes for the separation of PDE enantiomers [58].

An interesting feature of this system is that both adsorption isotherms and solubility data were determined in the same pure solvent (acetonitrile). This is expected to simplify a transition between chromatography and crystallisation in the process combination.

3.3.1 Chromatographic Separation

KNIEP *et al.* [123] determined adsorption isotherms for PDE in pure acetonitrile at 20 °C. They used an analytical 250 × 4 mm Chiralpack AS CPS column (Daicel, Japan) with $d_p = 20\mu\text{m}$ and $\epsilon = 0.73$ (system "B" in [123]). The determined selectivity at infinite dilution of $\alpha = 2.18$ is relatively high for enantiomeric systems. The following LANGMUIR isotherms were reported (units omitted; c_i, q_i in [g/l]):

$$q_1 = \frac{1.31c_1}{1 + 0.04c_1 + 0.022c_2} \quad (3.4a)$$

$$q_2 = \frac{0.6c_2}{1 + 0.04c_1 + 0.022c_2} \quad (3.4b)$$

These isotherms are valid up to a maximum concentration of $c_i = 20$ g/l. The corresponding single component isotherms are plotted in Fig. 3.9.

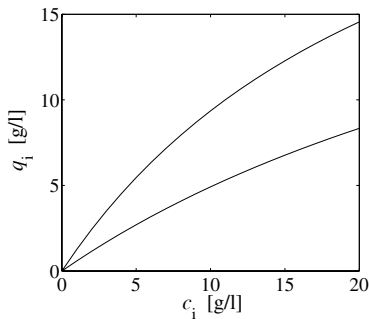


Figure 3.9. Single component adsorption isotherms for R- and S-PDE [123].

Pressure drop and column efficiency

The same approach was used as for systems I.f and II above. The resulting parameters for Eq. (3.1) are $A = 0.0161$ cm and $C = 0.0012$ min, respectively. For the pressure-drop correlation Eq. (3.2), a value of $k_0 = 0.0354$ bar min/cm² was found. The latter is significantly lower than for the other two systems. The reasons for this are the low viscosity of Acetonitrile and the somewhat larger particle size of this column ($d_p = 20$ μ m instead of 16 μ m for CSP3).

3.3.2 Solubility Equilibrium

Solubilities for PDE in pure acetonitrile were published in [118]. The ternary SLE is shown in Fig. 3.10. Raw data are compiled in Tab. B.5. The solubility of the enantiomers is very high. For example, at 40 °C the solubility of enantiomer 1 at racemic composition is $x_1 \approx 0.4$ (*i.e.*, the solubility of the racemate corresponds to almost 80%).

3.4 Chemicals and Equipment Used

S-(+)- and R-(-)-mandelic acid (both 99%+), D-threonine (98%+), and DL-threonine (98%+) were purchased from Sigma Aldrich (Steinheim, Germany), L-threonine (99%+) from Merck (Darmstadt, Germany). Both enantiomers and the racemate of PDE (system III) were provided by Schering (Berlin, Germany). All solvents (HPLC grade), and acetic acid (100% gradient grade)

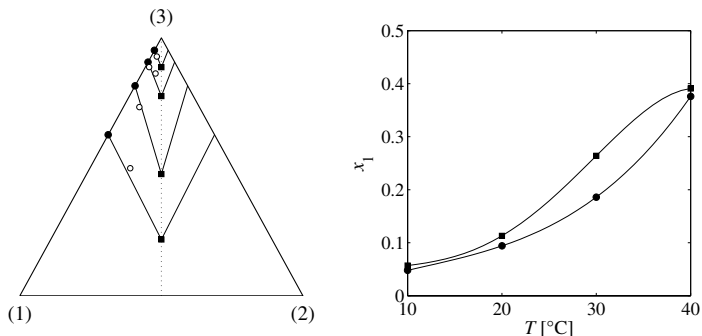


Figure 3.10. Solubility of PDE enantiomers between 10 and 40 °C in pure acetonitrile (system III). Data points from [118]; see Tab. B.5. For notation see Fig. 3.3.

were from Merck. Ammonium acetate (98%) was from Sigma-Aldrich. Triethyl ammonium acetate used was a 1% solution (Merck). Purified water was obtained from a Milli-Q gradient system (Millipore, Molsheim, France).

For isotherm measurements for system I.f (mandelic acid) the following HPLC setup was used: an HPLC pump (Model 2050; Kronlab Laborgeräte, Sinsheim, Germany), a manual injection valve, a dual-wavelength UV detector (K2600; Knauer GmbH, Berlin, Germany), and a liquid flowmeter (GJC Instruments, Merseyside, U.K.). An automated HPLC system (HP1000; Agilent Technologies, Waldbronn, Germany) was used for the perturbation measurements for system II (threonine). It consisted of a quaternary pump, a degasser, a thermostated column compartment, a diode array UV detector, and a workstation with software (Chemstations for LC 3D).

Density measurements of chromatographic solvents were performed at 25 °C using a pycnometer (Brand GmbH, Wertheim, Germany). For the results see Tab. B.9.

IMPACT OF ADSORPTION ISOTHERMS ON SMB PROCESSES

Motivation for the process combination suggested in Chapter 1 is the improvement of overall process performance. However, before investigating the integrated scheme as a whole, the behaviour of the individual unit operations should be examined under the specific requirements that result from coupling the two processes.

Of particular interest is here the impact of the involved thermodynamic equilibria on process performance. Since it is expected that the main benefit of the process combination results from the lowered purity requirements in the SMB separation, this chapter will address the impact of adsorption isotherms and lowered purity requirements on the productivity of SMB processes.¹

4.1 Background

Often there are several chromatographic systems (*i.e.*, combinations of mobile and stationary phase) available to perform a specific separation. Most probably, these systems will differ significantly with respect to their adsorption isotherm parameters, like separation factor, column efficiency, loading capacity, and isotherm nonlinearity. The impact of all these parameters on process performance appears to be well-understood for preparative batch chromatography. However, there is a lack in systematic studies of the impact of isotherm parameters on SMB performance; in particular, under reduced purity requirements.

In this study five different chromatographic systems capable of separating the enantiomers of mandelic acid (model systems I.a through I.e; see section 3.1) will be compared with respect to the achievable productivities using SMB chromatography. The analysis will be performed analytically based on an equilibrium model for the SMB process and, subsequently, numerically by using the equilibrium dispersive model (see section 2.1.4).

¹ A part of the results presented in this chapter were previously published by the author [57, 58].

4.2 Theoretical Fundamentals

4.2.1 Performance Parameters

The main parameters used in this section in order to characterise the performance of a continuous chromatographic separation are product purity and specific productivity. The purity at the ports for raffinate and extract, P^R and P^E , are defined with respect to their target components (see Fig. 2.1):

$$P^R = \frac{c_1^R}{c_1^R + c_2^R} \cdot 100\% \quad (4.1a)$$

$$P^E = \frac{c_2^E}{c_1^E + c_2^E} \cdot 100\% \quad (4.1b)$$

where c_1^R and c_2^E are the corresponding outlet concentrations. The specific productivity for component i , PR , will be defined as the ratio of feed flux and volume of stationary phase:

$$PR = \frac{Q^F c_i^F}{N_C (1 - \epsilon) V_c} \quad (4.2)$$

In Eq. (4.2), N_C , V_c , and ϵ are the number of columns in the SMB unit, their volume, and the porosity, respectively.

4.2.2 Isotherm Model

In this chapter the multi-component LANGMUIR adsorption isotherm defined in Eq. (2.4) will be considered. For the mentioned investigations based on an equilibrium model, thermodynamic consistency will be required (*i.e.*, $q_{s,i} = q_s$; see remarks on p. 25) [83]. In this case it follows from Eq. (2.5) for the equilibrium parameter $b_2 = \alpha b_1$. Further, it will be assumed that a racemic feed has to be separated, thus $c_1^F = c_2^F = c^F$. From this and from Eq. (2.4) one obtains the following two (thermodynamically consistent) adsorption isotherms:

$$q_1 = q_s \frac{b_1 c^F}{1 + (\alpha + 1) b_1 c^F} \quad (4.3a)$$

$$q_2 = q_s \frac{\alpha b_1 c^F}{1 + (\alpha + 1) b_1 c^F} \quad (4.3b)$$

Thus, in the equilibrium-based investigations of the SMB process only the isotherm parameters α , q_s , b_1 , and c^F have to be considered, which simplifies the analysis.

4.2.3 Equilibrium Design of SMB processes

A valuable tool in the design of continuous chromatography is the design procedure developed by STORTI, MAZZOTTI, MORBIDELLI, and co-workers (*e.g.*, [84, 103, 124, 125]), who derived solutions for the equilibrium model of a TMB process. Although their approach is valid only for the

case of complete separation (*i.e.*, pure extract and pure raffinate), it represents a helpful reference – even for SMB processes with reduced purity requirements. In the following, the optimum operational parameters derived in [103] for the linear and LANGMUIR isotherms will be summarised.

Dimensionless Flow Rates

The essential design parameters in continuous chromatography are the dimensionless flow rate ratios, γ^j , which are defined as

$$\gamma^j = \frac{Q_{\text{TMB}}^j}{Q_S}, \quad j = (I, II, III, IV) \quad (4.4)$$

where Q_{TMB}^j is the flow rate of the liquid in zone j of a TMB unit and Q_S the flow rate of the solid phase. To apply the γ^j to an SMB process, one has to consider that with each switching event the liquid inside the columns is moved together with the solid phase. Due to this, the actual flow rates in a TMB and an SMB are different for the same values for γ^j . The according definition of γ^j for an SMB process is

$$\gamma^j = \frac{Q_{\text{SMB}}^j t_S - V_c \epsilon}{V_c (1 - \epsilon)} \quad (4.5)$$

where t_S stands for the switching time.

Optimum Operating Points for Ideal Systems

As concerns the actual separation of the two components, it is most critical to properly adjust the operating conditions in the two separation zones *II* and *III* of an SMB unit (provided that regeneration is sufficient in the regeneration zones *I* and *IV*; see Fig. 2.1).

Based on the equilibrium model, a triangular region of complete separation in the two-dimensional parameter space $\gamma^{\text{II}}/\gamma^{\text{III}}$ was derived in [103]. Figure 4.1 shows this solution for a linear and a LANGMUIR isotherm, respectively. Any operating point inside the regions will result in pure raffinate and extract products. Operation outside the “triangle” will lead to impure raffinate, extract, or both. The optimal operating point in terms of throughput and desorbent consumption is represented by the vertices of the regions in Fig. 4.1, because the distance towards the 45°-line is directly proportional to the feed flow rate. See [103] for details on the construction of the separation regions.

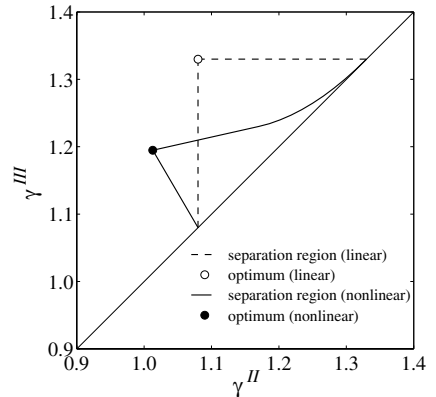


Figure 4.1. Regions of complete separation points for system I.d (see section 3.1.1).

In the case of linear adsorption isotherms, Eq. (2.2), the optimal operating point is given by the following values for the flow rate ratios γ^j :

$$\gamma_{\text{opt}}^I = \gamma_{\text{opt}}^{III} = H_2 \quad (4.6a)$$

$$\gamma_{\text{opt}}^{II} = \gamma_{\text{opt}}^{IV} = H_1 \quad (4.6b)$$

where H_1 and H_2 are the HENRY coefficients of the less and stronger adsorbing components 1 and 2, respectively.

Using the thermodynamically consistent LANGMUIR isotherm, Eq. (4.3), the following optimal γ^j for complete separation can be derived from the expressions given in [103]:

$$\gamma_{\text{opt}}^I = \alpha q_s b_1 \quad (4.7a)$$

$$\gamma_{\text{opt}}^{II} = \frac{\omega_G}{\alpha} \quad (4.7b)$$

$$\gamma_{\text{opt}}^{III} = \omega_G \frac{\omega_F(\alpha - 2) + q_s b_1}{\alpha q_s b_1 - \omega_F} \quad (4.7c)$$

$$\gamma_{\text{opt}}^{IV} = \frac{1}{2} \left(K - \sqrt{K^2 - 4q_s b_1 \gamma_{\text{opt}}^{III}} \right) \quad \text{whith } K = q_s b_1 + \gamma_{\text{opt}}^{III} + b_1 c^F (\gamma_{\text{opt}}^{III} - \gamma_{\text{opt}}^{II}) \quad (4.7d)$$

In the above, $\omega_G > \omega_F > 0$ are the solutions of the quadratic equation

$$(1 + b_1 c^F + \alpha b_1 c^F) \omega^2 - (1 + \alpha + 2\alpha b_1 c^F) q_s b_1 \omega + \alpha q_s^2 b_1^2 = 0 \quad (4.8)$$

From Eqs. (4.7) and (4.8) it can be seen that the optimal operating point for nonlinear isotherms depends on the feed concentration c^F .

Operating Points for Real Systems

The relations above were derived from an equilibrium model (*i.e.*, for infinite column efficiency). The reader will find it plausible that these values do not apply to real systems with finite efficiency. A simple way, which is often used in practise, to consider the deviation from ideal behaviour is to introduce safety factors, β^j , in order to correct the flow rate ratios, γ^j , in the direction required:

$$\gamma^j = \beta^j \gamma_{\text{opt}}^j, \quad j = (I, III) \quad (4.9a)$$

$$\gamma^j = \frac{1}{\beta^j} \gamma_{\text{opt}}^j, \quad j = (II, IV) \quad (4.9b)$$

For complete separation, $\beta^j \geq 1$. In general, the stronger the dispersive effects, the higher the safety factors that have to be chosen.

Switching Time and Flow Rates from Pressure Drop Correlation

The productivity optimum of preparative chromatographic separations is often achieved at the highest flow rate possible [63]. Thus, usually constraints related to pressure drop and limits of the

pumps are essential.² The pressure drop, Δp , can roughly be estimated as a function of flow rate according to [63]:

$$\Delta p = \frac{uL_c\eta}{kd_p^2} \quad (4.10)$$

with u from Eq. (2.9). In Eq. (4.10) k , η , and d_p are the permeability, the viscosity, and the particle diameter, respectively. Note that Eq. (4.10) differs from Eq. (3.2), which applies only for a given column (in contrast to the relation above). Within an SMB unit Δp depends on the configuration of the plant (*i.e.*, type, number, and arrangement of columns; positioning of the pumps). Since here such aspects are of less interest, the highest flow rate within the unit is taken as a critical measure for Δp . This highest flow usually occurs in zone I . Therefore, it follows from Eqs. (4.5) and (4.10) for the maximum flow rate, Q_{\max}^I :

$$Q_{\max}^I = k_0 \frac{\epsilon A_c d_p^2}{L_c \eta} \Delta p_{\max} \quad (4.11)$$

where Δp_{\max} is the maximum tolerable pressure drop in zone I . If γ^I is given from the design equations above, it follows from Eqs. (4.11) and (4.5) for the switching time, t_S

$$t_S = \frac{V_c [\gamma^I(1 - \epsilon) + \epsilon]}{Q_{\max}^I} \quad (4.12)$$

With the γ^j and t_S known, all internal flow rates, Q^j , can be calculated from Eq. (4.5), while the external streams (feed, raffinate, extract, and desorbent) correspond to the differences between the streams in adjacent zones (see Fig. 2.1).

4.2.4 Determination of Productivities from Equilibrium Design

Under equilibrium conditions an analytical expression for the productivity can be derived on the basis of Eq. (4.2). Considering that the feed flow is equal to $Q^F = Q^{III} - Q^{II}$, it follows from Eqs. (4.2), (4.5), and (4.12)

$$PR = \frac{Q_{\max}^I c^F}{nV_c} \cdot \frac{\gamma^{III} - \gamma^{II}}{\gamma^I(1 - \epsilon) + \epsilon} \quad (4.13)$$

This is a rather general expression for the productivity of an SMB process. The highest productivity corresponds to the highest possible difference between γ^{III} and γ^{II} and to the lowest value for γ^I . However, Eq. (4.13) is yet of rather limited use since the products' purity depends on the values for γ^j . By substitution of the expressions for the optimal γ^j into Eq. (4.13), it follows from Eqs. (4.6) and (4.13) under linear conditions:

$$PR_{100}^{\text{opt}} = \frac{Q_{\max}^I c^F}{nV_c} \cdot \frac{H_1(\alpha - 1)}{H_1\alpha(1 - \epsilon) + \epsilon} \quad (4.14)$$

² It is worth mentioning that JUPKE *et al.* [99] found that there is an infinite number of possible designs for maximum productivity which do not necessarily require maximum pressure drop. However, since in this work column efficiency is considered independent of flow rate, the above approach holds.

Here the index "100" denotes complete separation (100% product purity). An analogous expression can be derived for the case of the consistent nonlinear LANGMUIR by using Eqs. (4.7) and (4.13):

$$PR_{100}^{\text{opt}} = \frac{Q_{\text{max}}^I c^F \omega_G}{nV_c [\alpha q_s b_1 (1 - \epsilon) + \epsilon]} \cdot \frac{(\alpha - 1)^2}{\alpha^2 q_s b_1} \quad (4.15)$$

From expressions (4.14) and (4.15) the maximum productivity achievable in an ideal SMB unit can be explicitly calculated under the assumptions of infinite column efficiency and complete separation. Based on this, in the next section an analysis of the model systems will be performed.

Note that for real systems (finite efficiency, incomplete separation) such analysis can be performed only by numerical simulations. The results of such a study will be compiled in section 4.4.

4.3 Analysis for Pure Products Based on Equilibrium Design

4.3.1 Parameter Specifications

As mentioned before, for this study were used five of the mandelic acid systems (I.a through I.e). For a summary of the chromatographic parameters see Tabs. 3.1 and 3.2. Since the volume of stationary phase is needed in order to calculate the specific productivity, the number of columns had to be specified. Here an SMB unit with one column per zone was assumed.

For the two chromatographic columns, the maximum tolerable pressure drop is approximately $\Delta p_{\text{max}} = 100$ bar. Eq. (4.11) was used to determine maximum flow rates, Q_{max}^I from this value. For this purpose, the viscosity and permeability of water at 20 °C (*i.e.*, $k_0 \approx 10^{-3}$ and $\eta = 1.0$ cP) were applied. The results were $Q_{\text{max}}^I = 1.135$ ml/min (systems I.a – I.d) and 0.713 ml/min (system I.e), respectively. To allow for a comparison based on the adsorption isotherms rather than on hydrodynamic constraints, in the following the same maximum flow rate of $Q_{\text{max}}^I = 1.0$ ml/min will be assumed for all systems.³

4.3.2 Definition of Reference Isotherms

As shown above, the use of thermodynamically consistent LANGMUIR adsorption isotherms simplifies the analysis of continuous chromatographic enantioseparations. However, the experimental isotherms for mandelic acid deviate more or less from the consistency condition of equal saturation

³ This represents a rather low value when considering preparative applications. The reason for this is that analytical columns (small particle sizes, high length/diameter ratios) were examined here. However, the determined productivities are scalable, since in this work it is assumed that there is no impact of the flow rate on column efficiency.

capacities, q_s . Since system I.c reveals the smallest deviations from this condition (see Tab. 3.2), the parameters of this system were used to derive a set of consistent reference isotherms. The separation factor was held constant; therefore $\alpha^{\text{ref}} = \alpha = 1.14$. For q_s and b_1 resulted 180 g/l and 0.0057 l/g, respectively. The two reference isotherms corresponding to Eq. (4.3) are

$$q_1^{\text{ref}} = q_s^{\text{ref}} \frac{b_1^{\text{ref}} c^F}{1 + (\alpha^{\text{ref}} + 1) b_1^{\text{ref}} c^F} = \frac{1.026 c^F}{1 + 0.0122 c^F} \quad (4.16a)$$

$$q_2^{\text{ref}} = q_s^{\text{ref}} \frac{\alpha^{\text{ref}} b_1^{\text{ref}} c^F}{1 + (\alpha^{\text{ref}} + 1) b_1^{\text{ref}} c^F} = \frac{1.1696 c^F}{1 + 0.0122 c^F} \quad (4.16b)$$

Assuming the hypothetical situation that the initial isotherm slopes in Eqs. (4.16) continue to hold also at higher concentrations, the following linear reference isotherm equations were obtained:

$$q_1^{\text{ref}} = H_1^{\text{ref}} = 1.026 c^F \quad (4.17a)$$

$$q_2^{\text{ref}} = \alpha^{\text{ref}} H_1^{\text{ref}} = 1.1696 c^F \quad (4.17b)$$

4.3.3 Results for the Model Systems

As can be seen from Fig. 3.2, the adsorption isotherms of the model systems differ significantly with respect to separation factor, loading capacity, and concentration range. While three isotherms for the Teicoplanin stationary phase (systems I.b through I.d) appear somewhat similar with respect to their selectivity and their slope at infinite dilution, for system I.d (Cyclodextrine CSP) a steep slope at infinite dilution but a lower selectivity can be observed. Since the (unbuffered) system I.a reveals a complex behaviour (*i.e.*, a selectivity reversal at higher concentrations), this system was not considered further in the study presented here.

Using the parameters listed above, the productivities for the different chromatographic systems were calculated from Eqs. (4.14) and (4.15), respectively. The maximum productivities (obtained from maximum feed concentrations) are listed Tab. 4.1. The results reveal that – as one would expect – the productivity rises with increasing separation factor, α . Due to this, for system I.d a very low productivity is obtained that must be considered unsatisfactory for preparative purposes. Furthermore, isotherm nonlinearity has a strong influence and limits achievable values for PR .

Figure 4.2 shows the influence of the feed concentration. For all systems PR increases monotonously with increasing c^F and reaches a saturation level for $c^F \rightarrow \infty$. This is in agreement with the findings in [103]. Note that the results for the reference isotherms, Eq. (4.16), are in reasonably close agreement to the results for the isotherms they were derived from (system I.c).

In the next section, the influence of the individual isotherm parameters will be investigated in more detail.

Table 4.1. Maximum theoretical productivities obtained for a four-column SMB unit for the complete separation of mandelic acid enantiomers (using $c_i^F = c_{\max}^F$, see Tab. 3.2).

| system | α [-] | PR_{100}^{opt} [$\text{g} \cdot \text{l}^{-1} \cdot \text{d}^{-1}$] | |
|--------|-----------------|--|-----------|
| | | linear | nonlinear |
| I.a | 4.33 | n.e. | n.e. |
| I.b | 1.4 | 835.4 | 461.7 |
| I.c | 1.14 | 1010.6 | 188.7 |
| I.d | 1.24 | 1183.1 | 381.3 |
| I.e | 1.07 | 143.3 | 7.9 |
| ref | 1.14 | 984.2 | 177.9 |

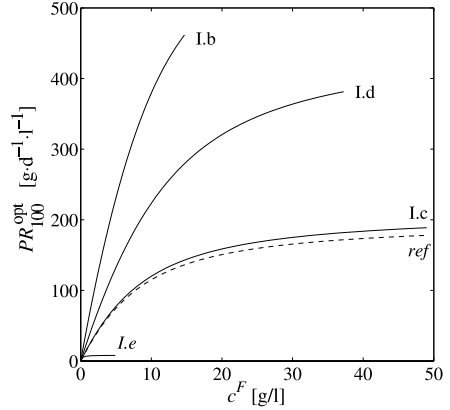


Figure 4.2. Dependence of theoretical productivities on feed concentration for the nonlinear isotherms. Dashed line – reference isotherm; solid lines – systems I.b through I.e.

4.3.4 Parametric Study Based on a Reference Isotherm

A parametric study was performed using the reference isotherms, Eqs. (4.16), to examine the role of the individual isotherm parameters. These were separation factor and HENRY constant in the linear case, and separation factor, saturation capacity, and energy parameter in the LANGMUIR case, respectively. Each parameter was varied systematically and the according productivities were calculated from Eqs. (4.14) and (4.15), respectively.

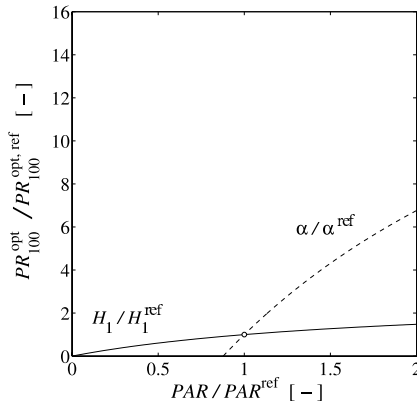


Figure 4.3. Dependence of productivity on separation factor α and HENRY constant H_1 for the linear reference isotherm.

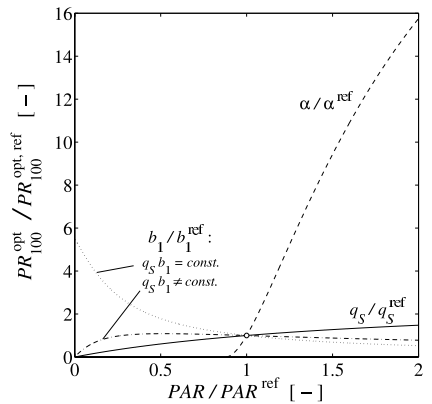


Figure 4.4. Dependence of productivity on separation factor α , saturation capacity q_s , and energy parameter b_1 for the LANGMUIR reference isotherm.

Figure 4.3 illustrates the effects of separation factor, α , and HENRY constant, H_1 , on the productivity for linear isotherms. The abscissa shows the ratio of the actual parameter (α or H_1) to the respective reference parameter (α^{ref} or H_1^{ref}), while the ordinate is the ratio of the actual productivity to the corresponding productivity for the reference parameters (see Tab. 4.1). It can be estimated that a hypothetical doubling of the HENRY constant H_1 (while keeping all other parameters constant) leads to a 1.5-times higher productivity. However, the impact of the separation factor is much more significant. For $\alpha = 2\alpha^{\text{ref}}$ the productivity increases to the seven-fold value. This indicates the trivial rule that high selectivities are desirable. Note, that the observed impact of the HENRY constants on PR is in conflict with the claim made in [126] that low HENRY constants are preferable in SMB applications.

Fig. 4.4 shows the impact of the parameters q_s , α , and b_1 on productivity in an analogous manner as in Fig. 4.3. Obviously, the dependencies are more complex in the nonlinear case. However, it is evident that again the most significant impact on process productivity originates from the separation factor. The strongly increasing PR for very low values of the equilibrium parameter b_1 emphasises again the significance of isotherm nonlinearity.

Parameter Sensitivities

The role of an individual parameter can be better quantified using the sensitivity of the productivity with respect to this parameter. A normalised sensitivity is defined by

$$S_{PR}^{PAR} = \frac{PAR}{PR} \cdot \frac{\partial PR}{\partial PAR} \quad (4.18)$$

where S_{PR}^{PAR} is the sensitivity of the productivity, PR , with respect to a certain parameter, PAR . A value for S_{PR}^{PAR} can be understood as the change of productivity in percent that results from a corresponding change of the actual isotherm parameter.

In the hypothetical linear case, the partial derivatives in Eq. (4.14) can easily be calculated. The resulting parameter sensitivities are

$$S_{PR}^{\alpha} = \frac{H_1(1 - \epsilon) + \epsilon}{\alpha H_1(1 - \epsilon) + \epsilon} \cdot \frac{\alpha}{\alpha - 1} \quad (4.19a)$$

$$S_{PR}^{H_1} = \frac{\epsilon}{\alpha H_1(1 - \epsilon) + \epsilon} \quad (4.19b)$$

The following sensitivities result from Eq. (4.19): $S_{PR}^{\alpha} = 7.79$ and $S_{PR}^{H_1} = 0.65$. These results emphasise the finding described above that the separation factor, α , has a dominating impact on productivity. Increasing α by 1% will lead to a remarkable increase in productivity (about 8%). Increasing the HENRY constant will also lead to higher PR , but the improvement is less than 1%.

For the nonlinear isotherms, the according derivatives of Eq. (4.15) are rather “voluminous”. In this case it was found more expedient to approximate the sensitivity by the corresponding finite differences

$$S_{PR}^{PAR} = \frac{\overline{PAR}}{\overline{PR}} \cdot \frac{\Delta PR}{\Delta PAR} \quad (4.20)$$

For the reference isotherm parameters the following values were calculated from Eq. (4.15) for shifting each parameter PAR by 1%: $S_{PR}^{\alpha} = 13.6$, $S_{PR}^{q_s} = 0.65$, $S_{PR}^{b_1} = -0.24$ (for $q_s b_1 \neq \text{const.}$), and $S_{PR}^{b_1} = -0.89$ (for $q_s b_1 = \text{const.}$). Obviously, the influence of the separation factor is even more pronounced in the nonlinear case than for a linear isotherm. The magnitude of the effects q_s and b_1 are comparable to that of the HENRY constant above.

4.4 Analysis for Variable Purity Based on Numerical Simulations

It is clear in general that prediction based on Eq. (4.13) will be too optimistic when considering the limited efficiency of real SMB plants. Furthermore, the mentioned equation applies for complete separation only. Therefore, in this section numerical simulations using a more detailed model will be applied to study the impact of reduced purity requirements on SMB performance.

4.4.1 Parameter Specifications

Figure 4.2 emphasises that the highest productivity in an SMB process is achieved for the highest feed concentrations [57, 103]. Therefore, in the numerical study of the SMB process below, again the highest feed concentrations was assumed. For the flow rate in zone I , again the value of $Q^I = 1$ ml/min was applied.

To solve the equilibrium dispersive model (section 2.1.4), it was necessary to specify the number of theoretical plates, NTP . The value determined experimentally for both column types was $NTP \approx 1000$ at a flow rate of $Q = 1.0$ ml/min [57]. The application of this number in the model requires rather long computation times. However, since it is well known that for a sufficiently high number of theoretical plates the SMB process becomes less sensitive to NTP (e.g., [63]), the application of lower numbers was possible without considerably affecting the accuracy of the results. Satisfactory convergence of the solutions was observed for plate numbers higher than 250 for each column. Hence, for all SMB calculations presented below, 300 theoretical stage per column were applied. For the SMB unit, again a configuration with one column per zone was used.

4.4.2 Separation Regions for Varying Outlet Purity

The representation of operating points in the γ^{II}/γ^{III} -diagram is a comprehensive tool when analysing SMB separations. However, the separation regions defined in Fig. 4.1 apply to complete separation in an infinitely efficient TMB process only. If, in contrast, column efficiency is limited and purity requirements are reduced, the analytical solution above may only serve as a rough indication. In this case, it is expedient to define separation regions for certain minimum values of the

outlet purities P^R and P^E . Such region is then defined by

$$\{(\gamma^{II}, \gamma^{III}) : P^R \geq P, P^E \geq P\} \quad (4.21)$$

To answer the question, how these regions and the according optimal γ^j depend on purity requirements, a systematic numerical “scan” over a sufficiently narrow equidistant grid in the γ^{II}/γ^{III} -plane was performed. For each operating point, the steady-state solutions of the mathematical model were calculated. In the calculations, γ^I and γ^{IV} were specified from the optimal values according to equilibrium theory, that is from Eqs. (4.9a) and (4.9b), in combination with a “small” safety factor $\beta = \beta^I = \beta^{IV}$. The value of β was determined in preliminary calculations for each chromatographic system by checking for selected operating parameters whether in zones *I* and *IV* complete regeneration was achieved. The lowest acceptable value of β was chosen. The switching time, t_S , was calculated from Eq. (4.12) using $Q^I = 1$ ml/min and the determined value for γ^I . Finally, all remaining internal and external flow rates were calculated.

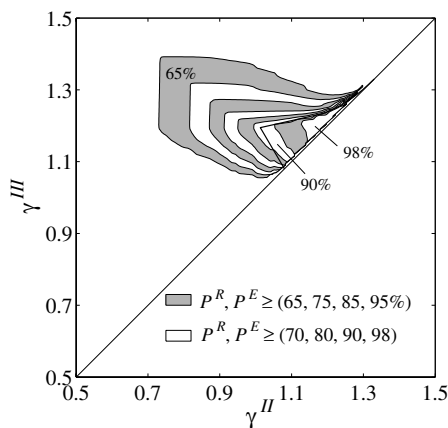


Figure 4.5. Example for separation regions as function of purity. Bold line – complete separation (equilibrium theory, section 4.2.3). Parameters: system I.d, $c^F = 10$ g/l, $\beta^I = \beta^{IV} = 1.2$. Regions derived from 1480 calculations.

for all systems studied, with lower outlet purity the positions of the vertices change in a similar way as shown in Fig. 4.5. That is, at first the optimum moves towards lower γ^{II} and γ^{III} . After falling below a certain intermediate purity, optima move towards higher γ^{III} while γ^{II} is decreasing. Finally, it is worth emphasising that (at least for the parameters used in this study) in the optimal operating point the purity is identical for both outlets (*i.e.*, in the vertex of each region holds $P^R = P^E$).

Typical results are shown in Fig. 4.5. The bold line depicts the region of complete separation from equilibrium theory. The regions correspond to different minimum outlet purities. Obviously, the lower the purity the larger the separation region. For example, it can be seen that the region for 90% purity almost coincides with the theoretical region of complete separation. This means that for the four-column SMB system studied here, the theoretical productivity resulting from equilibrium theory can be achieved only if the purity requirements are lowered to about 90%.

It should be noted that the shape of the regions and the position of their vertices (*i.e.*, the most productive operating points) depend strongly on the isotherm parameters and the feed concentrations. However, for

4.4.3 Productivity as Function of Feed Concentration and Purity

In order to identify the operating point delivering the maximum productivity for a desired product purity and feed concentration, the vertex of the respective purity region in the $\gamma^{\text{II}}/\gamma^{\text{III}}$ -plane has to be found (cf. Fig. 4.5). This can be done either via extensive simulations analysing all intercepts of an equidistant grid as demonstrated above, or by implementing an optimisation approach. The latter option was chosen in this section.

For the optimisations, a semi-heuristic approach was used similar to the algorithm described in [127]. The main idea of the search strategy is to identify an optimum based on the finding that in the vertex of a separation region for a certain purity P , the purities of raffinate and extract are equal to this minimum value (i.e., $P^R = P^E = P$). As will be shown in section 5.3, this assumption holds only true if complete regeneration is achieved in zones I and IV . To guarantee regeneration, safety factors were applied to γ^I and γ^{IV} (see page 61).

In the optimisations, design parameters from equilibrium theory were chosen as starting values for γ^{II} and γ^{III} . Calculation was stopped when the periodic steady state was reached (the stop criterion of KNIEP [95] was used to verify this). Similar to a simplex algorithm, the search direction was fixed based on the outlet purities calculated for neighbouring grid points and the trends in the location of optima that were found in the study on separation regions above. A simplified program flow chart of the approach is included in Appendix A.2. Using this approach it was possible to find operation points that provided the desired equal product purities and – presumably – met the requirement of maximal productivity. The method proved to be relatively fast – usually less than 20 function evaluations were required. Some selected results (essential design parameters and obtained productivities) are listed in the Appendix (Tab. A.1).

Fig. 4.6 summarises all optimisation results for the considered model systems. In the diagram, the productivity is shown as a function of the required outlet purities, $P^R = P^E$, and the feed concentrations.

Each point in the diagrams corresponds to the vertex of a region like the one shown in Fig. 4.5. For all systems, the productivity increases with increasing feed concentration. Furthermore, PR rises rapidly if the required purity is lowered. In contrast to the situation at higher purities, the productivities do not reach maximum values at lower purities (at least not for the concentration ranges examined here). As expected, the SMB process based on the isotherms with the highest separation factor of $\alpha = 1.4$ (system I.b) is most productive for high purities. However, for low purities the highest productivity is obtained for system I.d. Obviously, in this case the higher applicable feed concentration is advantageous. Such type of isotherms might be of interest if a low purity is required and the feed solution can be introduced very concentrated. Although the feed concentration for system I.c is the highest, it does not lead to high productivities, since the separation factor is not sufficiently large. Because of the very low separation factor (1.07) and the low maximum feed concentration (5 g/l), the productivity for the isotherms measured on the cyclodextrine column (system I.e) is negligible in comparison to the other systems.

It should be noted, that with increasing productivity also the specific desorbent requirement (i.e.,

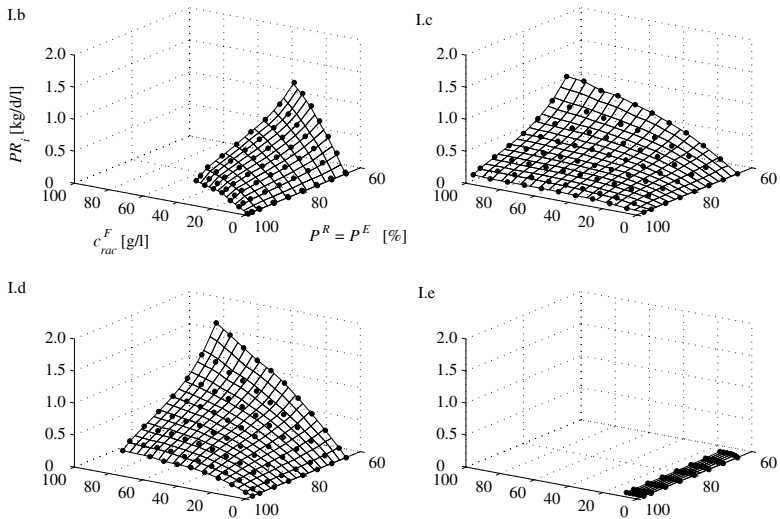


Figure 4.6. SMB productivity for four experimental systems as a function of product purity and feed concentration. Each point represents a vertex of the corresponding separation regions in Fig. 4.5.

the ratio of the necessary amount of chromatographic solvent introduced with feed and desorbent, respectively, to the mass fluxes of the products) is decreasing significantly. For reasons of clarity the desorbent requirement will not be discussed further in this chapter. However, this aspect will be treated in detail in Chapter 7.

Some first examinations of the dependency of productivity on feed concentration and outlet purity were performed by SHEEHAN *et al.* [56]. Comparing their results to the trends in Fig. 4.6, a difference will be noticed. While in [56] a productivity maximum at intermediate feed concentrations was observed when optimising the process for a purity of 70%, such a maximum was not observed in this work. It can be shown from some model calculations that the reason for the maximum observed in the case of [56] lies in insufficient regeneration of zone *IV* of the SMB. By adjusting a proper value for the safety factor, the productivity can be improved and this maximum will shift towards $c^F \rightarrow \infty$. Obviously, regeneration becomes critical with lower outlet purity and higher feed concentrations. Thus, an optimised design of SMB processes for limited outlet purities has to include the regeneration zones, which results in a numerically challenging problem. This aspect will be addressed in detail in Chapter 5, where all four zone flow rates of a continuous chromatographic process will be optimised using a computationally less expensive TMB model.

Finally, it should be emphasized that the numerical results presented above hold for a four-column SMB system that was restricted by a low maximum flow rate typical for lab-scale columns. Using preparative-scale columns will allow for higher flow rates and, thus, for higher absolute values of the productivity – without affecting the main tendencies presented in Fig. 4.6.

4.5 Conclusions

The results above emphasise the dominating impact of adsorption isotherm parameters on achievable productivity in SMB separations. Based on an equilibrium model, algebraic expressions for the theoretical productivity as a function of isotherm parameters were derived. A parametric study and a sensitivity analysis affirmed that out of the individual isotherm parameters, the separation factor α has the strongest impact on performance, in particular for nonlinear equilibria. Besides this, the analysis further revealed that limitations of productivity are also induced by the possible feed concentration and the isotherms' nonlinearity.

A simulation study based on the equilibrium dispersive model and considering a four-column SMB showed that separation regions in the $\gamma^{\text{II}}/\gamma^{\text{III}}$ -plane become larger if purity requirements are lowered. The productivity in optimum operating points rises strongly with lower outlet purities. Simultaneously, the desorbent requirement of the process is decreasing. More details on this can be found in [57]. Thus, reducing purity requirements affords significant enhancement of process performance, in particular for systems with low separation factors. These findings are encouraging when considering a coupling of SMB chromatography and crystallisation for enantioseparations.

A comparison of the result to literature sources emphasised the necessity to include all four zone flow rates in the optimisation of continuous chromatographic processes, since regeneration can become critical, in particular under reduced purity requirements. This important aspect will be addressed in the next chapter.

DESIGN OF SMB PROCESSES FOR PREDEFINED PURITY

The last chapter demonstrated that the performance of SMB processes increases significantly under reduced purity requirements. In the design approach used there, complete regeneration was required in the outward zones of the SMB. However, from engineering experience it is expected that operation under reduced purity requirements should also allow for a less restrictive design of these regeneration zones.

In this chapter this issue will be addressed on the basis of a parametric study. Two design options will be compared – a restrictive that requires complete regeneration, and a non-restrictive that includes all zone flow rates in an optimisation, respectively. It will be demonstrated that the latter approach facilitates significant performance improvements. Furthermore, it will be investigated how the different designs affect process robustness.

5.1 Background

Despite the substantial achievements in understanding of the SMB process, rather simple approaches are still common in its practical design for concrete separation problems. The "triangle theory" (section 4.2.3) predicts design variables valid only for ideal systems and complete separation of the components. For real systems, usually numerical simulations of an SMB model are applied to determine flow rates in the separation zones that account for nonideal behaviour. In contrast, the flow rates in the regeneration zones are often corrected only by using simple safety factors as were introduced in Eqs. (4.9) [125, 127, 128].¹ This might represent a reasonable engineering practice as long as very high product purities have to be achieved and solvent usage does not govern the total separation costs. However, this approach certainly entails a loss in process performance if lower product purities are of interest, since it is well known from other separation

¹ Some authors also suggest to use the optimal flow rates determined from the triangle theory and to subsequently optimise other design parameters (like column length or efficiency) [82].

processes that with lower purity requirements facilitate less restrictive designs, which in turn lead to higher throughputs.

An appealing strategy is certainly the application of control strategies to adjust automatically proper flow rates in the individual zones. However, in the corresponding publications so far either only high product purity was considered, or the complete regeneration in zones *I* and *IV* was required as a prerequisite [97, 129–133]. Another option is the application of multi-objective optimisation procedures that include all zone flow rates. Results of recent works in this context indicate that a "violation" of the requirement of complete regeneration might be desirable (*e.g.*, [100, 134, 135]). Although such optimisation approach is very useful, due to its complexity and the implementation efforts necessary, the application of the mentioned safety factors is still common practice.

However, so far only few attempts have been made to study systematically the influence of the operating parameters in the regeneration zones. Some investigations were presented in [136]. Yet, the authors considered only one of the two regeneration zones and a system with linear adsorption isotherms.

In this chapter, a systematic parametric study will be performed to study the impact of the design of the regeneration zones in continuous chromatography for nonlinear isotherms. The performance of the process will be compared for a *restrictive* design approach (*i.e.*, a design that requires complete regeneration in zones *I* and *IV*, respectively) and a *non-restrictive* design (in which this regeneration is not predefined). Finally, process robustness will be addressed by means of a sensitivity analysis.

5.2 Model and Parameters

It was already pointed out in Chapter 4 that the flow rates in the regeneration zones should be included in an optimised design of SMB processes for limited outlet purities. The use of an SMB model proved to be computationally too expensive to perform this task for the different systems and the several parametric studies within this work. Therefore, in this chapter the equilibrium stage model of a TMB process will serve as a reduced model for SMB chromatography. The model, which was implemented in the simulation environment DIVA [96], has already been explained in section 2.1.5.

For the optimisation of the TMB process, a sequential quadratic programming (SQP) method available in DIVA [137] is used. SQP was already used successfully by other authors for SMB optimisations, see for example [138]. Optimisation variables are the dimensionless internal flow rates, γ^j , for the zones of the TMB (for details see also Chapter 4). In the restrictive design approach only γ^{II} and γ^{III} were subject to optimisation, while in the non-restrictive designs all four γ^j were considered.

As the objective function the ratio of desorbent stream and product flux was found appropriate, since this simultaneously minimises desorbent requirement while it maximises productivity:

$$OF = \frac{Q^D}{Q^R c_1^R + Q^E c_2^E + 1.0 \cdot 10^{-8}} \rightarrow \min \quad (5.1a)$$

$$\text{s.t. } P^R \geq P_{\min}^R \quad (5.1b)$$

$$P^E \geq P_{\min}^E \quad (5.1c)$$

The term $1.0 \cdot 10^{-8}$ in Eq. (5.1a) was introduced to prevent numerical difficulties if the remaining denominator is equal to zero. The outlet purities are guaranteed by the nonlinear constraints (5.1b) and (5.1c). Additionally, it was found useful to include the following linear constraints:

$$\gamma^I \geq \gamma^{II} + \Delta\gamma \quad (5.2a)$$

$$\gamma^{III} \geq \gamma^{II} + \Delta\gamma \quad (5.2b)$$

$$\gamma^{III} \geq \gamma^{IV} + \Delta\gamma \quad (5.2c)$$

$$\gamma^I \geq \gamma^{IV} + \Delta\gamma \quad (5.2d)$$

where $\Delta\gamma = 10^{-2}$. These constraints prevented numerically expensive function evaluations at economically useless operating points (e.g., for extremely low feed flow rates). Furthermore, they guaranteed for the proper direction of flows, prohibited flow rates equal to zero, and also led to faster convergence.

5.2.1 Generic Example System

For illustrative purposes, a simple generic example system will be used in the following model calculations. A moderately nonlinear LANGMUIR isotherm with a separation factor of 1.5 will be considered. All parameters are listed in Table 5.1. The table contains also the optimum values for the dimensionless flow rates, γ^i , as predicted by equilibrium theory, Eqs. (4.7). These will serve as reference values in the following study.

Table 5.1. Parameters for TMB model calculations (generic example system).

| | | |
|--------------------------------------|---|--|
| Discretisation | 100 stages per zone | |
| Isotherm parameters (LANGMUIR) | $a_1 = 2.0$ $b_1 = 0.002$ | $a_2 = 3.0$ $b_2 = 0.002$ |
| Feed concentration | $c_1^F = 20.0 \text{ g/l}$ | $c_2^F = 20.0 \text{ g/l}$ |
| Zone length | $L = 20.0 \text{ cm}$ | |
| Column diameter | $D = 1.0 \text{ cm}$ | |
| Porosity | $\epsilon = 0.7$ | |
| max. internal flow rate | 10.0 ml/min | |
| opt. γ^j from triangle theory | $\gamma^I = 3.0$ $\gamma^{III} = 2.0644$ | $\gamma^{II} = 1.7423$ $\gamma^{IV} = 1.5799$ |

5.3 Influence of the Regeneration Zones

5.3.1 Internal Concentration Profiles

The values adjusted for the dimensionless flow rates in the regeneration zones I and IV will naturally influence the internal concentration profiles of a continuous chromatographic process. This is illustrated in Fig. 5.1 for three characteristic examples. For the upper plot, the parameters for complete separation as predicted from triangle theory were used (see Table 5.1). Additionally, to guarantee complete regeneration, a safety factor $\beta = 1.1$ was applied to the flow rates in the corresponding zones I and IV (restrictive design).

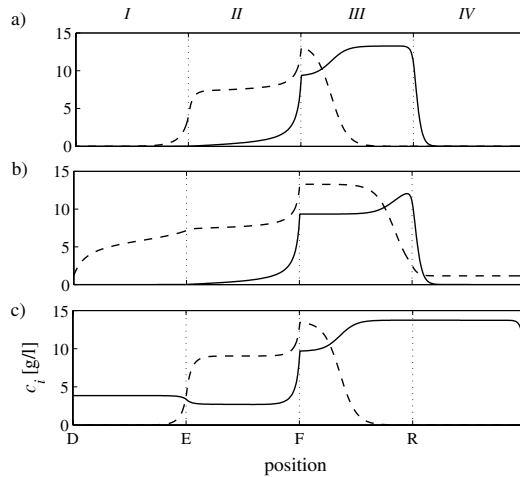


Figure 5.1. Internal concentration profiles for the TMB process in Tab. 5.1. Solid lines – fast component 1, dashed – slow component 2. a) Restrictive design of regeneration zones with 10% safety margin ($\beta^I = \beta^{IV} = 1.1$); b) violation of constraint in zone I ($\beta^I = 0.8$, $\beta^{IV} = 1.1$); c) violation of constraint in zone IV ($\beta^I = 1.1$, $\beta^{IV} = 0.8$).

Figure 5.1 a) reveals that the restrictive design provides for both, complete separation in zones II and III , as well as complete regeneration in zones I and IV . The next two panels show results for situations where the regeneration requirement was violated. Fig. 5.1 b) corresponds to a violation in zone I only ($\beta^I = 0.8$, while $\beta^{IV} = 1.1$). A breakthrough of the dispersive wave of the slow component into zone IV can be observed, which contaminates the raffinate. For Fig. 5.1 c) such a violation was applied to zone IV (i.e., $\beta^I = 1.1$, while $\beta^{IV} = 0.8$). Here, the shock wave of the fast component migrates into zone I and leads to a significant contamination of the extract product.²

² Since for LANGMUIR-type isotherms higher concentration levels migrate faster than lower concentrations, a desorption front undergoes dispersion, while an adsorption front will develop a shock wave (see, e.g., [139]).

This behaviour is not surprising. However, the question to be answered is, to which extent such breakthroughs are acceptable when aiming at improved process performance for reduced purity requirements.

5.3.2 Separation Regions

In Chapter 4 separation regions in the $\gamma^{\text{II}}/\gamma^{\text{III}}$ -plane were used to assess the performance of SMB processes for complete separation as well as under reduced purity requirements (see Fig. 4.5).

Figure 5.2 contains a corresponding plot of separation regions for different outlet purities for the generic example considered here. Like for the example shown in Fig. 4.5, for this diagram the restrictive design was applied ($\beta^{\text{I}} = \beta^{\text{IV}} = 1.1$). The regions become larger for lower purity requirements and their vertices move along a parabolic line away from the diagonal, which indicates the possibility to increase the feed flow rate.

However, a different picture is obtained when lowering the safety factors. Figure 5.3 shows separation regions for $P^{\text{R}}, P^{\text{E}} \geq 0.9$ (i.e., at least 90% product purity at both outlets) for varying values of the safety factors β^{I} and β^{IV} . To construct the diagrams the $\beta^{\text{I}}, \beta^{\text{IV}}$ -values were decreased stepwise starting from $\beta = 1.1$. In both panels the largest region is identical to the 90%-region in Fig. 5.2.

The results indicate that when lowering β^{I} the separation region shrinks starting from the diagonal (Fig. 5.3, left). For $\beta^{\text{I}} = 0.8$ the region vanished completely (i.e., the minimum purity of 90% could not be achieved anymore in one or both of the outlets). Note, that position of the vertex corresponding to the highest feed throughput remains almost constant for a rather wide range of β^{I} , which allows to maintain the maximum feed flow rate. In contrast, when lowering β^{IV} , the separation region shrink starting from the outside. Due to this, the vertices move towards the diagonal, even for small deviations from $\beta^{\text{IV}} = 1.1$. In turn this means that a violation of the regeneration constraint in zone IV might lead more or less promptly to a lower feed flow rate.

An interesting fact is that for violated constraints in zone I a second vertex develops at the lower border of the separation region (circle in Fig. 5.3, left). In this point it holds $P^{\text{R}} = P^{\text{E}}$ – just as for the vertices that correspond to maximum feed flow rates (see section 4.4.3). The throughput for this second vertex is much lower in comparison to the optimum vertex (denoted by the triangle). However, this finding emphasises that the condition $P^{\text{R}} = P^{\text{E}}$ (as it was used in Chapter 4 and

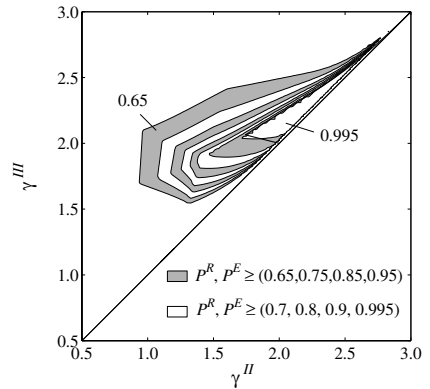


Figure 5.2. Separation regions for different outlet purities P^{R} and P^{E} for a restrictive design of the regeneration zones. Solid line – complete separation (equilibrium theory, see section 4.2.3).

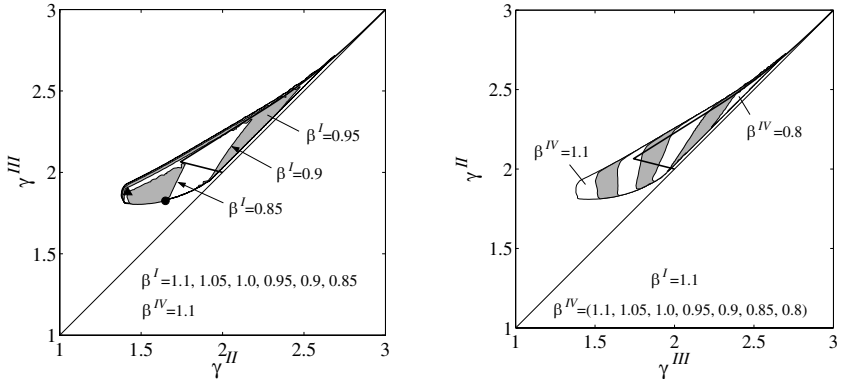


Figure 5.3. Separation regions for $P^R, P^E \geq 0.9$ under violated design restrictions in zone I (left) and zone IV (right). Two vertices in the left mark operating points with $P^R = P^E = 0.9$ for $\beta^I = 0.85$.

in [127]) does not represent an appropriate criterion for the optimisation of continuous chromatographic processes. It can be used only if complete regeneration is guaranteed, which actually was required for the investigations performed in Chapter 4.

5.4 Optimisation of Restrictive and Non-restrictive Designs

5.4.1 Process Performance

The results described above indicate that the separation regions shrink if the regeneration conditions are relaxed. Since in the above only one of the zone flow rates was varied and all others were kept constant, a separation region shrinking towards the diagonal simultaneously entails a decreasing feed flow rate. In order to clarify whether this also holds if all four flow rates are optimised, the optimisation procedure described in section 5.2 was applied.

Figure 5.4 contains the results of the optimisations for the restrictive and non-restrictive designs. For the restrictive design, a safety margin of 10% was applied to the regeneration zones, while for the non-restrictive design all zone flow rates were optimised. For all design points, the flow rate in zone I was set to 10 ml/min (arbitrarily assuming that this corresponds to the highest tolerable pressure drop of within the unit; cf. section 4.2.3). The results are very promising. Obviously, relaxing the regeneration conditions increases process performance significantly. The lower the purity requirements, the higher this effect. The productivity, PR , Eq. (4.2), and the specific solvent consumption, SC , which corresponds to the objective function, Eq. (5.1a), can be improved by up to 25% (Figs. 5.4 a and b). The latter is particularly due to the strongly increasing concentration of the extract (Fig. 5.4 c).

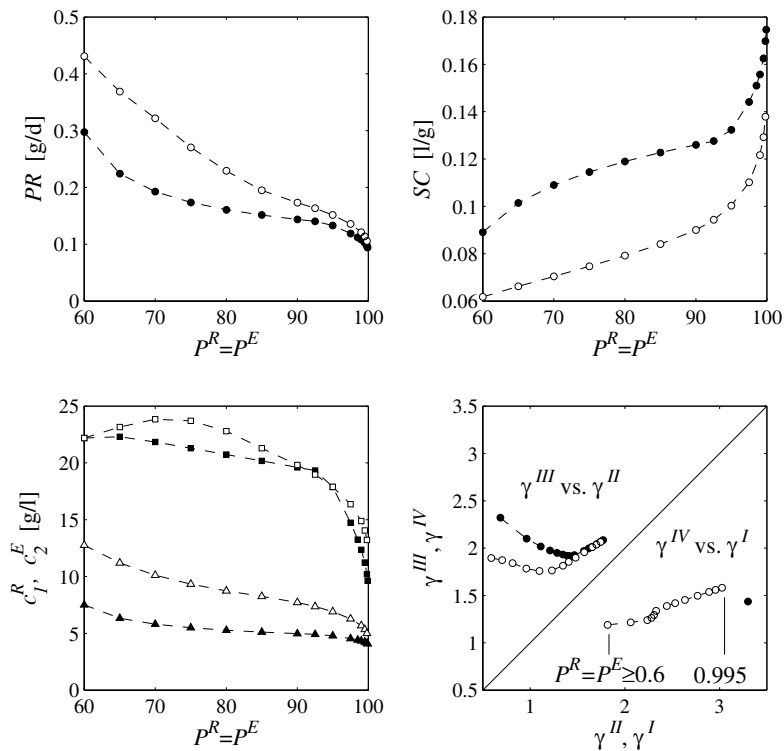


Figure 5.4. Comparison of non-restrictive (open symbols) and restrictive design (filled symbols). a) productivity, b) eluent consumption, c) product concentrations (squares – raffinate, triangles – extract), d) operating points in γ^{II}/γ^{III} and γ^I/γ^{IV} planes, respectively.

A very important finding is that also the positions of the optima in the γ^{II} - γ^{III} -plane are different for the two design approaches (Fig. 5.4 d). Surprisingly, in case of the non-restrictive design, the operating points move towards lower γ^{II} -values, apparently leading to lower feed flow rates. However, in parallel the value for γ^I decreases significantly, while γ^{IV} remains more or less constant (while γ^I, γ^{IV} are constant for the restrictive design; see the plot below the diagonal in Fig. 5.4 d). Since in all design points the same flow rate of $Q^I = 10$ ml/min was applied to zone I, these values for γ^I, γ^{IV} lead to overall lower desorbent consumption and higher throughput. This indicates that the benefit of a non-restrictive design is actually due to an interplay of the design conditions in the whole unit, and does not only result from relaxing the conditions in the regeneration zones.

It should be emphasised, that from the above follows that the possible benefit expected from the coupling of SMB chromatography and enantioselective crystallisation is not fully accessible if only the separation zones are considered in the design of the SMB step.

5.4.2 Internal Concentration Profiles

Figure 5.5 illustrates the differences between the internal concentration profiles for the two design options as obtained from the optimisations. For the restricted design, again $\beta^I = \beta^{IV} = 1.1$ was applied. In the example shown the minimum outlet purity was set to $P = 0.95$ for both outlets.

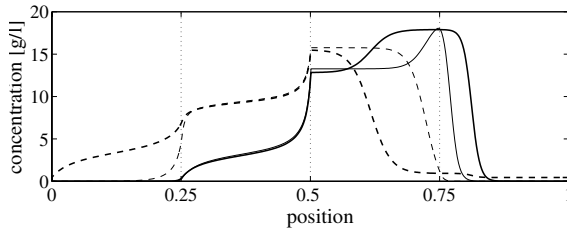


Figure 5.5. Comparison of optimised operating points for $(P^R, P^E) \geq 0.95$. Solid lines – component 1, dashed – component 2. Thin lines – restrictive design, thick lines – non-restrictive design.

It can be seen that in the restrictive design any breakthrough of concentrations waves from zone *I* into zone *IV*, or *vice versa*, is prevented. In contrast, the non-restrictive design prevents only the breakthrough of the shock wave of the less adsorbing component from zone *IV* into zone *I*, while the dispersive wave of the strong adsorbing component in zone *I* is allowed to partially migrate into zone *IV*. This leads to almost constant concentrations plateaus of this component in zones *III* and *IV*, respectively, which determine the purity of the raffinate. This situation was also observed for other purity requirements and isotherm parameters. To the authors opinion this rather simple scenario is a motivation for future investigations on the basis of equilibrium theory. However, this is beyond the scope of this work.

Although the above must be considered a phenomenological finding (since it cannot be ruled out that the optimisation results represent local minima), it deserves some more consideration. The prevention of a breakthrough of the shock wave from zone *IV* into zone *I* appears desirable, since such breakthrough would lead to immediate and strong contamination of the extract product. Obviously, this problem is less pronounced when considering a breakthrough of the dispersive wave from zone *I* into zone *IV*. In the next section a sensitivity analysis will be applied for a quantification of these effects.

5.4.3 Process Robustness

An important result of the investigations above is, that in an optimised design for reduced purity requirements the dispersive wave of the stronger adsorbing compound is allowed to migrate into zone *IV* of the unit. This raises the question, whether an optimised non-restrictive design results in lower process robustness in comparison to a restrictive design.

Here the steady state sensitivities of the raffinate and extract purity with respect to the flow rate ratios will be used as a measure for robustness. To calculate these sensitivities, the deviations of the purities at steady state will be considered after a step-change of the flow rates in the individual zones. A general definition for the sensitivity is given by Eq. (4.18). Here, the normalised sensitivities will be approximated numerically by

$$S_{P^j}^{\gamma^i} = \frac{\gamma_0^i}{P_0^j} \frac{\partial P^j}{\partial \gamma^i} \approx \frac{\gamma_0^i}{P_0^j} \frac{P_+^j - P_-^j}{\gamma_+^i - \gamma_-^i}, \quad i = (I, \dots, IV), j = (E, R) \quad (5.3)$$

The index 0 denotes the operating point for which the steady state sensitivity is determined. Terms with + and - correspond to values that were calculated by changing γ^i by +0.5% and by -0.5%, respectively, around the original design point, γ_0^i .

The resulting sensitivities are shown in Fig. 5.6. The values in the upper row correspond to the restrictive design (*i.e.*, safety factors $\beta_I = \beta_{IV} = 1.1$); the lower row contains the sensitivities for the non-restrictive design.

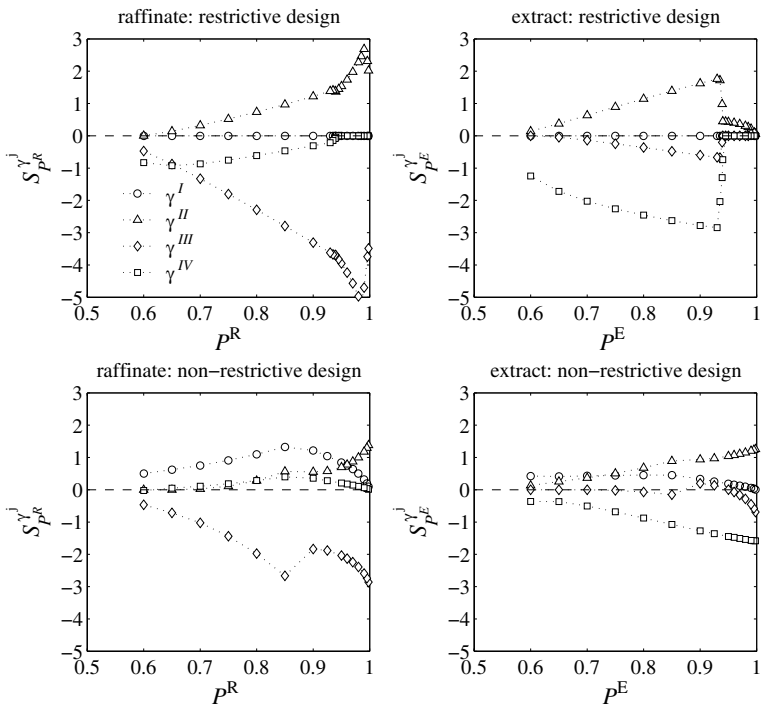


Figure 5.6. Steady state sensitivities of raffinate and extract purity with respect to the flow rates in the four zones of a TMB unit. Comparison of optimised restrictive designs and non-restrictive designs.

In the restrictive design, the sensitivities for the extract, $S_{pE}^{\gamma^j}$, are initially (*i.e.*, for high purity) low, while they are rather high for the raffinate, $S_{pR}^{\gamma^j}$. With decreasing outlet purities, in particular $S_{pR}^{\gamma^j}$ is affected, while $S_{pE}^{\gamma^j}$ remains stable between $P^j = 100\%$ and $P^j \approx 93\%$. This behaviour can be explained (and was also confirmed by the analysis of internal concentration profiles) by the nature of the concentration waves within the unit. For purities below approximately 93%, the sensitivities of the extract purity with respect to γ^{IV} and γ^{III} increase strongly, since the concentration and the corresponding migration velocity of the shock front in zone *IV* increase until, finally, a breakthrough of this front into zone *I* occurs. Thereafter, the sensitivities decrease gradually. Obviously, a higher safety factor for zone *IV* would be necessary to counterbalance this effect.

In the non-restrictive design, the highest observed sensitivities were lower than in the restrictive design. They were more or less of the same magnitude for all γ^j . For the raffinate purity, γ^{III} had the strongest impact. Surprisingly, γ^{IV} did not play a major role, which might be an indication for a better convergence of the SQP algorithm at low γ^{IV} -values (since it could be expected that optimal operating points would correspond to the highest γ^{IV} values possible). In such situation a small perturbation would cause the mentioned breakthrough of the shock wave, which should be observable in the calculated sensitivities.

Summarising the above, it can be concluded that stable operation of SMB processes can be achieved only for complete separation while simultaneously applying safety factors to *all* flow rates. In a restrictive design for lower purities, the use of inappropriate safety factors for the regeneration zones leads to strong sensitivities of the purities and, thus, to unstable operation. An encouraging finding with respect to the process combination of chromatography and crystallisation is that robustness of the process is not significantly decreased if all zone flow rates are optimised in comparison to a restrictive design.

5.5 Conclusions

A systematic study was performed to investigate the impact of the design of the regeneration zones on the performance of continuous chromatography under nonlinear conditions. The commonly used restrictive design (*i.e.*, the use of safety factors for zones *I* and *IV*, respectively) was compared to a non-restrictive design (*i.e.*, optimisation of all flow rates).

The results are promising with respect to the process combination of chromatography and crystallisation. The relaxation of the constraint of complete regeneration in zones *I* and *IV* allows for significant improvement of process performance. In the generic example studied, both throughput and eluent consumption can be improved by up to 25%.

Furthermore, it could be shown that the possible benefit expected from a coupling of SMB chromatography and enantioselective crystallisation is not fully accessible if only the separation zones

are considered in the design of the SMB step.

The optimisation results indicate that the performance optima are characterised by the prevention of breakthroughs of shock fronts from zone *I* into zone *IV*, while the dispersive wave of the strong adsorbing component is allowed to migrate in the opposite direction. A sensitivity analysis showed that process robustness is not significantly affected by the application of a non-restrictive design, which should be useful when considering the development of control strategies for continuous chromatographic processes under reduced purity requirements. Furthermore, it is worth investigating, whether it is possible to derive algebraic design expressions from equilibrium theory for the scenario shown above. This would represent an important tool in the design of continuous chromatography.

IMPACT OF SOLUBILITY EQUILIBRIA ON ENANTIOSELECTIVE CRYSTALLISATION

The previous two chapters addressed the influence of adsorption equilibria and process design on SMB performance. Analogously, in this chapter the design of enantioselective crystallisation and the effects of the solid-liquid equilibrium (SLE) on process performance will be demonstrated. Special emphasis will be put on modelling of ternary SLE for mixtures of enantiomers in a solvent, since this is crucial for process design.

An SLE model will be derived that allows for an equilibrium-based design of enantioselective cooling crystallisation. Subsequently, the impact of the SLE on the performance of enantioselective crystallisation is investigated for the different model systems.

6.1 Modelling of Ternary Solid-Liquid Equilibria

In the following, two approaches for modelling of ternary solid-liquid equilibria (SLE) of enantiomers in a solvent will be introduced. The first model is based on thermodynamics. Such models are generally desirable, since they might allow for the *a priori* prediction of equilibria. However, it will be demonstrated that this approach does not necessarily guarantee the required accuracy. As an alternative, a second modelling approach will be suggested, which is based on the interpolation of experimental SLE data. This model is considered appropriate for practical use.

6.1.1 Thermodynamic Models

The equilibrium composition in a two-phase system can be described by the SCHRÖDER-VAN LAAR-equation [7, 140]. This relation can be derived from classical thermodynamics (iso-fugacity

condition) or from a thermodynamic cycle (considering heating of sub-cooled melts, melting, and mixing of liquids). An elaborated version of this equation reads:

$$\ln \frac{\gamma_i^L x_i^L}{\gamma_i^S x_i^C} = \frac{\Delta h_{m,i}}{RT} \left(\frac{T}{T_{m,i}} - 1 \right) + \frac{\Delta c_{p,i}}{R} \left(\frac{T_{m,i}}{T} - 1 - \ln \frac{T_{m,i}}{T} \right) \quad (i = 1, \dots, n) \quad (6.1)$$

In this equation, x_i and γ_i are the compositions and activity coefficients, respectively. The indices L and C denote the liquid and the solid (crystal) phases, respectively. T is the current temperature, while $T_{m,i}$ is the melting temperature of the pure compound. $\Delta h_{m,i}$ is the heat of fusion at $T = T_{m,i}$ and $\Delta c_{p,i} = c_{p,i}^L - c_{p,i}^S$ is the difference of the specific heats in the liquid and solid states, respectively.

Eq. (6.1) can be simplified, since $\Delta c_{p,i}$ is approximately temperature-independent and, generally, the second term is very small in comparison to the first. Usually, ideal behaviour and immiscibility can be assumed for the solid phase (*i.e.*, $\gamma_i^C x_i^C = 1$). Using these assumptions, Eq. (6.1) reduces to

$$\ln (\gamma_i^L x_i^L) = \frac{\Delta h_{m,i}}{RT} \left(\frac{T}{T_{m,i}} - 1 \right) \quad (i = 1, \dots, n) \quad (6.2)$$

In addition, the mass balance condition has to be fulfilled:

$$\sum_{i=1}^n x_i = 1 \quad (6.3)$$

On the basis of Eqs. (6.2) and (6.3), it is often possible to describe the binary melting diagram of two enantiomers that form a conglomerate (see section 2.2.2) with reasonable accuracy. In Eq. (6.2) frequently ideal behaviour of the compounds in the liquid state (*i.e.*, $\gamma_i^L = 1$) is assumed. In this case, the melting temperature of the racemate can be predicted from the melting temperatures and enthalpy of fusion of the pure enantiomers only.

For compound forming systems, the melting equilibrium between the two eutectic compositions of an enantiomeric system is described by the PRIGOGINE-DEFAY equation [7, 140, 141]:

$$-\ln(\gamma_i^L x_i^L)(1 - \gamma_i^L x_i^L) + \ln(\gamma_i^C x_i^C)(1 - \gamma_i^C x_i^C) = \frac{\Delta h_m}{R} \left(\frac{1}{T} - \frac{1}{T_m} \right) \quad i = (1, 2) \quad (6.4)$$

SLAUGHTER *et al.* [109] successfully used Eqs. (6.2) and (6.3) together with a model for γ_i^L , to calculate ternary melting equilibria of simple eutectic systems and systems with compound formation. For the latter, they did not use the PRIGOGINE-DEFAY equation (6.4), but introduced an additional relation that accounts for reactions in the solid phase. WIBOWO *et al.* published some considerations on the use of this approach for modelling multi-component SLE, including enantiomer and diastereomeric systems with dissociating solutes [108].

In principle, the model above is sufficient to describe ternary solubility equilibria of two enantiomers in solvents for systems with either conglomerates or racemic compound formation. However, there are several reasons why this model is not used in this work. First, in any case it requires a

numerical solution [109], which is not desirable for a process model. Second, applying a thermodynamically consistent model to experimental SLE data is difficult if the necessary parameters are unknown (for example, enthalpies of fusion and mixing, melting temperatures, specific heats, etc.). Finally, solubility equilibria can be distinctively non-ideal and suitable models might not be available for the corresponding activity coefficients.

The latter problem is exemplified in Fig. 6.1 which shows activity coefficients of pure mandelic acid enantiomer dissolved in water. Using SLE data (solubilities, enthalpy of fusion, and melting temperature of the pure enantiomer) from [120], the activity coefficients of mandelic acid, γ_1^L , were calculated from Eq. (6.2). The figure reveals a rather extreme course, which is possibly caused by some ionic or enantiomer–enantiomer interactions in the liquid phase. Common expressions for activities like the regular solution model, as well as the MARGULES, VAN LAAR, and NRTL models [142] do not provide for a satisfactory prediction of $\gamma_1^L(T)$; in particular at lower temperatures, where γ_1^L first rises and then drastically decreases with increasing T . Even the best-fitting model

(MARGULES) introduces deviations up to 50% (at $T > 70^\circ\text{C}$). The application of more advanced models like UNIQUAC was not possible, because necessary critical data were not available for mandelic acid. The use of group group contribution methods provided unsatisfactory results [119]. A stepwise linearisation of the activity coefficients, as was proposed by LORENZ *et al.* [120], might actually provide a better fit for $\gamma_1^L(T)$. However, this is not considered as suitable here, because the discontinuous character of such description could in turn introduce numerical difficulties in a process model.

Summarising the above, it is concluded that the *a priori* prediction of solubility equilibria for enantiomeric systems based on pure component data (enthalpies of fusion and melting temperature) remains a difficult task, since for heterogeneous multi-component equilibria there is usually a lack of data that allow for the prediction of deviations from ideal phase behaviour. This is particularly true if essential solute properties (*e.g.*, data on the critical point) are not known.

6.1.2 SLE Model based on Solubility Approximation

Because of the problems related to the application of a thermodynamic model (see previous section), an alternative SLE modelling approach suitable for practical implementation is suggested.

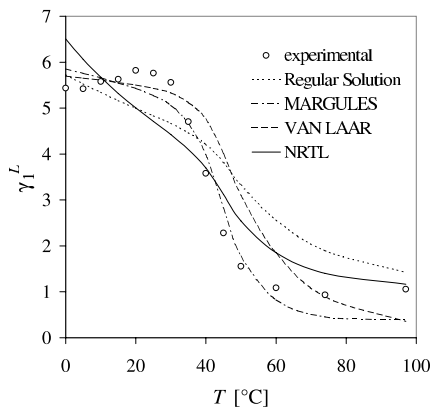


Figure 6.1. Activity coefficients for pure mandelic acid enantiomer dissolved in water. Symbols – γ_1^L from experimental data. Lines – different models for activity coefficients.

Concept

The model is based on the interpolation of solubility data and a linearisation between different solubilities. A major advantage of this approach is that it can be applied directly to experimental solubility data. Further parameters (*e.g.*, activity coefficients or pure component properties) are not required.

The main assumption of the concept is that isothermal solubility limits of mixtures between the eutectic through¹ and pure dissolved enantiomer (*i.e.*, $P_e \leq P \leq 1$) can be described by linear functions. This will be explained using again experimental data for the system mandelic acid / water (Fig. 6.2).

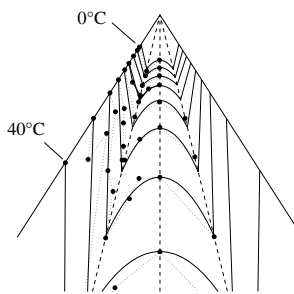


Figure 6.2. Experimental data for mandelic acid solubilities in water between 0 and 40 °C (inset of Fig. 3.5). Data (dotted lines with circles) and fit by SLE model (solid lines).

For this rather well-studied system (experimental data from [120]), a reasonable number of equilibrium points with intermediate purity are known. From the figure, two important aspects can be deduced: *i*), the eutectic composition ($P_e = 0.69$) is independent of temperature, and *ii*), isothermal mixture solubilities for $P_e \leq P \leq 1$ indeed follow – besides small deviations – straight lines. This was also stated by LORENZ *et al.* [120].

should yield a straight line for the solubility limit, the activity coefficient γ_1^L needs to be constant. That is, interactions between the dissolved enantiomer 1 and the solvent, as well as interactions between to two enantiomers, must remain constant for $T = \text{const.}$ and $P_e \leq P \leq 1$. This is a reasonable assumption, in particular for lower temperatures, where each solubility isotherm covers only a small concentration range. Furthermore, it might be expected that interactions of the two dissolved enantiomers are independent of enantiomeric purity.

The assumption of a linear course of the isothermal solubility between eutectic through and enantiomerically pure solution can be supported when considering Eq. (6.2). If this equation

As a consequence of the above it is sufficient to model the temperature dependence of the solubilities of the pure enantiomer, $x_{1,p}(T)$, and of the same enantiomer along the eutectic through, $x_{1,e}(T)$. Subsequently, intermediate points with $P_e \leq P \leq 1$ can be calculated from a linearisation between $x_{1,p}(T)$ and $x_{1,e}(T)$. Note that, since phase diagrams of enantiomeric systems are perfectly symmetric, it is sufficient to model only one half of a ternary or binary phase diagram – the second results from simple reflection over the racemic composition line. Therefore, in the following derivations only enantiomer 1 will be considered.

¹ For a fundamental introduction to ternary SLE of enantiomers in solvents see section 2.2.2.

Interpolation of Solubility and Linearisation

To approximate the experimental solubilities of enantiomer 1 for the pure enantiomer ($P^L = 1$) and along the eutectic through ($P^L = P_e$), the following polynomials were applied:

$$x_{i,j}(T) = \sum_{k=1}^5 a_{k,j} T^k \quad (j = p, e, r) \quad (6.5)$$

Note that the solubility along the racemic through, $x_{1,r}(T)$, is needed only if the whole ternary diagram should be plotted.

Once the parameters of the polynomials are known, the mixture compositions of an isothermal solubility limit, $x_i^*(T)$, can be described by the linearisation

$$x_1^*(T, \bar{x}_i) = \psi x_{1,p}(T) + (1 - \psi) x_{1,e}(T) \quad (6.6a)$$

$$x_2(T, \bar{x}_i) = (1 - \psi) \frac{1 - P_e}{P_e} x_{1,e}(T) \quad (6.6b)$$

Here ψ is a running parameter with $\psi = 1$ for $P^L = 1$ and $\psi = 0$ for $P^L = P_e$, respectively. If the purity of the saturated solution, P^L , is known, one can eliminate x_1^* and x_2 from Eqs. (6.6), since $x_2 = x_1^*(1 - P^L)/P^L$. One obtains the following useful expression for the linearisation factor ψ as a function of purity and temperature

$$\psi(T, P^L) = \frac{1}{1 + \frac{x_{1,p}(T)}{x_{1,e}(T)} \cdot \frac{P_e(1 - P^L)}{P^L - P_e}} \quad (6.7)$$

Note that in the above all enantiomeric purities are defined with respect to enantiomer 1.

The solubility approximations for the system mandelic acid / water are shown in Fig. 3.5 (right). The fit is considered to be good. By substitution of these polynomials into the linearisation Eqs. (6.6), the isothermal solubility limits can be plotted in the ternary diagrams. This is shown in Fig. 3.5 (left). A good overall agreement between experimental values and prediction can be concluded; in particular, when considering that the mandelic acid / water system actually represents the system with the strongest deviations from ideal behaviour (see previous section) and that the data points are scattered due to limited experimental accuracy [120].

Note that an analogous procedure was applied for calculating the parabolic lines between the two eutectic throughs in Fig. 3.5 (left). The solubility of enantiomer 1 at racemic composition was interpolated from Eq. (6.5) with $j = R$. Instead of the linearisation (6.6), a quadratic function was used. This is in correspondence to the quadratic PRIGOGINE-DEFAY equation (6.4) for compound forming systems. However, the region described by this border is not of interest if only the pure enantiomer should be crystallised. Note further, that the same modelling approach holds for conglomerate systems (here $P_e = P_r = 0.5$).

The solubility interpolations and the resulting model predictions for all experimental systems are included in Chapter 3 (Figs. 3.3 – 3.5, 3.8, and 3.10). The according polynomial coefficients and

temperature ranges are summarised in Tab. B.2. The coefficients were determined by minimising the sum of the absolute values of the relative errors. This was found to improve the fit in the lower temperature range, which is important when designing practical crystallisation processes.

Remarks

It was found useful to model all SLE in terms of mass fractions rather than concentrations, because this allows to subsequently introduce corrections for the liquid density (this aspect will be discussed later; see section 6.3.4). Furthermore, since for the model system III the molar weight is not known, mole fractions could not be used.

The solvent was always treated as a single component, independently whether it actually represents a mixture of different liquids or not.

The reader will have noticed that for the system mandelic acid / water the SLE was modelled only up to 40 °C. There were several reasons for this, namely the decreasing accuracy of the experimental data at higher temperatures [120], the low number of data points at these temperatures, and the decreasing accuracy of the polynomial solubility interpolations. It should be noted that a thermodynamic model suffers from the same shortcoming, since it would provide accurate predictions only if a detailed model for the activity coefficients is available (see Fig. 6.1).

6.2 Equilibrium Design of Enantioselective Crystallisation

Below the application of the SLE model from section 6.1.2 will be demonstrated to design enantioselective cooling crystallisation processes. In order to simplify the discussion, all derivations will be made with respect to the process example in Fig. 6.3.

In the example, an initial mixture (index 0) is concentrated by removal of solvent (*e.g.*, by evaporation or reverse osmosis) in order to achieve a suitable concentration level for crystallisation. The resulting stream (F) is introduced into a continuous crystalliser that has an operating temperature $T = T^L$. The mixture decomposes into a solid phase that contains only the desired enantiomer 1 (point C) and the remaining mother liquor in equilibrium (point L). Maximum yield of pure solid enantiomer is achieved if the operating temperature is lowered to $T = T_e$ (point E). This temperature obviously represents an important quantity, because it also represents the minimum temperature allowed when pure enantiomer has to be guaranteed.

Considering the process shown in the figure, obviously two main design questions arise: *i*) the determination of equilibrium *compositions* (*e.g.*, in points F , L , or E), and *ii*) the determination of according equilibrium *temperatures*. Both can be determined on the basis of Eqs. (6.5) – (6.7). Compositions can be derived explicitly from the SLE model, see section 6.2.2. This represents an advantage in comparison to a thermodynamic model, which does not provide explicit expressions.

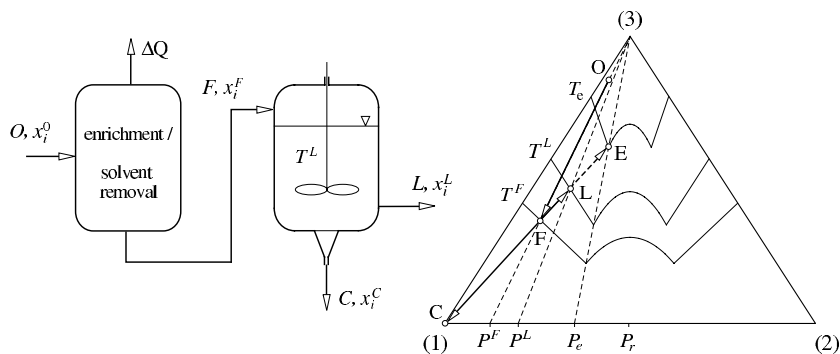


Figure 6.3. Enantioselective crystallisation. Left – continuous crystalliser decomposing a feed (F) into solid product (C) and mother liquor (L). Component 1 corresponds to the target enantiomer. Right – ternary representation of the process.

6.2.1 Mass Balances and General Relations

The global mass balance around the crystalliser in Fig. 6.3 reads

$$F = C + L \quad (6.8)$$

where F , L , and C denote the total masses of feed, mother liquor, and crystals, respectively. Since only enantiomer 1 crystallises, for the mass fractions in the crystal phase hold $x_1^C = 1$ and $x_2^C = 0$. From this and Eq. (6.8) one obtains the following mass balances for the two enantiomers:

$$F x_1^F = C + (F - C) x_1^L \quad (6.9a)$$

$$F x_2^F = (F - C) x_2^L \quad (6.9b)$$

An equation for the third component (the solvent) is obsolete, since $\sum x_i = 1$. The enantiomeric purity will be defined with respect to component 1, *i.e.*,

$$P^j = \frac{x_1^j}{x_1^j + x_2^j} \quad j = (F, L, C) \quad (6.10)$$

From the above equations it follows for the mass of pure solid enantiomer, $m_1^C = C$,

$$m_1^C = F x_1^F \frac{P^F - P^L}{P^F(1 - P^L)} \quad (6.11)$$

Since $F x_1^F = m_1^F$ corresponds to the mass of the same enantiomer introduced with the feed, from this equation an expression for the yield of the crystallisation process, $Y = m_1^C / m_1^F$, can be derived. Eq. (6.11) readily delivers for Y

$$Y = \frac{m_1^C}{m_1^F} = \frac{1}{P^F} \frac{P^F - P^L}{1 - P^L} \quad (6.12)$$

Furthermore, from Eq. (6.9) and Eq. (6.10), Y can also be obtained in terms of mass fractions:

$$Y = \frac{1}{x_1^F} \frac{x_1^F - x_1^L}{1 - x_1^L} \quad (6.13)$$

As will be shown below, (6.12) and (6.13) are very useful expressions for the design and evaluation of enantioselective crystallisation processes.

6.2.2 Determination of Compositions

From Eqs. (6.9) and (6.10) any equilibrium composition along the mass balance line C–F–L–E in Fig. 6.3 can be determined, if one composition along this line plus one additional parameter (like temperature, purity, or composition) is specified. Below some typical design examples will be explained.

Compositions from Specified Purities

A common situation in the design of an enantioselective crystallisation process is to determine the composition of the mother liquor (see point L in Fig. 6.3) from a given feed (point F). If the desired purity, P^L , is specified, x_1^L can easily be calculated. From Eqs. (6.10) and (6.13) one obtains

$$x_1^L(x_1^F, P^L, P^F) = x_1^F \frac{1 - Y(P^F, P^L)}{1 - x_1^F Y(P^F, P^L)} \quad (6.14a)$$

$$x_2^L(x_1^F, P^L, P^F) = x_1^L \frac{1 - P^L}{P^L} \quad (6.14b)$$

Note, that $Y(P^F, P^L)$ has to be calculated from Eq. (6.12). For the important case that the process should deliver maximum yield, the according compositions $x_i^L = x_{i,e}$ follow from the above equations with $P^L = P_e$.

Another important task is to calculate the mass fractions of the feed as a function of the purity if the composition of the mother liquor is known. In this case, Eq. (6.14 a) can be re-arranged to

$$x_1^F(x_1^L, P^L, P^F) = x_1^L \frac{1}{1 - (1 - x_1^L)Y(P^F, P^L)} \quad (6.15a)$$

$$x_2^F(x_1^L, P^L, P^F) = x_1^F \frac{1 - P^F}{P^F} \quad (6.15b)$$

Please note, that these expressions provide no statement whether these compositions can actually be achieved within the temperature range of the SLE. For a verification, the corresponding equilibrium temperatures must be determined. This will be explained in section 6.2.3.

Compositions from Specified Temperatures

Often the operating temperature of the process, T^L , will be fixed from some practical considerations. If the purity of the mother liquor, P^L is not known, but a value for the feed purity, P^F , is given, the composition of the mother liquor, x_i^L , can be calculated from Eqs. (6.6), (6.7), and (6.9a):

$$x_1^L(T^L, P^F) = \frac{P^F(1 - P_e)k_{e,F}(1 - x_1^F) + P_e(1 - P^F)(k_{e,F} - k_{p,F})}{x_{1,e}(T^L)P^F(1 - P_e) + k_{e,F}(P_e - P^F) - P_e k_{p,F}(1 - P^F)} \quad (6.16)$$

$$\text{where } k_{i,j} = x_{1,i}(T^L)x_{1,j}(T^L), \quad i, j = (p, e, F)$$

where $x_{1,p}(T^L)$ and $x_{1,e}(T^L)$ have to be determined from Eq. (6.5). For the purity of the solution at equilibrium one finds:

$$P^L(T^L, P^F) = \frac{k_{p,e}(1 - x_1^F)P^F(1 - P_e) - k_{p,F}P_e(1 - P^F) + k_{e,F}P_e(1 - P^F)}{k_{p,e}(P^F - x_1^F)(1 - P_e) - k_{p,F}P_e(1 - P^F) + k_{e,F}(1 - P^F)} \quad (6.17)$$

The mass fraction of the counter-enantiomer, x_2^L , then can be calculated from (Eq. 6.14b).

6.2.3 Determination of Temperatures

As was shown above, equilibrium concentrations can easily be calculated from simple expressions, if a composition along the mass balance line C–F–L–E in Fig. 6.3 is known. However, another important task is the determination of operating temperatures that correspond to pre-defined compositions.

If a composition is specified, the equilibrium temperature can be determined from the roots of Eqs. (6.5). However, since the linearisation factor ψ and $x_{1,j}$ in Eq. (6.5) are usually unknown, it is expedient to use a simple iteration procedure. For example, if operating point L in Fig. 6.3 is known (*i.e.*, x_1^L and P^L are specified), from an estimated value for the temperature, T , the solubilities $x_{1,p}(T)$ and $x_{1,e}(T)$ are calculated according to Eqs. (6.5). The linearisation factor ψ follows from Eq. (6.7) and a value for $x_{1,\text{calc}}^L$ from Eq. (6.6). T is changed iteratively until $x_{1,\text{calc}}^L = x_1^L$. No convergence problems were encountered when using this approach.

Some aspects should be considered during the calculation of equilibrium temperatures. *i)* It must be verified that determined temperature values lie within the temperature interval where the SLE model is valid. *ii)* A working temperature of $T = T_e$ provides maximum yield. However, during design it should be taken into account, that T_e represents a critical property, because temperatures $T < T_e$ will lead to the crystallisation of the counter-enantiomer.

In the next section, the performance of enantioselective crystallisation will be evaluated for the three model systems. The determination of the critical temperature T_e and the design restrictions that follow from the limited temperature intervals of the SLE models will be included in the discussion.

6.3 Performance of Crystallisation for the Model Systems

6.3.1 Theoretical Yield

The most important performance parameter in an enantioselective crystallisation is the yield for the target component. The highest yield, Y_{\max} , is obtained if the mother liquor just reaches eutectic composition (*i.e.*, if $P^L = P_e$). Thus, for Y_{\max} follows from Eq. (6.12)

$$Y_{\max} = \frac{1}{P^F} \frac{P^F - P_e}{1 - P_e} \quad (6.18)$$

The dependence of the yield on feed purity is shown in Fig. 6.4 for the different model systems. Parameter is the eutectic composition, P_e . It can be seen that Y decreases strongly with lowering feed and increasing eutectic purity, respectively. For example, since in the case of the conglomerate systems threonine and PDE (systems II and III) the eutectic purity is $P_e = 0.5$, a feed purity of $P^F = 0.8$ allows for a yield of 75%. In contrast, for the compound-forming mandelic acid systems it is $P_e = 0.69$. For the same feed purity only a yield of 41% can be achieved.

An important conclusion from the above with respect to the process combination of chromatography and crystallisation is that the SMB should deliver streams with high purity to achieve high yields in the crystallisation step. However, since the performance of SMB improves when lowering the purity requirements (see Chapters 4 and 5), it can be expected that these contrary effects lead to an intermediate value for the optimal transition purity between the two processes. Furthermore, since Y is limited by the eutectic composition, P_e , and the costs for chiral feed material are usually high, it is useful to recycle unresolved mother liquor from crystallisation back to the SMB unit. This recycle causes an additional load on the SMB process and has a major impact on overall process performance (see Chapter 7).

6.3.2 Operating Temperatures

Figure 6.4 emphasises that maximum yield is achieved if the operating of the crystalliser is adjusted to $T^L = T_e$. However, for all model systems studied the temperature range of the ternary SLE is limited. An important consequence of this is that achievable compositions and yields are also limited.

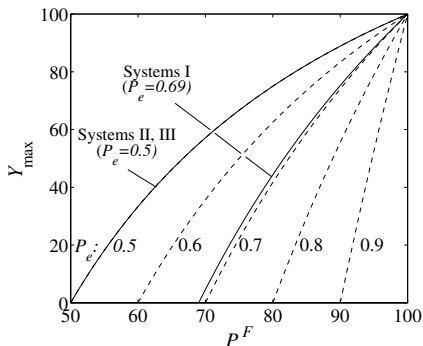


Figure 6.4. Theoretical yield of crystallisation, Y_{\max} , as function of feed purity and position of the eutectic.

Using the iterative procedure explained in section 6.2.3, feasible operating temperatures for maximum yield can be calculated as a function of the feed composition. An example is shown in Fig. 6.5 for the system mandelic acid / water.² To construct the diagram, the feed purity, P^F , and its equilibrium temperature, T^F , were varied. For each pair (P^F, T^F) , the corresponding equilibrium temperature along the eutectic through, $T^L = T_e$ was determined as follows: first, the feed composition, x_i^F was calculated from Eqs. (6.5) – (6.7). The according mother liquor composition then followed from Eqs. (6.14) with $P^L = P_e$. Finally, the temperature $T^L = T_e$ was obtained iteratively.

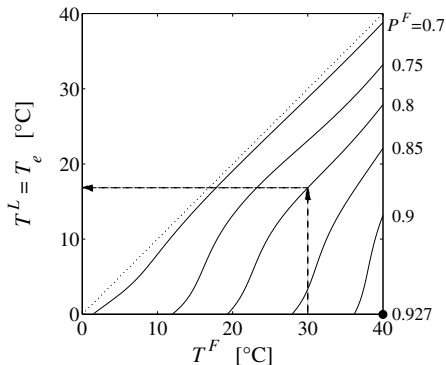


Figure 6.5. Operating temperature diagram for enantioselective crystallisation of mandelic acid in water. Parameter: feed purity, P^F ; circle – P^F_{\max} .

The diagram contains two important information: *i*) For given feed compositions, the operating temperatures for maximum yield can be determined. In the example marked by the arrows in Fig. 6.5, a feed stream saturated at $T^F = 30^\circ\text{C}$ and a purity of $P^F = 0.8$ requires a crystallisation temperature of $T^L = T_e = 17^\circ\text{C}$ to reach the eutectic through. Analogously, if a certain crystallisation temperature is given, the diagram allows to choose T^F and P^F , from which the feed compositions can be calculated. *ii*) The highest feed purity that still allows to reach $P^L = P_e$ is denoted by the point in the lower right (in the example $P^F_{\max} = 0.927$). Any higher feed purity will lead to a mother liquor with $P^L > P_e$ and, thus, to $Y < Y_{\max}$. This important aspect will be discussed below.

The corresponding diagrams for the other experimental systems are given in Figs. 6.6 a–d. The values for P^F_{\max} differ significantly. Furthermore, while for system II (threonine, Fig. 6.6 c) the purity-isopleths are almost linear, a certain nonlinearity can be observed for the other systems.

6.3.3 Yield Limitation and Stepwise Crystallisation

As already mentioned, the yield is limited by the temperature interval of each SLE. The highest yield that can be achieved in a crystallisation step can be calculated from Eq. (6.12) by using $P^F = P^F_{\max}$ and $P^L = P_e$. The values for P^F_{\max} are given in Figs. 6.5 and 6.6, respectively. The results for the different model systems are shown in Fig. 6.7. For systems I and III, the yields are in the range of 82%...98%. However, for system II (threonine) the change of solubilities is very low in the temperature interval of the SLE (see Fig. 3.8). Due to this fact, for this system only an unsatisfactory value of $Y = 54.4\%$ can be achieved.

² For corresponding SLE see section 3.1.2.

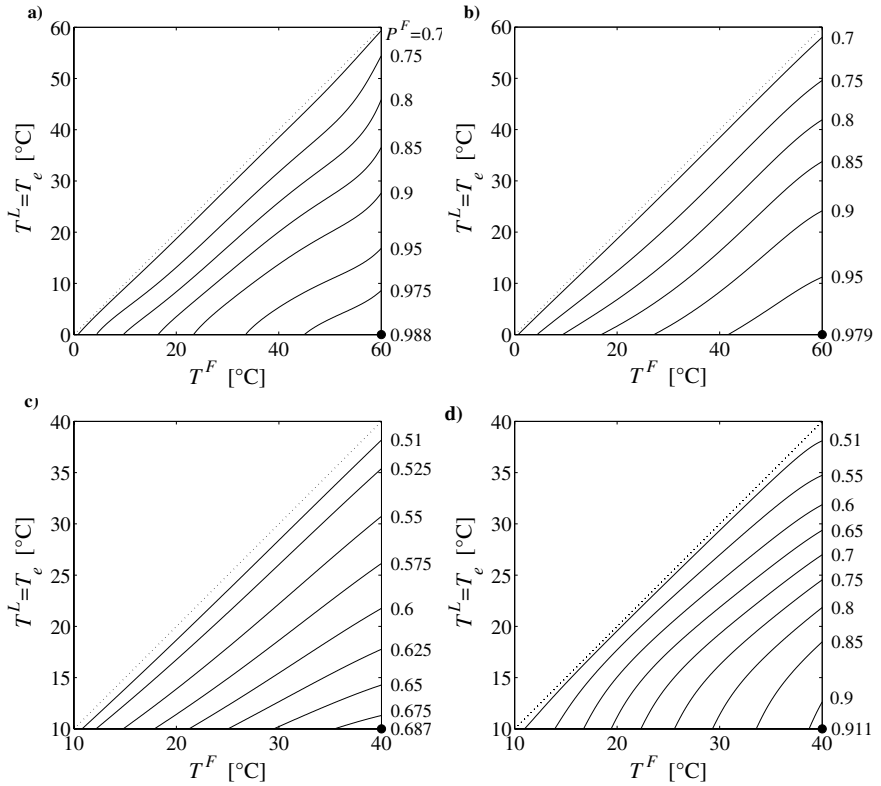


Figure 6.6. Operating temperature diagrams for the model systems. a) Systems I.b, I.f; b) system I.e; c) system II; d) system III. For notation see Fig. 6.5. The corresponding SLE data are given in Chapter 3.

A possible solution for this limitation is a process with alternating steps of crystallisation and solvent removal. Since this allows to use feed purities with $P^F > P^F_{\max}$, a maximum theoretical yield, Y_{\max} , can be achieved that is defined by Eq. (6.18).

Figure 6.8 shows such a process for the example of the strongly limited system II. In the first crystallisation step, the initial feed solution is used and equilibrium is reached at the minimum temperature of $T = 10$ °C. Then, the solution is heated up to 40 °C and solvent is removed until the mother liquor reaches equilibrium again. The next crystallisation is again performed at 10 °C. These steps are repeated until the eutectic through is reached (in the example at $T = 29$ °C). The figure also contains the purities in each crystallisation step and the development of the overall yield during the process. These values were determined from the design procedures given in section 6.2.

It should be noted, that an evaporative crystallisation process might be an alternative way to handle yield limitations. However, in this case the rate of solvent removal must be carefully adjusted to guarantee $P^L < P_e$.

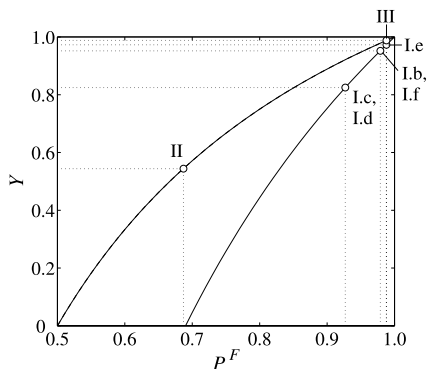


Figure 6.7. Maximum one-step yields of crystallisation for the model systems.

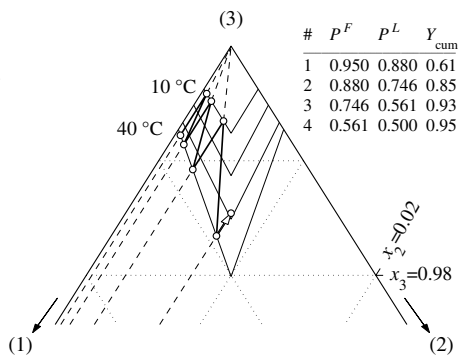


Figure 6.8. Example for stepwise cooling crystallisation to achieve Y_{max} (system II, initial feed purity of $P^F = 0.95$).

6.3.4 Considerations on Solution Density and Concentrations

In order to provide for "compatibility" with typical mathematical models for chromatographic processes, it will often be necessary to specify compositions in terms of concentrations. To convert mass fractions into concentrations, the density of the solution, ρ , must be known. Then

$$c_i = x_i \rho(T, x_i) \quad (6.19)$$

Unfortunately, the dependence of the liquid density in Eq. (6.19) on the amounts of dissolved components is usually not known. For a prediction of the density data on the critical point of the dissolved components are necessary. These are not available for the enantiomeric systems studied here.

The dependence of density on the amount of dissolved solute was investigated experimentally for aqueous solutions of racemic mandelic acid. Figure 6.9 shows measured liquid densities at 20 °C. The density rises only slightly with increasing concentration. At the rather high value of $x_r = 0.25$ the density deviation from pure water is only 5.7% .

The experimental determination of the density as a function of concentration and temperature for all model systems was beyond the scope of this work. It would be most efficient to collect such data during solubility measurements. As a simplification, in this work it will be assumed that the solution density is constant and corresponds to that of the pure chromatographic solvent, ρ_{sol} , at standard conditions ($T = 25$ °C). This assumption is supported by the low deviations for the mandelic acid system above. The results of the corresponding measurements for all systems are listed in Tab. B.9.

6.3.5 Specific Solvent Removal in a Process Combination

In the process combination, crystallisation is applied to a stream delivered by chromatography. Typically, the concentration levels of a chromatographic process are well below those in crystallisation. For all model systems studied here it is necessary to increase the concentration of the enantiomers before starting a cooling crystallisation. For this purpose, a certain fraction of the solvent has to be withdrawn, which is also indicated in Fig. 6.3. This enrichment will usually be performed by means of distillation or pervaporation.

As a quantification for the efforts related to this, the specific solvent removal, SR , is introduced. SR will be defined as the ratio of the amount of solvent that has to be removed and the mass of crystals created in crystallisation, m_1^C . From this definition and Eq. (6.12), SR can be expressed as a function of the composition of the initial process stream and of the yield of the crystallisation:

$$SR = \frac{Q^0 - Q^F}{Y m_1^F} \quad (6.20)$$

The indices 0 and F denote the streams before and after the enrichment unit, respectively (see Fig. 6.3). Since the enrichment unit should remove only solvent, the mass of enantiomers in the solution remains constant (*i.e.*, $m_1^0 = m_1^F$). From this and Eq. (6.19) follows

$$Q^0 \rho^0 x_1^0 = Q^F \rho^F x_1^F \quad (6.21)$$

One obtains for SR from Eqs. (6.20) through (6.21) and the yield expression (6.12):

$$SR = \frac{1}{Y} \cdot \frac{\rho^F x_1^F - \rho^0 x_1^0}{\rho^F \rho^0 x_1^F x_1^0} \quad (6.22)$$

A Priori-Estimation for the Model Systems

A first estimation of the specific solvent removal for the different model systems can be performed on the basis of Eq. (6.23).

For the estimation it was assumed that the outlet concentrations of the SMB process are approximately equal to its feed concentrations. Since the highest productivity of an SMB process is achieved for the highest feed concentration (see section 4.4.3), the highest value will be used of the concentration range for each adsorption isotherm (*i.e.*, $c_1^0 = c_{\max}$). Furthermore, since it was assumed that the liquid density is equal to the density of the solvent, it holds $\rho^F = \rho^0 = \rho_{\text{sol}}$. Finally, conditions

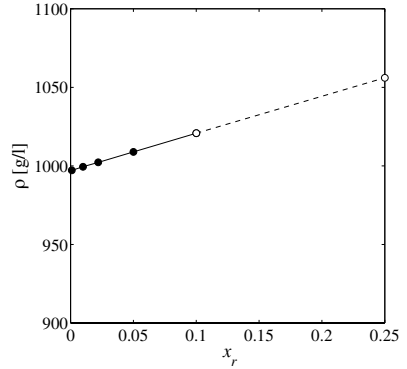


Figure 6.9. Liquid density as function of concentration (racemic mandelic acid/water, 20 °C). Note, that at $x_r = 0.25$ the solution already contained few small crystals.

for maximum yield in crystallisation were assumed (*i.e.*, $P^L = P_e$ and $P^F = P_{\max}^F$). Using these assumptions, from Eqs. (6.12) and (6.22) follows

$$SR = \frac{c_1^F - c_1^0}{c_1^F c_1^0} \cdot \frac{P_{\max}^F (1 - P_e)}{P_{\max}^F - P_e} \quad (6.23)$$

The feed concentration, c_1^F , was calculated from Eqs. (6.5), (6.7), and (6.19) using $P^L = P_{\max}^F$ and the maximum temperatures that were determined in section 6.3.2. Values for c_{\max} and ρ_{sol} can be found in Chapter 3 and Tab. B.9, respectively.

Figure 6.10 shows that the specific solvent removal is inversely proportional to the concentration presumably delivered by the SMB and that SR increases strongly for very low c_1^0 . It is noticeable that the values for SR follow almost perfectly a common course. An analysis of Eq. (6.23) reveals that – for the values used here – c_1^0 has the dominating influence.

It should be emphasised that the above results represent only a rough approximation, since the outlet concentrations of SMB processes depend on the actual operating conditions and decrease with increasing purity. Furthermore, for LANGMUIR adsorption isotherm, the extract stream usually does not reach the concentration level of the chromatographic feed. However, the estimation gives a fair basis for a first comparison.

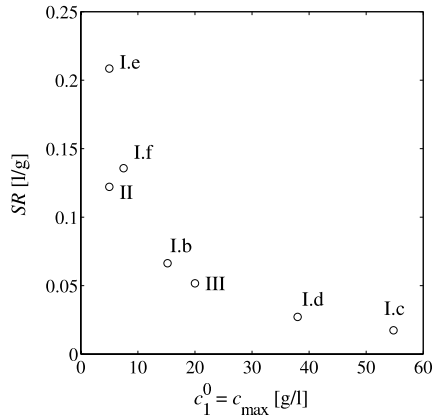


Figure 6.10. Specific solvent removal for the model systems under conditions for maximum yield.

6.3.6 Supersaturation

The supersaturation is a fundamental variable in crystallisation processes, since it represents the driving force for crystal growth and nucleation (see section 2.2).

The highest supersaturation that can occur in a crystalliser connected to an SMB process was estimated for the model systems. For this purpose, a similar procedure as in section 6.3.5 was applied. Using again the parameters for maximum yield, Eq. (2.27) delivers for σ_1 :

$$\sigma_1 = \frac{c_1^F - c_{1,e}}{c_1^F} \quad (6.24)$$

The results are summarised – together with other performance factors – in Tab. 6.1. The supersaturation differs significantly for the model systems, and a few rather high values were obtained ($1.2 \leq \sigma_1 \leq 8.6$).

It should be noted, that for the continuous crystallisation processes which are in the scope of this work, σ_1 represents the *local* supersaturation at the feed inlet of the crystalliser. The supersaturation in the bulk depends on the residence time and will be much lower. Therefore, even the values for σ_1 found for systems I.b and I.f might be applicable in a practical process. However, since such high local supersaturations might cause undesired nucleation, it might be expedient to apply a series connection of crystallisers with descending operating temperatures in order to limit local supersaturations.

6.3.7 Summary of Performance for the Model Systems

In order to simplify a comparison between the different model systems, the design and performance parameters determined in this chapter are summarised in Tab. 6.1. The results in the table correspond to the conditions that are necessary to achieve maximum yield.

The individual systems show distinct differences with respect to yield, solvent removal, and local supersaturation. For example, system II allows for only 54% yield in a single crystallisation step, which is very low in comparison to the other systems. On the other hand, the low concentration range covered by the SLE of system II also facilitates a low local supersaturation of only $\sigma_1 = 1.2$, which is more appropriate for practical realisations than, for example, the high value of $\sigma_1 = 8.6$ that was estimated for system I.f.

Table 6.1. Design and performance of a crystallisation process according to Fig. 6.3 for the model systems.

| | ρ_{sol} [g/l] | P_e | P_{max}^F | T_e [°C] | T^F [°C] | c_1^0 [g/l] | c_1^F [g/l] | c_1^L [g/l] | Y_{max} | SR [l/g] | σ |
|------------------|------------------------------|-------|--------------------|---------------|---------------|------------------|------------------|------------------|------------------|---------------|----------|
| I.b | 1059 | 0.69 | 0.988 | 0 | 60 | 15.2 | 806.9 | 84.3 | 0.973 | 0.066 | 8.6 |
| I.c ³ | 997 | 0.69 | 0.927 | 0 | 40 | 54.8 | 256.1 | 57.0 | 0.825 | 0.017 | 3.5 |
| I.d ³ | 997 | 0.69 | 0.927 | 0 | 40 | 38.0 | 256.1 | 57.0 | 0.825 | 0.027 | 3.5 |
| I.e | 1010 | 0.69 | 0.979 | 0 | 60 | 5.0 | 685.9 | 92.7 | 0.952 | 0.208 | 6.4 |
| I.f | 1059 | 0.69 | 0.988 | 0 | 60 | 7.5 | 806.9 | 84.3 | 0.973 | 0.136 | 8.6 |
| II | 902 | 0.5 | 0.687 | 10 | 40 | 5.0 | 7.5 | 3.4 | 0.544 | 0.122 | 1.2 |
| III | 776 | 0.5 | 0.911 | 10 | 40 | 20.0 | 295.6 | 44.2 | 0.902 | 0.052 | 5.7 |

It should be noted, that the concentrations and supersaturations in the table should be handled with care, since *i*) the density of the solution is not known accurately (see section 6.3.4), and *ii*) the accuracy of the solubility interpolation is limited.

³ Due to a lack of SLE data, for systems I.c and I.d the surrogate SLE (mandelic acid / water, Fig. 3.5) was used.

6.4 Conclusions

This chapter addressed the design and evaluation of enantioselective cooling crystallisation processes based on an equilibrium approach. A simple ternary SLE model was established to describe the solubilities of two enantiomers in a solvent. A good agreement between predictions and experimental data was achieved. The model is considered suitable for practical implementations.

The SLE model together with the mass balances for the crystallisation process allow for an equilibrium-based design. Expressions for the most important performance parameters yield, solvent removal, and supersaturation were established as a function of distinct purity specifications, which greatly simplifies the analysis. A comparison of the results for the different model systems revealed the pronounced impact of the SLE on process performance. It should be noted that operating parameters and, accordingly, performance are limited by the specific temperature range of each SLE.

Some important conclusions with respect to a process combination of crystallisation and SMB chromatography can be drawn. To achieve high yields in crystallisation, the SMB process should deliver streams with high purities (which is contradictory to the improving performance of SMB for lower purity requirements; see Chapter 4). Furthermore, the crystallisation yield is maximised if the composition of the mother liquor just reaches the eutectic through. This aspect deserves experimental investigation. Finally, the solvent removal between the two processes depends strongly on the concentration level delivered by the SMB and, to a lower extent, on the purity of the SMB outlet and the mother liquor, respectively. This interplay between the two unit operations will be investigated in more detail in the following chapter.

EVALUATION AND DESIGN OF THE PROCESS COMBINATION

The behaviour and the design of the single unit operations SMB chromatography and enantioselective crystallisation was investigated in the previous chapters. It was demonstrated in Chapters 4 and 5 that a certain economic potential results from reduced purity requirements in SMB processes, which might be further increased by an according design. On the other hand, the results of Chapter 6 indicate that the constricted yield in crystallisation will certainly limit the performance of the integrated process.

In this chapter, the process combination is studied as a whole. The two contrary effects above obstruct intuition-based process analysis and constitute a complex optimisation problem. A shortcut method is proposed that contributes to both process understanding and design, while it requires only a minimum of information.¹

7.1 Detailed Concept of the Process Combination

The basic scheme of the process combination that was introduced in Chapter 1 (Fig. 1.6) will be refined here based on the conclusions from the previous chapters. Figure 7.1 contains a suggestion for a more detailed flow chart of an integrated process of SMB chromatography and enantioselective crystallisation.

The process in the figure incorporates primarily an SMB plant (unit *I*) and two crystallisers (units *II* and *III*, respectively). An external racemic feed is introduced (*F*₀). The feed of the SMB (inlet *F*₁) is split into two fluxes – the raffinate containing an excess of the less retained enantiomer 1 (outlet *A*₁), and the extract that contains more of the stronger retained enantiomer 2 (outlet *B*₁). Note that the minimum purity of these streams corresponds to the eutectic purity (see section 2.2). The subsequent crystallisers deliver pure solid enantiomers at their corresponding outlets (*i.e.*, enantiomer 1 at *A*_{II} and enantiomer 2 at *B*_{III}, respectively). As was demonstrated in Chapter 6, recycling of mother liquor from the crystallisation back to the SMB is required for high yields.

¹ A part of the results presented in this chapter was published in [61].

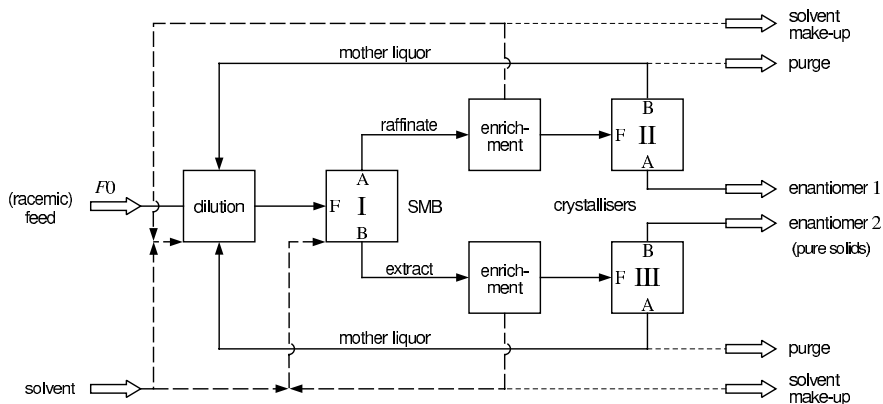


Figure 7.1. Flow chart for the combination of SMB chromatography and crystallisation. Solid lines denote streams containing the two enantiomers. Dashed lines mark fluxes of pure solvent.

Correspondingly, the scheme contains recycle streams (starting from outlets *BII* and *AIII*). Also in Chapter 6 it was found that pre-enrichment steps are necessary between the two unit operations in order to adjust appropriate concentration levels for crystallisation. In turn this means that solvent must be added to the recycle streams in order to dilute them before the SMB process. For this purpose, the solvent that is removed in the enrichment steps might be used.

Note that the type of the enrichment units in Fig. 7.1 (e.g., distillation or pervaporation) is of no particular interest in the following analysis. Note further, that the purge streams shown in the figure are optional and have to be considered only if the accumulation of impurities must be prevented.

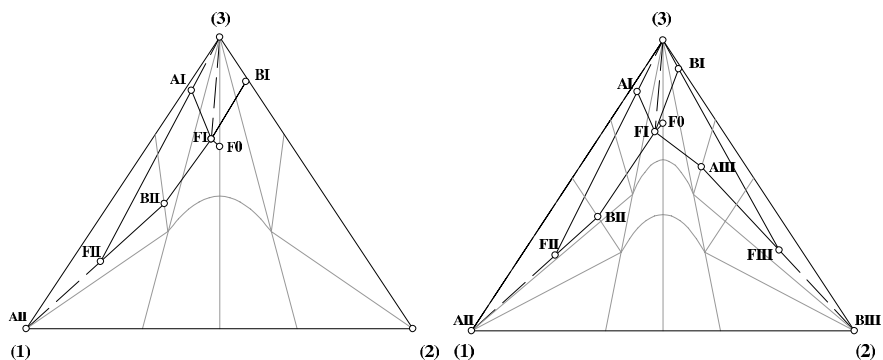


Figure 7.2. Two operating options for the process in Fig. 7.1 in the ternary diagram. Left – process for one target compound (enantiomer 1 obtained from the raffinate). Right – process with both enantiomers desired.

The main design parameters for the scheme in Fig. 7.1 are obviously the parameters (state variables) at the transition points between the SMB unit and the crystallisation step (*i.e.*, the purity and outlet compositions of the SMB and the two crystallisers, respectively). Figure 7.2 illustrates the course of composition change for distinct positions of the process scheme in Fig. 7.1. Two different configurations are considered. In the first, only enantiomer 1 is desired (Fig. 7.2, left). In this case, crystalliser *III* and the corresponding streams in Fig. 7.1 will be omitted. Note that, although there is a racemic external feed (F_0), the stream that enters the SMB (F_I) is non-racemic (asymmetric) due to the recycling of mother liquor. This has to be accounted for in model calculations. In the second configuration both enantiomers are desired (Fig. 7.2, right). Accordingly, the whole scheme in Fig. 7.1 applies. Note that in this case the adjustment of different purities in the two branches will also result in an asymmetric composition of the SMB feed in point F_I .

It is worth mentioning that a process combination as shown in Fig. 7.1 basically represents a separator network with internal recycles, which in this case involves a complex, hybrid, and nonsharp separator (unit *I*), and two rather simple, sharp separators (*II*, *III*).² It should be emphasised that networks of this type cannot be designed or evaluated on the basis of intuition only and that there is a lack of systematic studies to analyse such arrangements. Therefore, before investigating in detail the specific process combination that is subject of this work, in the next section an approach will be suggested that simplifies the formulation of mass balances for networks that include nonsharp separators. This approach will subsequently be used in section 7.3 to derive a shortcut method for evaluation and design of the process combination discussed here.

7.2 Mass Balancing Approach for Separator Networks

The process shown in Fig. 7.1 involves three components – the two enantiomers that have to be separated, and the solvent that is necessary to perform this task. At a first stage, the solvent might be considered as an auxiliary and therefore disregarded. This reduces the problem to be examined to a binary separation. Furthermore, here the steady-state performance of the system is of main interest. These two aspects greatly simplify the derivation of expressions for steady-state mass balances of networks with nonsharp binary separators and recycles.

7.2.1 Nonsharp Binary Separators

Fig. 7.3 shows a single unit for the separation of two components (1 and 2). The module basically consists of a feed node (F) and two outlet nodes (A , B). Since here no restrictions are applied

² In chemical engineering a *nonsharp* separator is a process with outlet streams that may contain all of the feed components. In contrast, *sharp* separators perform at least one perfect (sharp) split between these components (*i.e.*, at least one of the product streams contains only a pure component). Thus, the sharp separator is a special case of the nonsharp separator.

with respect to the outlet purities, this unit is a nonsharp binary separator. In the special case that it delivers one or two pure outlet streams, it represents a sharp binary separator.

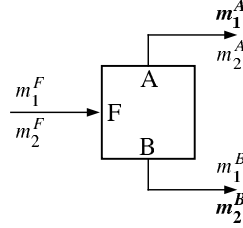


Figure 7.3. Single nonsharp binary separator with inlet and outlet nodes.

The compositions (or purity, respectively) at the three nodes j of the module, P^j , will be defined with respect to their target components - compound 1 at outlet A and compound 2 at outlet B , respectively. The composition of the feed is defined (arbitrarily) with respect to component 1:

$$P^A = \frac{m_1^A}{m_1^A + m_2^A} \quad (7.1a)$$

$$P^B = \frac{m_2^B}{m_1^B + m_2^B} \quad (7.1b)$$

$$P^F = \frac{m_1^F}{m_1^F + m_2^F} \quad (7.1c)$$

where m_i^j denotes the mass or molar flux of component i at node $j = (A, B, F)$. Obviously, for a "successful" separation holds $P^A > P^F$ and $P^B > (1 - P^F)$. The target component fluxes leaving the unit, m_1^A and m_2^B , depend on the inlet fluxes m_i^F and the values for the purity, P^j . The following relative mass fluxes, y_i , can be defined for the target compounds:

$$y_1(P^j) = \frac{m_1^A}{m_1^F} \quad (7.2a)$$

$$y_2(P^j) = \frac{m_2^B}{m_2^F} \quad (7.2b)$$

These y_i can be denoted as segregation factors [143]. The definitions 7.2 are useful, because in the case of a binary separator, the segregation factors obviously correspond to the yields achieved at the outlets for the two components. It is straightforward to show that from mass balances around the unit illustrated in Fig. 7.3 follows

$$y_1 = \frac{P^A}{P^F} \cdot \frac{P^F + P^B - 1}{P^A + P^B - 1} \quad (7.3a)$$

$$y_2 = \frac{P^B}{1 - P^F} \cdot \frac{P^A - P^F}{P^A + P^B - 1} \quad (7.3b)$$

Thus, the relative fluxes of the target components now are given with Eqs. (7.1) – (7.3). For the fluxes of the non-target compounds (component 2 at outlet A and component 1 at outlet B , respec-

tively) holds

$$\frac{m_1^B}{m_1^F} = 1 - y_1 \quad (7.4a)$$

$$\frac{m_2^A}{m_2^F} = 1 - y_2 \quad (7.4b)$$

It is important to note that the segregation factors in Eqs. (7.2) through (7.4) are functions of the compositions at the characteristic nodes only. Therefore, the specification of the purities at the nodes of a unit is sufficient to determine all relative fluxes of this unit. Similar approaches are well known in chemical engineering problems. For example, DOHERTY and MALONE [144] used a comparable method for the modelling of flash cascades.

7.2.2 Networks of Nonsharp Separators with Recycles

The conventions made above for a single binary separator provide a basis for the analysis of networks of nonsharp binary separators. Fig. 7.4 shows two simple examples of such networks. The units are connected via the outlets of unit *I* (dashed lines mark possible recycles).

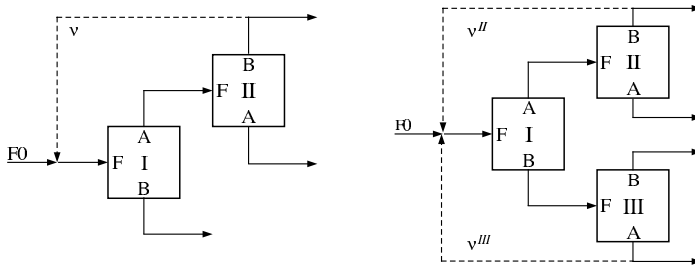


Figure 7.4. Simple networks of binary separators with and without recycles.

One can establish relations for all relative fluxes m_i^{jk}/m_i^{FI} as a function of the y_i^k given by Eqs. (7.3) (j denotes the node, $j = F, A, B$, of the k th unit, $k = I, II, \dots$). As an example, in the following derivations the relative outlet flux of component 1 at outlet *AII*, m_1^{AII} , will be considered.

The balancing of the system in Fig. 7.4 (left) is straightforward. If there is no recycle stream, one obtains for m_1^{AII}

$$\frac{m_1^{AII}}{m_1^{F0}} = \frac{m_1^A}{m_1^{FI}} = y_1^I y_1^{II} \quad (7.5)$$

If a recycle stream is turned on, it can be shown that

$$\frac{m_1^{AII}}{m_1^{F0}} = \frac{y_1^I y_1^{II}}{1 - \nu y_1^I (1 - y_1^{II})} \quad (7.6)$$

In this equation, ν is the recycle ratio, which is defined as

$$\nu = \frac{m_i^{BII}}{m_i^{AI}} \quad (7.7)$$

Now the system with three units in Fig. 7.4 (right) will be considered. If there are no recycles, for the mass flux m_1^{AII} still holds Eq. (7.5). For the case that the two recycles are turned on, one finds

$$\frac{m_1^{AII}}{m_1^{F0}} = \frac{y_1^I y_1^{II}}{1 - \nu^{II} y_1^I (1 - y_1^{II}) - \nu^{III} y_1^{III} (1 - y_1^I)} \quad (7.8)$$

It should be noted that in order to calculate the segregation factors for unit I from Eqs. (7.3), the feed composition of this unit, P^{FI} , must be specified. This composition can differ from the composition of the external feed, P^{F0} , since it depends on the recycle streams. From a mass balance around the feed node one obtains the following general expression for this composition:

$$P^{FI} = \frac{K^I K^{II} K^{III} + \nu^{II} K^{III} (1 - P^{BI}) (P^{AI} - P^{AII}) (1 - P^{BII} - P^{F0}) + \nu^{III} K^{II} P^{AI} (P^{AIII} - P^{F0}) (P^{BIII} - P^{BI})}{K^I K^{II} K^{III} + \nu^{II} K^{III} (P^{AI} - P^{AII}) (1 - P^{F0} - P^{BII}) + \nu^{III} K^{II} (P^{AIII} - P^{F0}) (P^{BIII} - P^{BI})} \quad (7.9)$$

$$\text{where } K^k = 1 - P^{Ak} - P^{Bk}, \quad k = (I, II, III)$$

Note that, although Eq. (7.9) is rather "voluminous", it will be shown below that for most realistic applications it can be reduced to much simpler expressions.

Since the process in the left of Fig. 7.4 is obviously a subset of the scheme on the right (*i.e.*, the three-unit network represents a superstructure of the two-unit process), it is sufficient to derive expressions for the three-unit network only. Table 7.1 contains all relative mass fluxes in this network expressed in terms of segregation factors. To determine the actual fluxes, all compositions (purities), P^{jk} , at all nodes of the system, as well as one flux (usually the feed flow, m_i^{F0}) must be specified. The segregation factors y_i^{jk} then follow from Eqs. (7.3). Note that proper transition conditions between the units have to be specified. These conditions read for the processes in Fig. 7.4:

$$m_i^{FII} = m_i^{AI} \quad (7.10a)$$

$$P^{FII} = P^{AI} \quad (7.10b)$$

$$m_i^{FIII} = m_i^{BI} \quad (7.10c)$$

$$P^{FIII} = 1 - P^{BI} \quad (7.10d)$$

The last line of Tab. 7.1 contains the ratio of external (or total) feed to internal feed of unit I . This ratio represents an important quantity because it is a measure for the additional demand on this unit due to the recycles.

The examples above demonstrate that the use of segregation factors simplifies the determination of mass fluxes in networks of nonsharp separators with recycles. The clear and symmetrical structure of the equations in the table reveal that mass fluxes at specific points in a network are just

Table 7.1. Relative mass fluxes of the two components for the network in Fig. 7.4 (right).

| unit | component 1 | component 2 |
|--------------|--|--|
| <i>I</i> | $m_1^{AI}/m_1^{F0} = y_1^I$ $m_1^{BI}/m_1^{FI} = 1 - y_1^I$ | $m_2^{AI}/m_2^{FI} = 1 - y_2^I$ $m_2^{BI}/m_2^{FI} = y_2^I$ |
| <i>II</i> | $m_1^{AH}/m_1^{FI} = y_1^I y_1^H$ $m_1^{BH}/m_1^{FI} = y_1^I (1 - y_1^H)$ | $m_2^{AH}/m_2^{FI} = (1 - y_2^I)(1 - y_2^H)$ $m_2^{BH}/m_2^{FI} = (1 - y_2^I) y_2^H$ |
| <i>III</i> | $m_1^{AIII}/m_1^{FI} = (1 - y_1^I) y_1^{III}$ $m_1^{BIII}/m_1^{FI} = (1 - y_1^I)(1 - y_1^{III})$ | $m_2^{AIII}/m_2^{FI} = y_2^I (1 - y_2^{III})$ $m_2^{BIII}/m_2^{FI} = y_2^I y_2^{III}$ |
| <i>FO/FI</i> | $m_1^{F0}/m_1^{FI} = 1 - \nu^H y_1^I (1 - y_1^H) - \nu^{III} y_1^{III} (1 - y_1^I)$ $m_2^{F0}/m_2^{FI} = 1 - \nu^H y_2^H (1 - y_2^I) - \nu^{III} y_2^I (1 - y_2^{III})$ | |

the products of the segregation factors of the units passed in the corresponding pathway, which simplifies mass balancing. The extension of this approach to more complex networks as well as to multicomponent separations appears to be straightforward.

The reader will have noticed that the three-unit network in Fig. 7.4 is very similar to the scheme of the process combination that was introduced in Fig. 7.1. In fact, when disregarding the units for solvent removal and dilution, the two schemes are identical. Therefore, the simple relations listed in Tab. 7.1 can be directly applied to the process combination of SMB chromatography and enantioselective crystallisation. In the next section a shortcut method for design and evaluation of this specific process combination will be developed that makes use of the approach described above.

7.3 Shortcut Approach for Evaluation of the Process Combination

One obvious choice to solve the design problem for the process combination in Fig. 7.1 is the global optimisation based on a detailed mathematical model. In such approach a rather large number of variables would have to be considered; for example, flow rates, number and geometry of columns, size and operating temperatures of the crystallisers, recycle ratios, and removal of solvent. Obviously, this would lead to a computationally very expensive problem, in particular when considering the hybrid nature of the SMB process. Besides this, it could not be guaranteed or verified that the optimisation delivers the global optimum.

At this stage of development, it appears rather useful to perform parametric studies in order to gain insight into the behaviour of the process combination and to identify critical design parameters. Furthermore, in drug development important decisions with respect to process design have to be made at an early stage, even though often not enough information about the system of interest are

available to establish a detailed model for subsequent optimisation.

The above reasons favour the development of a shortcut method for the process combination that requires only a limited amount of information, while it is flexible enough to study general process behaviour. Such approach will be presented in this section.

7.3.1 Basic Concept

The fundamental idea of the shortcut method is to apply directly the mass balance equations derived in section 7.2 to the process combination of chromatography and enantioselective crystallisation. Since these expressions relate the mass fluxes in a network to the purities adjusted at each node, this can be done only if the throughput of the units is known as a function of the purity at the specific in- and outlets.

In Chapter 6 simple algebraic expressions were derived from an equilibrium model of enantioselective crystallisation that describe the above-mentioned dependency. However, such expressions cannot be established for the nonsharp SMB separation. Therefore, it is suggested to use characteristics that describe the throughput of an SMB as a function of the purity of its two outlets.³ These characteristics can then be inserted, together with the mentioned expressions for the crystallisation, into the mass balance equations for the process network listed in Tab. 7.1.

The characteristics for the SMB process have to be determined using optimisations of a suitable model. Since here evaluations will be performed for several experimental systems, the use of a detailed SMB model appears numerically too expensive for an efficient determination of the necessary characteristics. Therefore, the TMB model that was successfully applied in the optimisations presented in Chapter 5 will serve as a reduced model for the SMB process.

The suggested approach implies some assumptions. The most important are:

- The performance of SMB processes can be described appropriately using characteristics obtained from a TMB model.
- The use of a proper objective function in the optimisations of the TMB model leads to near-optimum results with respect to the performance of the process combination.
- Crystallisers can be treated as sharp separators (*i.e.*, delivering only pure enantiomers) that operates at equilibrium and can be modelled using the mass balances derived in section 7.2.

7.3.2 Derivation of Process Parameters for the Process Combination

Using the equations derived in section 7.2 and listed in Tab. 7.1, expressions for important parameters of the process combination can be derived. In particular these are mass fluxes in the network,

³ The use of characteristics for such purposes is an established method. For example, MALLIK *et al.* applied somewhat simpler characteristics in the design of nonsharp separator networks for the resolution of mineral mixtures. [145, 146].

feed composition of the SMB, recycle ratio, overall yield, and internal load of the SMB process.

Mass Fluxes, Yield, and Recycle Ratio

For the following derivations the example will be considered where only enantiomer 1 (enriched in the raffinate) represents the target product. Corresponding expressions for other cases will be summarised at the end of this section.

The target product (enantiomer 1) is withdrawn at node *AI* of the scheme in Fig. 7.1. Accordingly, crystalliser *III* and its recycle are omitted, thus $\nu^{III} = 0$ and $y^{III} = 0$. To allow for crystallisation of pure enantiomer ($P^{AII} = 1$), the purity of the raffinate should exceed the eutectic composition. As was demonstrated in Chapter 6, the highest yield is achieved for $P^{AI} = P_e$.⁴ From these conventions and Eqs. (7.3) it follows for the segregation factors of the target component (index "1" omitted):

$$y^I = \frac{P^{AI}}{P^{FI}} \cdot \frac{P^{FI} + P^{BI} - 1}{P^{AI} + P^{BI} - 1} \quad (7.11)$$

$$y^{II} = \frac{P^{AI} + P^{BII} - 1}{P^{AI} P^{BII}} \quad (7.12)$$

Equation 7.6 readily gives an expression for both, the relative mass flux of the target component as well as the overall yield of the process, Y :

$$Y = \frac{m_1^{AII}}{m_1^{F0}} = \frac{y_1^I y_1^{II}}{1 - \nu^{II} y_1^I (1 - y_1^{II})} \quad (7.13)$$

where the values for y_1^j are given by Eqs. (7.11). If a certain minimum overall yield, Y^* , has to be achieved, Eq. (7.13) can be rearranged to obtain the necessary recycle ratio:

$$\nu^{II} = \frac{Y^* - y^I y^{II}}{Y^* y^I (1 - y^{II})} \quad (7.14)$$

Feed Composition of SMB Chromatography

As already mentioned, due to the recycle stream the feed purity of the SMB, P^{FI} , will differ from the purity of the external feed, P^{F0} . Such situations also occur for recycled fractions in elution chromatography, see [147]. P^{FI} is given by Eq. (7.9). However, as mentioned earlier, this expression can be simplified significantly. Because enantiomers usually represent expensive products, very high yields appear desirable, which corresponds to high recycle ratios. Assuming complete recycle, $\nu^{II} = 1$, and a racemic total feed, $P^{F0} = 0.5$, Eq. (7.9) reduces to

$$P^{FI} (\nu = 1) = \frac{2P^{AI} P^{BI} P^{BII} + P^{AI} + P^{BI} + P^{BII} - P^{AI} P^{BI} - P^{BII} (P^{AI} + P^{BI}) - 1}{2P^{BII} P^{BI} + P^{AI} - 1} \quad (7.15)$$

⁴ In this example the eutectic purity is defined with respect to enantiomer 1. For conglomerate forming systems, $P_e = 0.5$; for compound forming systems $0.5 < P_e < 1$. See section 2.2.2 for details.

A further increase of the yield results from demanding that the extract BI should contain only the non-target enantiomer 2 (*i.e.*, $P^{BI} = 1$). From this and Eq. (7.15) follows

$$P^{FI}(\nu = 1, P^{BI} = 1) = \frac{P^{AI} P^{BII}}{2P^{BII} + P^{AI} - 1} \quad (7.16)$$

It should be noted that in this case the segregation factor y^I is unity, because all of enantiomer 1 leaves the SMB through the raffinate port. The assumption of pure extract at first might appear somewhat contradictory, because the economical advantage expected from the process combination is based on reducing purity requirements on SMB. However, since any amount of the target enantiomer that is contained in the outlet of the non-target species (in this example, the extract port BI) is lost, it can be mandatory for cost-limitation to adjust a very high purity for this outlet. In such cases, a possible benefit will result only from the lowered purity requirements on the outlet of the target enantiomer (in the example, the raffinate port AI).

Internal Load on SMB Separation

An important issue with respect to the process in Fig. 7.1 is that the yield of the crystalliser is restricted by the position of the eutectic. As was discussed in Chapter 6, the yield decreases with increasing eutectic purity. As a consequence, more material has to be recycled back to the SMB to maintain the overall yield. This recycling causes additional load on the SMB process and, therefore, decreases overall throughput.

In order to quantify this effect, an internal load of the SMB process, L , which will be defined as the ratio between SMB feed and total feed, that is, $L_i = m_i^{FI}/m_i^{F0}$. This ratio is already given by the expressions in the last two lines of Tab. 7.1. For the example that enantiomer 1 is the target product, one obtains for L_1

$$L_1 = \frac{m_1^{FI}}{m_1^{F0}} = \frac{1}{1 - \nu^{II} y^I (1 - y^{II})} \quad (7.17)$$

In a stand-alone separation by SMB, there is no recycle ($\nu^{II} = 0$). Correspondingly, $L_1 = 1$ and $m_1^{FI} = m_1^{F0}$. As soon as a recycle is present, the SMB has to process a mass flux higher than the external feed, that is, $L_1 > 1$ and $m_1^{FI} > m_1^{F0}$. Whether or not the throughput of the process combination will be higher than in a stand-alone SMB process depends on the specific throughput-characteristic of the SMB separation and the position of the eutectic.

Summary of Parameters for Different Process Configurations

For investigations of the process combination following in this chapter, three different process configurations that are related to the choice of the target enantiomer will be considered. In case (1), only enantiomer 2 is the desired target enantiomer. This enantiomer is delivered by the extract of the plant in Fig. 7.1. Correspondingly, the crystalliser III will be omitted. In the second scenario, case (2), the desired enantiomer 1 is delivered by the raffinate and unit II will be neglected (this

corresponds to the case used for the derivations above). In case (3), both enantiomers are desired and all units are required.

Table 7.2 contains expressions for the most important process parameters of the three process configurations. Note that for case (3) a “symmetrical” operation scheme is assumed. This means, that identical operating conditions are assumed for the two branches of the process (i.e., $P^{AI} = P^{BI} = P^I$, $P^{BII} = P^{AIII} = P^{II}$, $\nu^{II} = \nu^{III} = \nu$).

Table 7.2. Main process parameters and conventions for the three process options. P^{FI} , Y , L , and y^j are defined with respect to the target component. It is assumed that $P^{F0} = 0.5$. Given equations for P^{FI} apply for $\nu = 1$ and pure SMB outlets for the non-target components; otherwise see Eq. (7.15).

| | Case (1) (target: extract) | Case (2) (target: raffinate) | Case (3) (targets: extr. & raff.) |
|---------------------|--|---|---|
| Units | I, III | I, II | I, II, III |
| Conventions | $P^{BI} > P_e$ $P^{BIII} = 1$ $P^{FIII} = 1 - P^{BI}$ | $P^{AI} > P_e$ $P^{AII} = 1$ $P^{FII} = P^{AI}$ | $(P^{AI} = P^{BI}) > P_e$ $P^{AII} = P^{BIII} = 1$ $P^{FII} = P^{AI}$, $P^{FIII} = 1 - P^{BI}$ |
| Segregation factors | $y^I = \frac{P^{BI}}{1 - P^{FI}} \frac{P^{AI} - P^{FI}}{P^{AI} + P^{BI} - 1}$ $y^{III} = \frac{P^{AIII} + P^{BI} - 1}{P^{AIII} P^{BI}}$ | $y^I = \frac{P^{AI} P^{FI} + P^{BI} - 1}{P^{FI} P^{AI} + P^{BI} - 1} y^I = P^I$ $y^{II} = \frac{P^{AI} + P^{BII} - 1}{P^{AI} P^{BII}}$ | $y^I = P^I$ $y^{II} = \frac{P^I + P^{II} - 1}{P^I P^{II}}$ |
| Feed composition | $P^{FI} = \frac{P^{AIII}(2 - P^{BI}) + P^{BI} - 1}{2P^{AIII} + P^{BI} - 1}$ | $P^{FI} = \frac{P^{AI} P^{BII}}{2P^{BII} + P^{AI} - 1}$ | $P^{FI} = P^{F0}$ |
| SMB load | $L = \frac{1}{1 - \nu^{III} y^I (1 - y^{III})}$ | $L = \frac{1}{1 - \nu^{II} y^I (1 - y^{II})}$ | $L = \frac{1}{1 - \nu(1 - y^I y^{II})}$ |
| Yield | $Y = \frac{y^I y^{III}}{1 - \nu^{III} y^I (1 - y^{III})}$ | $Y = \frac{y^I y^{II}}{1 - \nu^{II} y^I (1 - y^{II})}$ | $Y = \frac{P^I + P^{II} - 1}{P^{II} - \nu(1 - P^I)}$ |
| Recycle ratio | $\nu^{III} = \frac{Y - y^I y^{III}}{Y y^I (1 - y^{III})}$ | $\nu^{II} = \frac{Y - y^I y^{II}}{Y y^I (1 - y^{II})}$ | $\nu = \frac{P^{II} Y - (P^I + P^{II} - 1)}{Y(1 - P^I)}$ |

7.3.3 Determination of Characteristics for SMB Processes

Characteristics for continuous chromatography describe the dependency of all flow rates and the corresponding outlet concentrations on the purity of the raffinate and the extract, P^{AI} and P^{BI} , respectively. Based on the promising results of Chapter 5, such characteristics will be determined here by optimisations of the four zone flow rates in a TMB model.

The model and the optimisation approach were explained in section 5.2. The objective function is given by Eq. (5.1a). This function is expected to reflect also the main performance parameters of the whole process combination, since it minimises the amount of solvent that is introduced into the process scheme in Fig. 7.1 (and of which a certain fraction has to be removed before crystallisation), while it simultaneously maximises the throughput of the SMB process (which is expected to be a limiting factor for the whole scheme).

It is useful to perform such optimisations for different efficiencies of the chromatographic process (*i.e.*, for different plate numbers, NTP ; see Eq. (2.16)).

7.3.4 Illustrative Example

Figure 7.5 contains a generic example of a characteristic for an SMB process. In the example shown, this function describes the dependency of the throughput of the SMB for component 1, m_1^{FI} , as a function of the purity at one of its outlets, P^I (the purity of the other SMB outlet is held constant). The shape of this function is typical for SMB processes, see Chapter 4 and [57, 58].

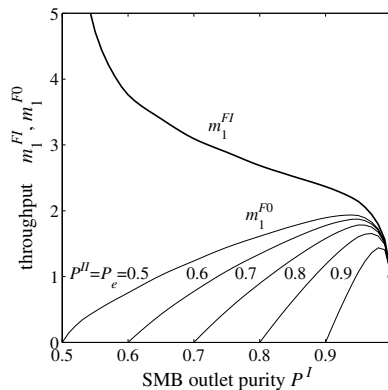


Figure 7.5. Evaluation of characteristics. Bold line – generic example for a throughput-characteristic of an SMB process as a function of its outlet purity, P^I . Thin lines – corresponding throughput of the process combination for different assumed values of the eutectic purity, P_e .

While the throughput of the SMB process, $m_1^{FI}(P^I)$, is given by this characteristic, the possible throughput of the whole process combination, m_1^{F0} , will depend on the purity of the mother liquor, P^{II} . By specifying a value for this purity and inserting the values for m_1^{FI} into Eq. (7.17), one obtains the corresponding throughput for the whole process combination, m_1^{F0} . In the figure, it is assumed that the mother liquor reaches eutectic composition (*i.e.*, $P^{II} = P_e$). Furthermore, complete recycle was assumed (*i.e.*, $\nu = 1$).

A pronounced maximum for each curve $m_1^{F0}(P^I, P^{II})$ can be observed, which demonstrates the usefulness of the equations derived above. The results emphasise the significant influence of the

eutectic purity of a system. It can be seen that for an (assumed) lower eutectic position P_e a higher maximum for m_1^{F0} can be achieved. This is due to the increasing yield of the crystallisation step and was already anticipated in Chapter 6. Further, it can be observed that also the optimum transition purity depends on the value for P_e .

The determination of other performance measures (e.g., flow rates in the different zones of the chromatographic process, amount of stationary phase, specific solvent removal between the units) will be explained in the following section.

7.4 Evaluation and Design of the Process Combination

In this section, the shortcut method introduced above will be applied to evaluate the process combination considering the three different configurations that result from the choice of the target enantiomer (see Tab. 7.2). Furthermore, the performance of the process will be evaluated for the three model systems I.f (mandelic acid), II (threonine), and III (PDE), respectively.

All results will be compared to a reference scenario, which applies an optimised stand-alone separation by an SMB process that achieves high product purity and yield. The process combination should achieve at least the same yield as this reference scenario, while it is assumed to deliver pure products.

7.4.1 Detailed Procedure

The following procedure was used as a shortcut method for design and evaluation of the process combination of SMB chromatography and enantioselective crystallisation:

1. *Determination of required experimental parameters.* These are adsorption isotherms, solubility data, and relations for pressure drop and plate number as functions of the flow rate. All parameters for the three model systems are specified in Chapter 3. It should be emphasised that, with respect to the SLE, it is sufficient for the application of the shortcut procedure to specify the eutectic *composition*, P_e . However, since here also the removal of solvent was considered, for each system the *solubility* at eutectic composition was specified, using the lowest temperature for which SLE data were available.
2. *Specification of process requirements.* The most important parameter is the overall yield. Corresponding to the chosen value, the recycle ratios and the purity of the SMB ports for the non-target component have to be adjusted using Eq. (7.14). Here it was assumed that a minimum yield of $Y^* = 0.998$ had to be guaranteed. With the simplifying assumption of complete recycle (i.e., $\nu = 1$) it followed from the equations in Tab. 7.2: $P^{AI} = 0.998$ in

case (1) and $P^{BI} = 0.998$ in case (2), respectively. The crystallisation step was required to achieve the eutectic composition.

3. *Calculation of purity-performance characteristics.* For this purpose the method explained in section 7.3.3 was applied. Optimisations were performed for different numbers of theoretical plates of the TMB unit ($8 \leq NTP \leq 400$) and for different purities of the outlet for the target component. Note that in case (3) (both enantiomers desired) it was set $P^{AI} = P^{BI}$. To maximise throughput, the maximum concentration for each adsorption isotherm was used (see Chapter 4). Note, that in the simulations for cases (1) and (2) the feed composition was adjusted according to complete recycle and eutectic composition of the mother liquor using the expressions for P^{FI} in Tab. 7.2.
4. *Determination of essential process parameters.* Since here a TMB model was used for the determination of characteristics, the bed lengths and flow rates that correspond to the use of packed columns (as are used in SMB processes) had to be determined. The corresponding calculation procedure is explained in Appendix A.4. For its application, the correlations for pressure drop and plate number were used that are reported in Chapter 3. In accordance to typical practical situations, the pressure drop in the unit was adjusted to 50 bar. Subsequently, for each optimisation performed, the load ratio, L , and the overall throughput, m_i^{F0} was calculated using the relations in Tab. 7.2. Finally, the specific solvent removal, SR , was calculated from Eq. (6.23).

It should be noted, that steps 2.–4. could also be performed in a single step by including all relations into a model describing the whole process. However, decomposing the problem into the steps listed above provides a certain flexibility, since the calculated characteristics can be re-used if conditions like solubility, column geometry, or pressure drop restriction are changed.

7.4.2 Evaluation for Different Process Configurations

For the investigations of the different process configurations in this section the mandelic acid system I.f will be used (for parameters see section 3.1). Further experimental model systems will be considered in section 7.4.3.

Case (1) – Target Enantiomer from SMB-Extract

Figure 7.6 shows characteristics determined for system I.f for the case that the stronger adsorbing enantiomer 2 is the target product. Each characteristic was obtained by optimisations of the TMB model for about 15 different values specified for the extract purity, P^{BI} , (denoted by the circles). In all calculations, the raffinate purity was held constant at a high value (*i.e.*, $P^{AI} = 0.998$, since at least 99.8% yield is required). Characteristics were determined for different total numbers of theoretical plates, NTP .

For the sake of simplicity, the figure shows the dimensionless throughput⁵. It can be seen that the throughput of the TMB process increases strongly with decreasing extract purity. For increasing plate numbers the throughput also increases; however, only small improvements can be achieved when increasing NTP beyond 120.

Furthermore, the figure shows the corresponding dimensionless throughputs for the process combination. They were calculated using the expression for the SMB load in Tab. 7.2 (with $P^{AIII} = 0.31^6$ and $\nu^{III} = 1$). It can be seen that from each characteristic follows for the process combination a throughput curve with a distinct maximum. These maxima are higher than the throughput of the reference scenario (*i.e.*, the stand-alone separation which is characterised by the values of the characteristics for $P^{BI} = 0.998$). Note that for $NTP < 60$ the efficiency of the unit is too low to achieve the extract purity required for the reference case, while the process combination is still able to deliver pure enantiomer at a considerable productivity.

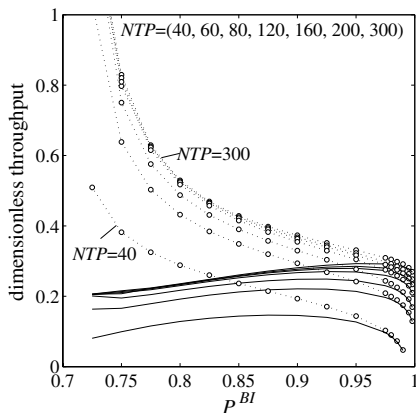


Figure 7.6. Characteristics for different NTP (dashed) and resulting feed fluxes of the process combination (solid). Variable purity of extract (P^{BI}) and constant purity of raffinate ($P^{AI} = 0.998$).

A better comparison of the process combination and the reference scenario can be obtained by determining the performance of SMB processes that correspond to the different operating points shown in Fig. 7.6. For this purpose it is necessary to “translate” the plate numbers, NTP , that were used in the TMB calculations, to bed lengths and flow rates that correspond to the use of packed (SMB) columns. The procedure to realise this is explained in detail in Appendix A.4. Figure 7.7 (left) shows the resulting values for throughput and bed length that correspond to the throughput-maxima in Fig. 7.6. The same parameters are displayed for the reference scenario.

For the separation by SMB alone, the calculations predict a throughput-optimum at 120 theoretical stages. However, the process combination clearly outperforms this. At only 80 theoretical stages the throughput is 43.6% higher than in the best stand-alone separation. Simultaneously, the zone length (and thus the volume of CSP) is 19.4% lower.

The right panel of Fig. 7.6 shows the specific solvent removal that was calculated from Eq. (6.23). Note that, since the process combination delivers a solid product, the same was required for the reference case. Therefore, a complete solvent removal from the stream that contains the target

⁵ The dimensionless throughput for this case was calculated as the difference between the dimensionless flow rates in zones I and II of the TMB process, multiplied by the ratio of extract and feed concentration, respectively.

⁶ This corresponds to the eutectic purity for systems I.f of 69%. Since the purity for outlet AIII is defined with respect to the counter-enantiomer, $P^{AIII} = 1 - 0.69$.

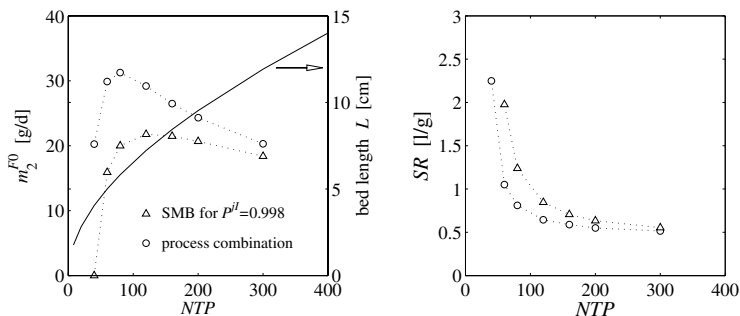


Figure 7.7. Performance of the process combination and the reference scenario if the extract delivers the target enantiomer. Throughputs and bed lengths (left), and specific solvent removal (right) as a function of NTP . Each point corresponds to a maximum in Fig. 7.6 (process combination) or to the value for $P^{AI} = P^{BI} = 0.998$ (reference scenario), respectively.

enantiomer was assumed (*i.e.*, for the reference scenario in case (1) holds $SR = 1/c_2^{BI}$). In the throughput-optimum of the reference scenario about 0.84 litres of solvent must be removed per gram target product. In the optimum for the process combination the value is slightly lower (0.81 l/g). For very low plate numbers SR rises strongly in both cases.

The transition purities that correspond to the maximum throughput of the process combination will be discussed later (see Tab. 7.3 on page 112).

A very important aspect is the required bed length shown in the figure. At the throughput maximum for the process combination, the bed length is one third lower than in the optimum for the reference scenario (*i.e.*, 80 vs. 120 stages). This means in turn, that about 33% of chiral stationary phase (CSP) can be saved. Since investment costs in chiral chromatography are often dominated by the costs for CSPs, this indicates a significant potential of the process combination with respect to the reduction of investment costs.

Case (2) – Target Enantiomer from SMB-Raffinate

Figure 7.8 shows the performance of the process combination and the reference scenario for case (2), where the less adsorbing enantiomer 1 is the desired product.

Obviously, in this case, throughput and relative solvent removal of the two process options are similar; the process combination appears to be only slightly better than the stand-alone SMB. Since the optima for both processes are located at $NTP = 120$, identical amounts of CSP are necessary.

The reason for the comparatively low benefit for this case is the behaviour of the concentration waves inside the SMB (or TMB) unit. For decreasing purity requirements, the internal shock waves become higher and, thus, travel faster within the separation zones [139]. At the same time, high extract purity has to be maintained to meet the yield requirements (see above). The optimiser

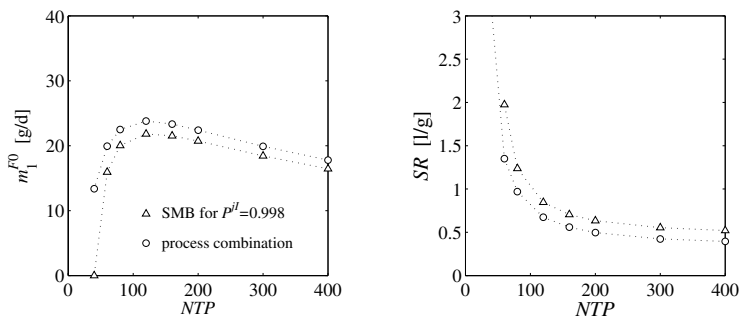


Figure 7.8. Throughput and specific solvent removal if the raffinate contains the target enantiomer.

counterbalances these effects by delivering for decreasing raffinate purity decreasing values for the flow rate in zone *IV*. This, in turn, restricts the possible throughput. This finding is consistent with the results of Chapter 5, where it was concluded that an optimisation of all flow rates in continuous chromatography is particularly beneficial with respect to the product concentrations of the stronger adsorbing component (see Fig. 5.4 c).

Case (3) – Two Target Enantiomers

For the case that both enantiomers are desired products, a “symmetrical” operation of the plant was assumed. This means, that during the determination of the characteristics identical values for the raffinate and the extract purity were used.

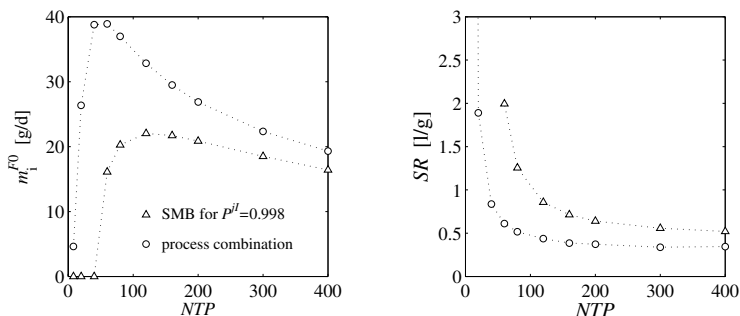


Figure 7.9. Throughput and specific solvent removal (averaged) if both enantiomers are desired.

Figure 7.9 shows the corresponding results for this case. Similar performance improvements as in case (1) can be achieved (see Fig. 7.8). Comparing the optima of the throughput for the stand-alone SMB process (at $NTP = 120$ stages) and for the process combination (at $NTP = 60$ stages), one finds that in the combined scheme the throughput is 77% higher, while simultaneously CSP volume and specific solvent removal are lower by 31% and 29%, respectively. Note that the figure contains the averaged values of SR for both enantiomers.

Comparison of the Different Cases

Table 7.3 compares the results for the three different process configurations of the process combination and the reference scenario. For the latter, the stand-alone separation by SMB with a plate number of $NTP = 120$ was considered, since for this value this process delivers the highest throughput under the purity constraint of $P^{AI} = P^{BI} = 0.998$.

It can be seen again that cases (1) and (3) provide for the best performance. In these cases, the process combination allows for significantly increased throughput in comparison to the reference scenario. The transition purities for highest throughput shifted towards lower values for decreasing plate numbers.

Table 7.3. Comparison of transition purity and throughput for the three cases. P_{opt}^I – transition purity for highest throughput, Δm_1^{F0} – change of throughput with respect to the reference scenario by application the process combination. Underlined – operating points for highest throughput.

| NTP | Case (1) | | Case (2) | | Case (3) | |
|-------|--------------------|-----------------------|--------------------|-----------------------|--------------------|-----------------------|
| | P_{opt}^I | Δm_1^{F0} [%] | P_{opt}^I | Δm_1^{F0} [%] | P_{opt}^I | Δm_1^{F0} [%] |
| 400 | n.a. | n.a. | 0.990 | -24.0 | 0.990 | -17.5 |
| 300 | 0.950 | -12.1 | 0.990 | -13.5 | 0.980 | -3.1 |
| 200 | 0.950 | +7.4 | 0.990 | -0.6 | 0.975 | +19.0 |
| 160 | 0.925 | +18.1 | 0.990 | +4.5 | 0.975 | +31.5 |
| 120 | 0.925 | +31.1 | <u>0.985</u> | <u>+7.7</u> | 0.965 | +47.7 |
| 80 | <u>0.900</u> | <u>+41.9</u> | 0.980 | +3.1 | 0.925 | +68.2 |
| 60 | 0.900 | +36.3 | 0.975 | -8.3 | <u>0.900</u> | <u>+77.5</u> |
| 40 | 0.875 | -7.5 | 0.900 | -38.8 | 0.875 | +77.4 |
| 20 | n.a. | n.a. | n.a. | n.a. | 0.85 | +19.4 |
| 8 | n.a. | n.a. | n.a. | n.a. | 0.75 | -82.4 |

As already mentioned, case (2) allowed only for a rather low improvement. Due to the additional efforts necessary for design and implementation of the process combination, this case was not regarded as advantageous. Here it appears reasonable to apply SMB chromatography in stand-alone mode.

It should be noted, that in all cases the transition purity, P_{opt}^I , lies above the maximum feed purity for the SLE of system I.f ($P_{\text{max}}^{FI} = 0.988$, see Tab. 6.1). Since also the temperature range of the SLE for system I.f is sufficiently large, for each operating point in the table the eutectic composition can be achieved in a single-step crystallisation, which facilitates maximum yield of this unit operation (see also the discussion in section 6.3.3). Note further, that this positive result could not be reported in [61], since there the stronger limited "surrogate" SLE for mandelic acid in water (Fig. 3.5) was applied.

7.4.3 Evaluation for Different Model Systems

In order to compare the performance of the process combination for different enantiomeric systems, the shortcut method was also applied to the model systems II and III (for the corresponding parameters see Chapter 3). For this comparison the already explained case (3) was applied that considers both enantiomers as target products.

Figure 7.10 summarises the results that were already obtained for system I.f (see section 7.4.2) together with those additionally determined for systems II and III. It can be seen that the performance is rather different for the three systems. While for system III remarkable productivities and very low solvent consumptions can be obtained, the performance of systems I.f and II is significantly lower. The reason for the high absolute performance of system III is that it actually combines several beneficial aspects. The chromatographic separation benefits from the relatively high separation factor and high possible feed concentrations, as well as from low slopes of the correlations for pressure drop and *HETP* as a function of flow rate (see Chapter 3 for details). In crystallisation, the favourable eutectic composition of this conglomerate system (*i.e.*, $P_e = 0.5$) allows for high yields. This in turn leads to a low load on the SMB unit due to recycles and, therefore, allows for a good performance of the process combination.

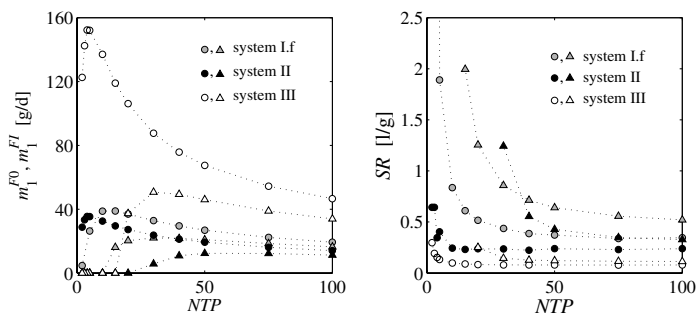


Figure 7.10. Comparison of process performance for systems I.f, II, and III if both enantiomers are desired. Left – throughput of the stand-alone process (triangles) and the process combination (circles). Right – specific solvent removal for the two options.

However, it is more expedient to compare the performance of the process combination and the reference scenario for each system separately. Table 7.4 lists the relative performances for both options in a similar manner as was already used in Tab. 7.3. It can be seen that the relative improvements with respect to the reference scenario are significant for all systems. For example, for system III the throughput was increased by up to 200% while simultaneously reducing the total bed length by about 65%. This corresponds to a remarkably increased specific productivity (*i.e.*, the ratio of throughput and volume of stationary phase; see Eq. (4.2)) of about 308%.

The relative improvements are highest for systems II and III, respectively. This is in particular due to the fact that these are conglomerate forming systems (*i.e.*, they have a favourable eutectic

Table 7.4. Evaluation of the three model systems. Throughput (m_1^{F0}), bed length (L), and solvent removal (SR) of the process combination relative to a stand-alone separation. Underlined – throughput-optima, *italicised* – operating points that require a step-wise crystallisation.

| <i>NTP</i> | system I.f | | | | system II | | | | system III | | | |
|------------|-------------|-------------------|------------|-------------|-------------|-------------------|------------|-------------|-------------|-------------------|------------|-------------|
| | <i>P</i> | Δm_1^{F0} | ΔL | ΔSR | <i>P</i> | Δm_1^{F0} | ΔL | ΔSR | <i>P</i> | Δm_1^{F0} | ΔL | ΔSR |
| | [%] | [%] | [%] | [%] | [%] | [%] | [%] | [%] | [%] | [%] | [%] | [%] |
| 400 | 97.5 | -12 | +94 | -60 | <i>92.5</i> | +14 | +42 | -44 | 90.0 | -8 | +91 | -45 |
| 300 | 96.5 | +1 | +65 | -61 | <i>90.0</i> | +30 | +23 | -46 | 85.0 | +7 | +64 | -46 |
| 200 | 96.5 | +22 | +32 | -57 | <i>90.0</i> | +56 | 0 | -44 | 85.0 | +33 | +31 | -46 |
| 160 | 95.0 | +34 | +17 | -55 | <i>85.0</i> | +71 | -11 | -48 | 85.0 | +49 | +17 | -45 |
| 120 | 92.5 | +49 | 0 | -49 | <i>85.0</i> | +92 | -23 | -45 | 85.0 | +73 | 0 | -44 |
| 80 | 92.5 | +68 | -19 | -40 | <i>80.0</i> | +121 | -37 | -45 | 80.0 | +109 | -19 | -42 |
| 60 | <u>90.0</u> | <u>+77</u> | <u>-31</u> | <u>-29</u> | <i>75.0</i> | +139 | -45 | -46 | 75.0 | +135 | -30 | -39 |
| 40 | 87.5 | +76 | -44 | -3 | <i>70.0</i> | +164 | -55 | -43 | 75.0 | +170 | -44 | -33 |
| 20 | 82.5 | +20 | -61 | 121 | 65.0 | +187 | -69 | -6 | <u>65.0</u> | <u>+200</u> | <u>-61</u> | <u>-9</u> |
| 16 | | | | | <u>60.0</u> | <u>+187</u> | <u>-72</u> | <u>-19</u> | 65.0 | +200 | -65 | +5 |
| 12 | | | | | <i>60.0</i> | +169 | -76 | +50 | <i>60.0</i> | +181 | -70 | +33 |
| 8 | 72.5 | -79 | -76 | +3009 | <i>55.0</i> | +132 | -80 | +50 | <i>60.0</i> | +142 | -75 | +105 |

purity of $P = 0.5$). It should be noted that for system II already at higher plate numbers and transition purities a certain benefit from the process combination can be observed (see the first few rows of the table). This is caused by the low separation factor and the steeper slope of the *HETP* function for this system (see Eq. (3.1) and parameters in Chapter 3). These two effects allow only very low improvements of the stand-alone separation by chromatography for the required purity of 99.8% (see Fig. 7.10). In turn, reduction of these high purity requirements immediately increases the throughput of the chromatographic process and, therefore, leads to a better performance of the process combination.

It can be expected that the process combination is particularly advantageous for enantiomeric systems with *i*), a limited performance of the chromatographic separation (for example, due to low separation factors or low column efficiency), and *ii*), a favourable SLE that reveals a low eutectic purity and that does not impose limitations with respect to feasible operating conditions (as is the case for system II, where feed purity and adjustable temperatures in crystallisation are restricted).

However, considering the results in Tab. 7.4, it must be taken into account that the composition range of the SLE is limited for each system (for a detailed discussion of this aspect see section 6.3). As already mentioned, for system I.f all operating points in the table are feasible. On the other hand, this is not true for the other two systems. For system II, the predicted optimum transition purities that correspond to plate numbers of $NTP \geq 40$ (*i.e.*, $P \geq 0.70$) are higher than the maximum feed purity of $P_{\max}^F = 0.687$ (*i.e.*, the highest feed purity that still allows to reach the eutectic composition in a single crystallisation step; see section 6.3.2 and Tab. 6.1). Therefore, a step-wise crystallisation process will be required for these operating points as was suggested in section 6.3.3. Furthermore, for points with $NTP \leq 16$, the necessary feed concentration is too low to be adjusted within the temperature range of the SLE. This case (which was not considered

in Chapter 6) will also require the mentioned step-wise procedure, since it is necessary to operate crystallisation at higher concentrations than originally assumed. In the table such unfavourable operating points are *italicised*.

Obviously, for system II only one of the optimisation results allows for a one-step crystallisation. The maximum feed purity for system III ($P_{\max}^F = 0.911$, see Tab. 6.1) is always higher than the optimum transition purity. Therefore, for this system limitations apply only for the operating points with $NTP \leq 12$, which would require lower temperatures than covered by the SLE.

7.4.4 Remarks and Limitations of the Approach

When applying the shortcut method that was introduced in this chapter, some limitations of this approach should be taken into account. First, the values for the performance parameters obtained will not match exactly the values that would result when using an SMB model. One issue is that the optimal bed lengths obtained are rather low (between 2 and 14 cm), while simultaneously high flow rates are applied (up to several hundred ml/min). These cannot be used in a real SMB, because this would cause impractically short switching times (in the range of a few seconds). Because of the high pressure drop and efficiency of the columns used, such high flow rates could not be covered by typical measurements. Another limitation is that a TMB model always over-predicts SMB performance. However, it can be shown that the purity-performance characteristics of SMB and TMB models are very similar with respect to their curvature. The main difference is that an SMB process will always need a higher plate number to achieve the same performance. It appears a valid strategy to compare selected SMB and TMB calculations for a given separation problem to quantify the differences between model predictions. However, this is out of the scope of this work.

It should be emphasised that - despite the aforementioned limitations - the approach presented will predict the trends of the system correctly, while the actual results will represent upper limits of the benefits achievable from the process combination.

It represents an interesting fact that very low values were found for the optimum number of theoretical plates (NTP). On one hand, this stresses the significant potential to save investment costs for chiral stationary phase (CSP) by combining SMB and crystallisation. Alternatively, less efficient (and less expensive) CSPs and solvents could be used to resolve the separation task without increasing operation costs. On the other hand, the low plate numbers indicate that the application of combined separation schemes might facilitate using simpler separation processes than SMB chromatography, since it actually appears rather contradictory to apply a complex separation process like the SMB process to a problem that requires only 10 theoretical stages. Less efficient techniques like membrane processes might be of interest as the first separation step.

When considering the results of the investigations presented above, the shortcut design method that was proposed in [59] appears inappropriate. A number of shortcomings of the approach used there (*e.g.*, the impact of column efficiency was not accounted for) will lead to inaccurate predictions

for the optimal transition purity. In particular the assumption of linear characteristics represents a misconception (as can be seen, for example, from Fig. 7.6).

7.5 Further Aspects of Process Engineering

There is quite a large number of questions that arise when trying to develop a combined process of SMB chromatography and enantioselective crystallisation. Since in this work focus was set on general evaluation and conceptual design of this process, by far not all of these issues could be covered exhaustively. In the following, a brief overview will be given about other important aspects of process engineering and further issues that should be investigated when attempting a practical implementation of the process combination considered.

Solvent-Related Issues

Some very important aspects are related to the choice of solvent and its removal between chromatography and crystallisation. One of them is that it is desirable to perform both unit operations using the same solvent (this is actually given for the three model systems I.f, II, and III examined above). However, for systems where crystallisation cannot be conducted in the chromatographic eluent, a complete solvent removal has to be applied before crystallisation *and* in the recycle streams back to chromatography.

Furthermore, it is useful to apply single-component solvents (with pure acetonitrile this applies here only to system III), since otherwise the enrichment step in Fig. 7.1 has to be either non-selective with respect to eluent components, or must deliver a liquid composition for which the ternary SLE is known. This problem will apply to many practical systems, since mixed eluents are very common in chiral chromatography (*e.g.*, aqueous solutions of alcohols like for systems I.f and II, respectively). In this context, the use of reverse osmosis for the enrichment step appears interesting.

Finally, for process design one should not only consider the specific solvent removal with respect to product flux, SR , but also the relative amounts that have to be removed in the enrichment unit. When analysing the results for the three systems presented in section 7.4.3, one finds at the optimum operating point for system I.f that the enrichment unit is required to remove 99.8% of the passing solvent. This is related to the high solubility for this system at transition conditions. This is less pronounced for system II (48.9%) and system III (88.9%). Since for a reasonable performance of the crystalliser it is necessary to adjust these values accurately, in cases like for system I.f also a complete removal of the solvent is worthwhile to consider.

Incorporation of Further Unit Operations

A very interesting field for further investigations is the use of alternative or additional unit operations. One example is the use of membrane-based enrichment processes like the already mentioned

reverse osmosis.

The coupling approach investigated here might be extended to the use of batch chromatography as the first separation step. Furthermore, since it was demonstrated that the optimal transition conditions correspond to very low efficiencies of the chromatographic process, the use of separation processes that are typically less effective (*e.g.*, chiral membranes) might be of interest.

In the present work it was not accounted for the solid-liquid separation after crystallisation. However, for a detailed process design it will be necessary to include also transport, filtering, and washing of the produced crystals.

Evaporative crystallisation can serve as an alternative to cooling crystallisation. Although its design is somewhat more complex, it could allow to perform solvent removal and crystallisation in one apparatus (provided that the rates of crystallisation and solvent evaporation are properly adjusted). This would make possible to circumvent restrictions due to limited ternary SLE.

It appears very attractive to apply a racemisation step in cases where only one enantiomer is desired. A racemisation converts an asymmetrical mixture of two enantiomers into the 1:1 mixture. This could be applied to the chromatographic outlet for the non-desired enantiomer. The resulting racemic mixture could be recycled back to the chromatographic step (see, for example Fig. 1.6). Such processes could theoretically achieve a yield of 100%.

Development of a Model for Further Investigations

In order to study many of the aspects listed above, it will be necessary to perform investigations on the basis of more advanced mathematical models than were used here. In particular, a fully coupled process model will be required to study the start-up behaviour and the dynamic properties of the process combination.

A suggestion for such a model can be found in Appendix C. The model was already implemented in the simulation environment PROMOT/DIVA [96, 98]. It mainly consists of a TMB stage model (see section 2.1.5) and a moment model for crystallisation that considers particle phenomena like crystal growth kinetics and nucleation on a simplified basis. The incorporation of further unit operations or a hybrid SMB model is straightforward. First studies that were performed for system I.f showed an excellent agreement between calculations using the detailed model and design predictions obtained in this chapter.

Process Robustness

For a continuous realisation of the process combination it will be mandatory to identify the parameters that influence most strongly the dynamic behaviour.

For this purpose, a first analysis of the steady state sensitivities of all performance measures (*e.g.*, yield, purity of mother liquor and SMB outlets, etc.) on the design parameters (*e.g.*, flow rates, recycle ratios, operating temperature in crystallisation, etc.) was performed using the developed dynamic model. For this study, system I.f and the optimal design point for case (1) (see section 7.4.2)

were considered. The sensitivities were determined using Eq. (4.20) from the deviations between two steady states after a small perturbation (0.5%) of each parameter. The results indicate that for this system the impact of the solvent removal is highest (which is not surprising when considering the high solvent removal reported above for this system), followed by the flow rates in the separation zones of the chromatographic process. Further investigations of this type appear desirable for other enantiomeric systems and operating conditions.

7.6 Conclusions

In this chapter, a shortcut method was developed that simplifies the design of the process combination of SMB chromatography and enantioselective crystallisation and allows for a straightforward estimation of its performance for a specific enantiomeric system. The method is based on a simplifying approach for mass balancing in networks of nonsharp binary separators and the application of performance characteristics for the SMB separation. These characteristics could be determined efficiently from optimisations of a TMB model which serves as a reduced model for SMB processes.

The application of the shortcut method to different configurations that result from the choice of the target enantiomer revealed that a coupling of chromatography and crystallisation is particularly advantageous in cases where either only the stronger adsorbing enantiomer or both enantiomers are desired. This was also confirmed by the results of Chapter 5, where it was demonstrated that a non-restrictive design of continuous chromatography particularly enhances the concentrations in the extract stream.

A comparison of the performance of the process combination was performed for three model systems. The results emphasise the significant potential that results from combining the two processes. Productivity enhancements of up to about 300% could be achieved at similar efforts for solvent removal. For all systems it is possible to operate the process combination at higher throughput while simultaneously decreasing the volume of CSP and the specific solvent removal.

It is noteworthy that a limited validity range of an SLE can entail restrictions with respect to the process combination (as was anticipated in Chapter 6). Some of the cases studied will require additional implementation efforts, since they require to apply step-wise crystallisation processes. This finding emphasises the necessity to study the SLE of an enantiomeric system over a wide range when considering the combination of enantioselective cooling crystallisation and chromatography.

An important conclusion from the results of this chapter is that the application of the combined process is particularly beneficial for enantiomeric systems with a limited performance of the chromatographic separation with respect to high product purity and, simultaneously, a favourable SLE with a low eutectic purity and a wide range of accessible compositions and temperatures.

At the end of the chapter a brief overview was given about aspects of process engineering that deserve to be included in further investigations of the process combination investigated.

SUMMARY AND CONCLUSIONS

A fundamental objective of chemical engineering is the development of economically and ecologically efficient processes. Certainly one of the most innovative strategies in this field is process integration. While this is often merely perceived as the incorporation of reaction and separation into a single apparatus, it should be recognised that likewise the combination of separation units on the flowsheet-level can comprise a significant potential with respect to performance enhancement.

Subject of this work was the investigation of such a process combination for the separation of enantiomers. A well-suited technology for this challenging and important separation problem is continuous Simulated Moving Bed (SMB) chromatography. Yet, the performance of this rather complex process is typically limited if a very high product purity is required. In contrast, a pure enantiomer can often be obtained by means of simpler crystallisation as long as a certain enrichment with respect to this enantiomers is provided. Consequently, in a process combination that incorporates SMB chromatography and enantioselective crystallisation, the purity requirements on the chromatographic process can be reduced, which in turn allows to enhance the performance of the whole separation process.

In this work, focus was set on conceptual design and evaluation of the potential that arises from applying this process combination. In order to contribute to process understanding and to reveal the origins of possible benefits of the approach, at first systematic model-based investigations of the single unit operations were performed under consideration of the specific design requirements of the process combination. Of particular interest in this context was the influence of the involved thermodynamic equilibria on process performance. To allow for general conclusions with respect to feasibility and possible limitations, these investigations were performed using experimental data of different enantiomeric model systems.

In case of the SMB process, a parametric study was performed to study the impact of individual adsorption isotherm parameters on productivity. The obtained results emphasise that in this connection the separation factor has the strongest influence. However, the achievable productivity depends also on the nonlinearity of the isotherms and the feed concentration. An encouraging finding with respect to the process combination of chromatography and crystallisation was that in each case the reduction of purity requirements allowed for significant improvements of process performance. However, it was also demonstrated that – in order to fully exploit this potential – it is necessary to consider all flow rates within an SMB unit as free parameters in the design. A corresponding method based on the optimisation of a suitable model was proposed and applied successfully.

Similar investigations were performed with respect to enantioselective crystallisation. Starting

from the development of a model for ternary solubility equilibria of two enantiomers in a solvent, a design approach was suggested for this process. It was shown that the performance of crystallisation is mainly determined by the eutectic composition of an enantiomeric system. Furthermore, restrictions could be revealed that result from limitations imposed by the solid-liquid equilibrium with respect to accessible compositions and temperatures.

Based on the results of the preceding examinations, a more detailed process scheme was suggested for the combination of the two processes. For investigations of this integrated process a shortcut method was proposed that is based on a mass balance approach for networks of nonsharp separators and the application of performance characteristics for the SMB separation. Such characteristics could be determined efficiently from optimisations of a reduced model for this process. The shortcut procedure simplified significantly the design of the process combination and allowed for a straightforward evaluation of its performance. Similar approaches should be applicable for the analysis of other process combinations involving complex nonsharp separation processes.

The application of the shortcut method to different process configurations that result from the choice of the target enantiomer revealed that for systems with LANGMUIR adsorption isotherms a coupling of chromatography and crystallisation is especially advantageous in cases where either only the stronger adsorbing enantiomer or both enantiomers are desired. A comparison of process performance for three different model systems underlined the significant potential that results from combining the two processes. Remarkable productivity enhancements of up to 300% were predicted in comparison to a stand-alone enantioseparation by SMB chromatography. Simultaneously, investment costs might be lowered significantly by a reduction of the necessary volume of expensive chiral stationary phase. The results further indicate that an implementation of the process combination is particularly beneficial for enantiomeric systems with limited performance of the chromatographic separation and, simultaneously, favourable SLE that have a low eutectic purity and that reveal a strong dependency on temperature.

Process combinations of the type considered here generally raise many questions, not all of which can be addressed in studies that aim at the evaluation of the general potential of an approach. Consequently, a number of interesting aspects remain that deserve to be included in further examinations. An example is the more detailed consideration of solvent-related issues, in particular the design of the enrichment between chromatography and crystallisation. Furthermore, investigations of the dynamic behaviour based on more detailed mathematical models appear to be desirable in order to promote the promising concept studied in this work.

Appendix A

SMB and TMB Models

A.1 Numerical Solution of Equilibrium-Dispersive Model

Here only a short description of the so-called ROUCHON algorithm for the solution of the equilibrium-dispersive model (section 2.1.4) will be given. Comprehensive reviews of this algorithm can be found, for example, in [63, 89, 94, 95].

Basis of this method is that at first the dispersive term in Eq. (2.19) is neglected. The resulting equilibrium model is solved using an explicit difference scheme. The accuracy of the solution is adjusted such that the numerical dispersion of the solution matches the physical dispersion term in Eq. (2.19). This is achieved by properly adjusting the ratio of the space and time increments. This ratio is derived from a stability criterion and the relation for the apparent dispersion coefficient (Eq. (2.20)).

Neglecting the dispersion in Eq. (2.19), the equilibrium mass balance reads:

$$\frac{\partial c_i}{\partial t} + F \frac{\partial q_i}{\partial t} + u \frac{\partial c_i}{\partial z} = 0, \quad (i = 1 \dots N) \quad (\text{A.1})$$

For the discretisation of this equation, a backwards-in-time and forwards-in-space approach was found useful [63]. After discretisation and re-arrangement of Eq. (2.19), the following equation for an unknown concentration at point $n + 1$ in space and j in time results:

$$c_{i,n+1}^j = c_{i,n}^j - \frac{\Delta z}{u \Delta t} \left[c_{i,n}^j - c_{i,n}^{j-1} + F(q_{i,n}^j - q_{i,n}^{j-1}) \right] \quad (\text{A.2})$$

For known initial and boundary conditions, Eq. (A.2) is an explicit expression for the unknown concentration $c_{i,n+1}^j$. From a stability analysis, the following convergence condition can be derived (see, e.g., [63, 89]):

$$a_{\text{cou}} = u_{\text{min}} \frac{\Delta t}{\Delta z} \geq 1 \quad (\text{A.3})$$

In this so-called COURANT-FRIEDRICHS-LEVY condition, a_{cou} is the COURANT number and u_{min} is the minimum migration velocity of the solute (*i.e.*, for LANGMUIR isotherms this is the migration velocity for $c_i \rightarrow 0$). For mixtures with nonlinear equilibria it is expedient to use the average value

of the different minimum velocities [89]. "Tuning" of the numerical accuracy (in order to match the physical dispersion term in Eq. (2.19)) is achieved by setting a proper ratio between the time and space increments of the difference terms above. It can be shown that the following holds for the apparent dispersion coefficient in Eq. (2.20) [89]:

$$D_{a,i} = \frac{\Delta z}{2}(a_{cou} - 1) \quad (\text{A.4})$$

From Eqs. (2.20) and Eq. (A.4) follows for the space increment

$$\Delta z = \frac{L_c}{NTP(a_{cou} - 1)} \quad (\text{A.5})$$

Thus, after specification of values for a_{cou} (in this work, $a_{cou} = 2$ will be used) and NTP , the space and time increments follow from Eqs. (A.5) and (A.3).

A.2 Steady-State Optimisation of SMB Processes

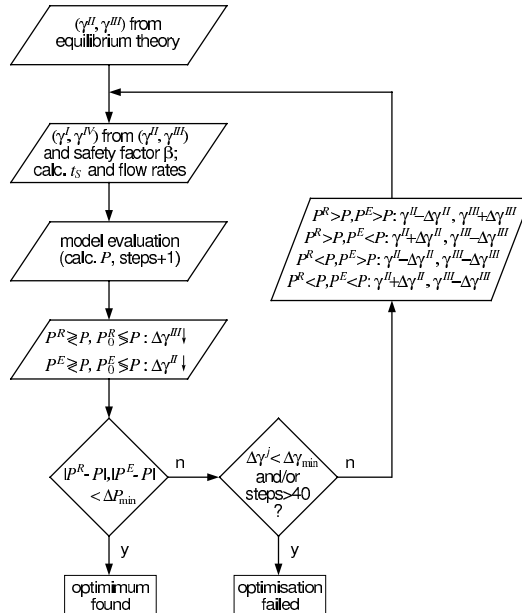


Figure A.1. Program flow chart for SMB optimisations in section 4.4.3.

The flow chart above describes the semi-heuristic approach used for the optimisations of the SMB process in Chapter 4.

A.3 SMB Performance under Reduced Purity Requirements

Table A.1 lists selected optimisation results for SMB processes under reduced purity requirements that were performed in section 4.4.3.

The first two lines contain for each system the theoretical productivities predicted from equilibrium theory using Eqs. (4.13) and (4.9) ($\beta = 1$ applied). The second line contains the theoretical productivity calculated using the necessary safety factors $\beta \geq 1$ that were estimated "manually" from preliminary numerical simulations. The difference between the corresponding productivities indicates the effect of the safety factors. The next three lines show results obtained from numerical simulations for three different values of the target purity.

Table A.1. Design parameters and selected predicted maximum productivities of the SMB process for separation of mandelic acid enantiomers using different chromatographic systems.

| System | α | c^F [g/l] | P [%] | β | γ^I | γ^{II} | γ^{III} | γ^{IV} | t_S^a [min] | PR [$\text{gl}^{-1}\text{d}^{-1}$] | ΔPR^b [%] | |
|--------|----------|------------------|--------------|---------|------------|---------------|----------------|---------------|--------------------|---|------------------------|--|
| I.b | 1.4 | 15 | 100 | 1.0 | 1.610 | 0.950 | 1.204 | 1.041 | 2.97 | 467.8 ^c | | |
| | | | 100 | 1.1 | 1.771 | 0.950 | 1.204 | 0.947 | 3.10 | 448.6 ^c | -4.1 | |
| | | | 99.0 | 1.1 | 1.771 | 1.031 | 1.243 | 0.947 | 3.10 | 367.2 ^d | -21.5 | |
| | | | 97.5 | 1.1 | 1.771 | 0.983 | 1.226 | 0.947 | 3.10 | 415.3 ^d | -11.2 | |
| | | | 65.0 | 1.1 | 1.771 | 0.432 | 1.549 | 0.947 | 3.10 | 1272.0 ^d | +172.9 | |
| I.c | 1.14 | 50 | 100 | 1.0 | 1.160 | 0.962 | 0.987 | 0.920 | 2.62 | 172.7 ^c | | |
| | | | 100 | 1.35 | 1.566 | 0.962 | 0.987 | 0.682 | 2.94 | 153.9 ^c | -10.9 | |
| | | | 99.0 | | | | | | | | | |
| | | | 97.5 | 1.35 | 1.566 | 1.040 | 1.050 | 0.682 | 2.94 | 57.2 ^d | -66.9 | |
| | | | 65.5 | 1.35 | 1.566 | 0.606 | 0.857 | 0.682 | 2.94 | 990.4 ^d | +473.5 | |
| I.d | 1.24 | 38 | 100 | 1.0 | 1.330 | 0.963 | 1.046 | 0.953 | 2.75 | 416.3 ^c | | |
| | | | 100 | 1.2 | 1.596 | 0.963 | 1.046 | 0.794 | 2.96 | 386.8 ^c | -7.1 | |
| | | | 99.0 | 1.2 | 1.596 | 1.191 | 1.195 | 0.794 | 2.96 | 130.5 ^d | -68.7 | |
| | | | 97.5 | 1.2 | 1.596 | 0.931 | 1.068 | 0.794 | 2.96 | 329.0 ^d | -21.0 | |
| | | | 65.5 | 1.2 | 1.596 | 0.520 | 1.104 | 0.794 | 2.96 | 1723.0 ^d | +313.9 | |
| I.e | 1.07 | 5 | 100 | 1.0 | 8.621 | 7.787 | 7.817 | 7.557 | 7.19 | 7.8 ^c | | |
| | | | 100 | 1.5 | 12.930 | 7.787 | 7.816 | 5.038 | 9.83 | 5.7 ^c | -26.9 | |
| | | | 99.0 | | | | | | | | | |
| | | | 97.5 | 1.5 | 12.930 | 8.213 | 8.221 | 5.038 | 9.83 | 1.4 ^d | -82.1 | |
| | | | 65.5 | 1.5 | 12.930 | 6.125 | 6.473 | 5.038 | 9.83 | 33.1 ^d | +324.4 | |
| ref | 1.14 | 50 | 100 | 1.0 | 1.170 | 0.966 | 0.992 | 0.924 | 2.63 | 178.3 ^c | | |

^a Calculated from Eq. (4.12) with $Q^I = 1.0$ ml/min.

^b Difference to maximum theoretical productivity ($P = 100\%$, $\beta = 1$).

^c Equilibrium theory with $P = 100\%$; Eqs. (4.13, 4.9).

^d Numerical simulations with $NTP = 300/\text{column}$.

A.4 Determination of Flow Rates and Bed Lengths

The TMB process is not used in practice because of the problems arising from solid handling (back-mixing and abrasion). Thus, for the calculations in section 7.4 flow rates and bed lengths have to be calculated that correspond to the use of packed columns (as are used in SMB processes).

The pressure drop in an SMB depends on the configuration of zones and pumps (see, for example, [138]). The highest internal flow rates and thus the highest throughputs are guaranteed if the maximum tolerable pressure drop, Δp_{\max} , is achieved. For the Chirobiotic T column, Δp is given by Eq. (3.2). In SMB systems with one internal recycle pump, Δp depends on all four internal flows. Assuming identical zone lengths, from Eq. (3.2) one obtains

$$\Delta p_{\max} = 4k_0 L_c \frac{Q_{t,\text{SMB}}}{\pi D^2} \quad (\text{A.6})$$

where Q_t is the sum of all four internal flow rates. For the maximum pressure drop tolerable, in the assume $\Delta p_{\max} = 50$ bar.

The relation between the height of a theoretical plate, $HETP$, and the flow rate is given by Eq. (3.1). For a plate number averaged over all four zones, \overline{NTP} , it follows from Eq. (3.1)

$$\overline{NTP} = \frac{L_c}{HETP} = \frac{L_c}{A\bar{u}_0 + B} = \frac{L_c}{A\frac{Q_{t,\text{SMB}}}{\pi D^2} + B} \quad (\text{A.7})$$

From Eq. (A.6) and Eq. (A.7) the flow rates and zone length can be calculated that correspond to the \overline{NTP} used in the TMB optimisations and to the tolerable pressure drop, Δp_{\max} and. Solving Eq. (A.6) and Eq. (A.7) one obtains for the bed length, L_c :

$$L_c = \frac{1}{2k_0} \left[NTP B k_0 + \sqrt{NTP k_0 (NTP k_0 B^2 + A \Delta p_{\max})} \right] \quad (\text{A.8})$$

For each TMB optimisation, the sum of the flow rates $Q_{t,\text{SMB}}$ and the bed length L_c now are calculated from Eqns. (A.6) and (A.8). Please note, that if the correlations for Δp_{\max} and $HETP$ are nonlinear, some simple iteration has to be used. The zone flow rates in an SMB, Q_{SMB}^j , depend on the dimensionless parameters γ^j (see section 4.2.3):

$$Q_{\text{SMB}}^j = \frac{\gamma^j V_c (1 - \epsilon_t) + V_c \epsilon_t}{t_S} \quad (\text{A.9})$$

Here, t_S and $V_c = \pi D^2 L_c$ are the switching time and column volume, respectively. From Eq. (A.9) and $Q_{t,\text{SMB}} = \sum_j \gamma^j$ follows for the flow rate in an individual zone

$$Q_{\text{SMB}}^j = Q_{t,\text{SMB}} \frac{\gamma^j (1 - \epsilon_t) + \epsilon_t}{(1 - \epsilon_t) \sum_j \gamma^j + 4\epsilon_t} \quad (\text{A.10})$$

From this expression, all individual zone flow rates can be obtained.

Appendix B

Data and Parameters for SLE Models

B.1 Experimental Data for Ternary SLEs

The following tables list the experimental data that were used to establish the SLE models in Chapter 6. These raw data were obtained from [118] and [119].

Table B.1. SLE data of mandelic acid enantiomers in methanol:water 20:80 (systems I_b and I_f in Tab. 3.1) from [119]. The corresponding ternary SLE is shown in Fig. 3.3.

| T [°C] | x_S [wt%] | x_R [wt%] |
|-------------|----------------|----------------|-------------|----------------|----------------|-------------|----------------|----------------|-------------|----------------|----------------|
| 0 | 6.9 | 0.0 | 20 | 19.1 | 0.0 | 40 | 53.4 | 0.0 | 60 | 76.8 | 0.0 |
| 0 | 7.9 | 3.6 | 20 | 29.7 | 13.4 | 40 | 48.5 | 21.8 | 60 | 59.2 | 26.6 |
| 0 | 5.2 | 5.2 | 20 | 18.0 | 18.0 | 40 | 33.3 | 33.3 | 60 | 41.2 | 41.2 |
| 10 | 11.0 | 0.0 | 30 | 35.3 | 0.0 | 50 | 66.1 | 0.0 | | | |
| 10 | 16.3 | 7.3 | 30 | 40.7 | 18.3 | 50 | 54.0 | 24.2 | | | |
| 10 | 9.5 | 9.5 | 30 | 27.0 | 27.0 | 50 | 37.5 | 37.5 | | | |

Table B.2. SLE data for mandelic acid enantiomers in acetonitrile:water 4.5/95 (system I_e in Tab. 3.1) from [118]. Corresponding ternary SLE shown in Fig. 3.4.

| T [°C] | x_S [wt%] | x_R [wt%] |
|-------------|----------------|----------------|-------------|----------------|----------------|-------------|----------------|----------------|-------------|----------------|----------------|
| 0 | 6.5 | 0.0 | 10 | 11.7 | 11.7 | 30 | 24.0 | 24.0 | 50 | 35.1 | 35.1 |
| 0 | 7.0 | 7.0 | 10 | 18.1 | 8.1 | 30 | 36.3 | 16.3 | 50 | 50.4 | 22.6 |
| 0 | 9.2 | 4.1 | 20 | 20.5 | 0.0 | 40 | 44.2 | 0.0 | 60 | 68.8 | 0.0 |
| 5 | 10.8 | 0.0 | 20 | 16.8 | 16.8 | 40 | 30.1 | 30.1 | 60 | 38.7 | 38.7 |
| 5 | 8.6 | 8.6 | 20 | 27.1 | 12.2 | 40 | 44.4 | 20.0 | 60 | 54.6 | 24.5 |
| 10 | 14.2 | 0.0 | 30 | 31.4 | 0.0 | 50 | 58.3 | 0.0 | | | |

Table B.3. SLE data for mandelic acid enantiomers in water (surrogate system) according to [118]. Corresponding ternary SLE shown in Fig. 3.5.

| T [°C] | x_S [wt%] | x_R [wt%] |
|-------------|----------------|----------------|-------------|----------------|----------------|-------------|----------------|----------------|-------------|----------------|----------------|
| 0 | 4.9 | 0.0 | 15 | 5.4 | 5.4 | 30 | 11.9 | 0.0 | 35 | 26.2 | 15.5 |
| 0 | 5.9 | 2.7 | 20 | 8.4 | 0.0 | 30 | 12.7 | 2.1 | 35 | 18.1 | 18.1 |
| 0 | 3.5 | 3.5 | 20 | 10.8 | 4.8 | 30 | 18.1 | 5.7 | 35 | 15.0 | 33.5 |
| 5 | 5.4 | 0.0 | 20 | 6.7 | 6.7 | 30 | 19.1 | 7.9 | 40 | 22.6 | 0.0 |
| 5 | 6.4 | 2.9 | 20 | 4.9 | 10.9 | 30 | 23.5 | 10.6 | 40 | 41.5 | 18.7 |
| 5 | 4.1 | 4.1 | 25 | 9.9 | 0.0 | 30 | 17.7 | 10.4 | 40 | 25.7 | 25.7 |
| 10 | 6.3 | 0.0 | 25 | 11.4 | 2.9 | 30 | 15.0 | 10.0 | 50 | 49.2 | 0.0 |
| 10 | 7.5 | 3.4 | 25 | 12.6 | 3.9 | 30 | 12.4 | 12.4 | 50 | 50.9 | 22.9 |
| 10 | 4.7 | 4.7 | 25 | 14.4 | 5.7 | 30 | 10.5 | 23.4 | 50 | 34.2 | 34.2 |
| 15 | 7.4 | 0.0 | 25 | 15.6 | 6.6 | 35 | 15.8 | 0.0 | 60 | 66.9 | 0.0 |
| 15 | 8.4 | 1.9 | 25 | 15.3 | 6.9 | 35 | 19.6 | 2.5 | 60 | 55.5 | 24.9 |
| 15 | 8.5 | 3.8 | 25 | 11.9 | 7.1 | 35 | 15.4 | 2.7 | 60 | 39.4 | 39.4 |
| 15 | 9.2 | 4.1 | 25 | 8.6 | 8.6 | 35 | 33.1 | 14.2 | | | |
| 15 | 7.0 | 4.3 | 25 | 6.7 | 15.0 | 35 | 33.7 | 15.2 | | | |

Table B.4. SLE data for system II according to [118]. Corresponding ternary SLE shown in Fig. 3.8.

| T [°C] | x_L [wt%] | x_D [wt%] |
|-------------|----------------|----------------|-------------|----------------|----------------|-------------|----------------|----------------|-------------|----------------|----------------|
| 10 | 0.370 | 0.000 | 20 | 0.510 | 0.000 | 30 | 0.670 | 0.000 | 40 | 0.730 | 0.000 |
| 10 | 0.380 | 0.380 | 20 | 0.565 | 0.565 | 30 | 0.755 | 0.755 | 40 | 1.005 | 1.005 |

Table B.5. SLE data for system III according to [118]. Corresponding ternary SLE shown in Fig. 3.10.

| T [°C] | x_S [wt%] | x_R [wt%] |
|-------------|----------------|----------------|-------------|----------------|----------------|-------------|----------------|----------------|-------------|----------------|----------------|
| 10 | 4.8 | 0.0 | 20 | 11.3 | 11.3 | 30 | 26.4 | 26.4 | 40 | 36.3 | 14.3 |
| 10 | 5.7 | 5.7 | 20 | 1.4 | 10.0 | 30 | 21.2 | 5.7 | | | |
| 10 | 5.2 | 2.1 | 20 | 9.1 | 4.8 | 40 | 37.6 | 0.0 | | | |
| 20 | 9.4 | 0.0 | 30 | 18.6 | 0.0 | 40 | 39.1 | 39.1 | | | |

B.2 Coefficients for SLE Models

Table B.2 contains the determined polynomial coefficients for the different enantiomeric systems that were used for the temperature-interpolation of solubilities at different compositions, Eq. (6.5).

Table B.6. Polynomial coefficients for temperature approximation of the solubility for the different experimental systems, Eq. (6.5). P – pure enantiomer, E – eutectic through, R – racemic through.

| System | | a_5 | a_4 | a_3 | a_2 | a_1 | a_0 |
|----------------------------------|-----|-------------|-------------|-------------|-------------|-------------|------------|
| MA/H ₂ O 0...40 °C | P | 8.0205E-09 | -5.3634E-07 | 1.3519E-05 | -1.3164E-04 | 2.2451E-03 | 4.4892E-02 |
| | E | 0.0000E+00 | -1.6197E-07 | 1.6516E-05 | -2.4289E-04 | 2.6283E-03 | 5.6939E-02 |
| | R | -5.6697E-09 | 5.6766E-07 | -1.4247E-05 | 1.4652E-04 | 6.7093E-04 | 3.4627E-02 |
| I.b, I.f (MA) 0...60 °C | P | 8.7708E-09 | -1.3312E-06 | 6.5150E-05 | -9.5673E-04 | 8.3834E-03 | 6.9060E-02 |
| | E | 0.0000E+00 | 1.2130E-07 | -1.5988E-05 | 5.9406E-04 | 4.2798E-03 | 7.8652E-02 |
| | R | 0.0000E+00 | 8.8598E-08 | -1.2671E-05 | 5.4155E-04 | -2.2794E-05 | 5.2260E-02 |
| I.e (MA) 0...60 °C | P | 0.0000E+00 | -1.1056E-07 | 1.1743E-05 | -2.8561E-04 | 9.0897E-03 | 6.6724E-02 |
| | E | 0.0000E+00 | 7.9716E-09 | -2.1200E-06 | 9.1496E-05 | 7.9843E-03 | 9.2249E-02 |
| | R | 0.0000E+00 | 5.8326E-09 | -2.1093E-06 | 1.4226E-04 | 3.0780E-03 | 6.9759E-02 |
| II 10...40 °C | P | 0.0000E+00 | 2.4772E-09 | -4.2100E-07 | 1.9685E-05 | -1.9315E-04 | 4.1058E-03 |
| | E=R | 0.0000E+00 | 0.0000E+00 | 9.1667E-08 | -5.2500E-06 | 2.7833E-04 | 1.4500E-03 |
| III 10...40 °C | P | 0.0000E+00 | 0.0000E+00 | 8.6667E-06 | -2.9000E-04 | 7.2333E-03 | 0.0000E+00 |
| | E=R | 0.0000E+00 | -8.9583E-07 | 6.9750E-05 | -1.4704E-03 | 1.4325E-02 | 0.0000E+00 |

B.3 Determination of Adsorption Isotherms from Perturbations

A perturbation method was applied for the determination of adsorption isotherms for systems I.f (mandelic acid on Chirobiotic T, see section 3.2) and system II (threonine on Chirobiotic T, see section 3.2). Tables B.7 and B.8 list the corresponding measured retention times.

Table B.7. Retention times measured in perturbation experiments for system I.f.

Flow rate: 2.50 ml/min, injections of 20 μ l pure eluent.

| c_{rac} [g/l] | t_1 [min] | t_2 [min] | c_{rac} [g/l] | t_1 [min] | t_2 [min] |
|--------------------|----------------|----------------|--------------------|----------------|----------------|
| 0.0 | 4.80 | 7.07 | 3.0 | 4.62 | 5.37 |
| 0.375 | 4.73 | 6.22 | 4.5 | 4.59 | 5.17 |
| 0.750 | 4.69 | 5.94 | 6.0 | 4.56 | 5.07 |
| 1.5 | 4.67 | 5.70 | 9.0 | 4.52 | 4.91 |
| 2.25 | 4.65 | 5.52 | 15.0 | 4.47 | 4.76 |

Table B.8. Retention times measured in perturbation experiments for system II. Left: flow rate Q of 0.98 ml/min, injections of 20 μ l pure eluent; middle: $Q = 1.97$ ml/min, 20 μ l pure eluent; right: $Q = 2.50$ ml/min, 20 μ l of asymmetrical enantiomeric mixtures.

| c_i | t_1 | t_2 | c_i | t_1 | t_2 | c_i | t_1 | t_2 |
|-------|-------------|-------------|-------|-------------|-------------|-------|-------|-------|
| [g/l] | [min] | [min] | [g/l] | [min] | [min] | [g/l] | [min] | [min] |
| 0.00 | 11.90 | 13.47 | 0.00 | 5.92 | 6.75 | 0.00 | 4.68 | 5.35 |
| 0.15 | 11.93 | 13.37 | 0.15 | 5.96 | 6.70 | 0.25 | 4.62 | 5.22 |
| 0.25 | 11.84 | 13.22 | 0.25 | 5.91 | 6.59 | 0.50 | 4.60 | 5.15 |
| 0.50 | 11.80 | 13.07 | 0.50 | 5.87 | 6.51 | 0.75 | 4.58 | 5.08 |
| 0.75 | 11.70 | 12.91 | 0.75 | 5.78 | 6.36 | 1.00 | 4.57 | 5.03 |
| 1.00 | 11.62 | 12.73 | 1.00 | 5.75 | 6.28 | 1.25 | 4.55 | 5.00 |
| 1.50 | 11.51 | 12.53 | 1.50 | 5.70 | 6.19 | 1.50 | 4.55 | 4.99 |
| 2.00 | 11.40 | 12.25 | 2.00 | 5.59 | 6.03 | 2.00 | 4.51 | 4.88 |
| 2.50 | 11.28 | <i>n.a.</i> | 2.50 | 5.59 | <i>n.a.</i> | 2.50 | 4.47 | 4.80 |
| 3.00 | 11.21 | <i>n.a.</i> | 3.00 | <i>n.a.</i> | <i>n.a.</i> | 3.00 | 4.45 | 4.77 |
| 3.50 | 11.05 | <i>n.a.</i> | 3.50 | <i>n.a.</i> | <i>n.a.</i> | 3.50 | 4.39 | 4.74 |
| 4.00 | <i>n.a.</i> | <i>n.a.</i> | 4.00 | <i>n.a.</i> | <i>n.a.</i> | 4.00 | 4.42 | 4.73 |
| 5.00 | <i>n.a.</i> | <i>n.a.</i> | 5.00 | <i>n.a.</i> | <i>n.a.</i> | 4.50 | 4.38 | 4.69 |
| | | | | | | 5.00 | 4.40 | 4.69 |

B.4 Densities of Chromatographic Solvents

Table B.9. Experimental densities of chromatographic solvents. For abbreviations see Table 3.1.

| System | Mobile phase composition | ρ [g/cm ³] |
|--------|--|-----------------------------|
| I.a | EtOH:H ₂ O (50:50) | 0.9222 |
| I.b | MeOH:0.3 M TEAAc (20:80) | 1.0059 |
| I.c | EtOH:0.36 M TEAAc (50:50) | 0.9233 |
| I.d | MeOH:MeCN:TEAAc:HOAc (54.5:45.1:0.2:0.2) | 0.7880 |
| II | EtOH:H ₂ O (60:40) | 0.9018 |
| III | MeCN | 0.7758 |

Appendix C

Dynamic Model for the Process Combination

In order to provide a tool for further investigations, a mathematical model was developed for a continuous scheme of the process combination. The model was implemented into DIVA using the modelling tool PROMOT. Basis for this model is the process scheme in Fig. 7.1.

The model basically consists of the equilibrium-stage approach for the TMB process that was explained in section 2.1.5, and a model for a continuous crystallisation process. The crystalliser was considered as a CSTR of the Mixed Suspension – Mixed Product Removal (MSMPR) type. The particle size distribution (PSD) was described by a moment approach. Moment models allow to quantitatively describe PSDs on the basis of ordinary differential equations. Due to this, they are numerically much less expensive than detailed models for PSDs (which represent systems of partial differential equations). More information on the model below can be found, for example, in [112]. A comprehensive overview on modelling of crystallisation processes is given in [113].

The following expressions are used to model the rates of particle growth, G , and nucleation, B , respectively:

$$B = k_b M_2 (c_1 - c_1^*)^b \quad (\text{C.1})$$

$$G = k_g (c_1 - c_1^*)^g \quad (\text{C.2})$$

Here c_1^* is the equilibrium concentration of component 1, which was calculated using the SLE model explained in section 6.1.2. It is assumed that only this component crystallises. The coefficients in the equations above have to be determined experimentally. Since detailed information with respect to these coefficients were missing for the enantiomeric systems considered, the following values were (arbitrarily) assumed: $k_b = 1000 \text{ m}/(\text{g}\cdot\text{s})$, $k_g = 2 \cdot 10^{-9} \text{ m}^4/(\text{g}\cdot\text{s})$, $b = g = 1$.

In Eq. (C.1), M_2 is the second moment of the PSD. The time-dependence of the different moments is given by

$$\frac{\partial M_0}{\partial t} = B - \frac{M_0}{\tau} \quad (\text{C.3a})$$

$$\frac{\partial M_i}{\partial t} = G - \frac{M_i}{\tau}, \quad i = (1, 2, 3) \quad (\text{C.3b})$$

Here, τ is the residence time in the crystalliser. For the concentration of component 1 in the mother liquor holds (under the assumption of spherical crystals):

$$\frac{\partial c_1}{\partial t} = \frac{c_1^{\text{in}} - c_1}{\tau} - 3\rho_s \frac{\pi}{6} G M_2 \quad (\text{C.4})$$

where ρ_s is the density of the solid phase. For the concentration of component 2 (which is not crystallising) applies

$$\frac{\partial c_2}{\partial t} = \frac{c_2^{\text{in}} - c_2}{\tau} \quad (\text{C.5})$$

For the solid phase mass balance the suspension density, $c_{1,s}$, was described by

$$\frac{\partial c_{1,s}}{\partial t} = 3\rho_s \frac{\pi}{6} G M_2 - \frac{c_{1,s}}{\tau} \quad (\text{C.6})$$

Correspondingly, since component 2 is not crystallising, it is set $c_{2,s} = 0$.

As initial values in the above equations it was applied $(B, G, M_i, c_1, c_2) = 0$. This corresponds to a crystalliser filled with pure solvent. A discrete event was applied for the addition of a certain amount of seed crystals if the liquid concentration exceeded the solubility limit (*i.e.*, if $c_1 > c_1^*$). Similarly, it was continuously checked if the composition of the mother liquor has under-run the eutectic through. Since in this case the SLE model explained in Chapter 6.1.2 does not hold, a certain penalty was set to some of the calculated states in order to "mark" the corresponding simulation results. This penalty was also applied if the liquid concentration fell below the saturation limit (*i.e.*, for $c_1 < c_1^*$), since dissolution kinetics were not implemented at this stage. It is emphasised that this modelling approach is consistent only for the crystallisation of pure enantiomer.

Design decisions are open for the unit operations in Fig. 7.1 that are related to solvent removal and dilution. Therefore, these units were modelled as continuous CSTRs with a low volume. The enrichment step was assumed to perform an ideal split (*i.e.*, to remove only solvent). For this purpose, a solvent removal ratio was specified.

It should be mentioned that the above model represents a basis for further model development. It is straightforward to expand this model using more advanced kinetic expressions or unit operations. For example, a distillation or membrane unit might be applied for solvent removal. Furthermore, a hybrid model for the SMB process might be implemented.

Bibliography

- [1] J. H. van't Hoff. Sur les formules de structure dans l'espace. *Archives Néerlandaises des Sciences Exactes et Naturelles* 9 (1874) 445–454.
- [2] J. A. Le Bel. Sur les relations qui existent entre les formules atomiques des corps organiques et le pouvoir rotatoire de leurs dissolutions. *Bulletin de la Societe Chimique de France* 22 (1874) 337.
- [3] E. L. Eliel, S. Wilen, and M. Doyle. *Basic Organic Stereochemistry*. Wiley-Interscience, New York, 2001.
- [4] E. Fischer. Ueber die Configuration des Traubenzuckers und seiner Isomeren: II. *Berichte der Deutschen Chemischen Gesellschaft* 24 (1891) 2683–2687.
- [5] R. Cahn, S. C. Ingold, and V. Prelog. Spezifikation der molekularen Chiralität. *Angewandte Chemie* 78 (1966) 413–447.
- [6] K.-H. Hellwich. *Stereochemie; Grundbegriffe*. Springer, Berlin, 2002.
- [7] J. Jacques, A. Collet, and S. Wilen. *Enantiomers, Racemates and Resolutions*. Krieger, Malabar, 1994.
- [8] G. Coquerel. Review on the Heterogeneous Equilibria between Condensed Phases in Binary Systems of Enantiomers. *Enantiomer* 5 (2000) 481–498.
- [9] W. A. Bonner. Parity violation and the evolution of biomolecular homochirality. *Chirality* 12 (2000) 114–126.
- [10] E. J. Ariëns. Stereochemistry, a Basis for Sophisticated Nonsense in Pharmacokinetics and Clinical Pharmacology. *European Journal of Clinical Pharmacology* 26 (1984) 663–668.
- [11] R. R. Shah, J. M. Midgley, and S. K. Branch. Stereochemical origin of some clinically significant drug safety concerns: lessons for future drug development. *Adverse Drug Reactions and Toxicological Reviews* 17 (1998) 145–190.
- [12] A. M. Rouhi. Chirality at work. *Chemical and Engineering News* 81 (2003) 56–61.
- [13] J. Blumenstein. Chiral Drugs: Regulatory Aspects. In: A. Collins, G. Sheldrake, and J. Crosby (Eds.): *Chirality in Industry II. Developments in the Manufacture of Optically Active Compounds*. John Wiley & Sons, Chichester, 1997, 11–18.
- [14] I. Agranat, H. Caner, and J. Caldwell. Putting chirality to work: the strategy of chiral switches. *Nature Reviews Drug Discovery* 1 (2002) 753–768.

- [15] S. C. Stinson. Chiral pharmaceuticals. *Chemical and Engineering News* 79 (2001) 45–57.
- [16] A. M. Rouhi. Chiral business. *Chemical and Engineering News* 81 (2003) 45–55.
- [17] S. Kotha. Opportunities in Asymmetric Synthesis: An Industrial Perspective. *Tetrahedron* 50 (1994) 3639–3662.
- [18] J. M. Brown and S. G. Davies. Chemical asymmetric synthesis. *Nature* 342 (1989) 631–636.
- [19] J. Crosby. Chirality in Industry: An Overview. In: A. Collins, G. Sheldrake, and J. Crosby (Eds.): *Chirality in Industry. The Commercial Manufacture and Applications of Optically Active Compounds*. John Wiley & Sons, Chichester, 1992, 1–66.
- [20] J. Crosby. Synthesis of Optically Active Compounds: A Large Scale Perspective. *Tetrahedron* 47 (1991) 4789–4846.
- [21] A. Collins, G. Sheldrake, and J. Crosby (Eds.). *Chirality in Industry. The Commercial Manufacture and Applications of Optically Active Compounds*. John Wiley & Sons, Chichester, 1992.
- [22] A. Collins, G. Sheldrake, and J. Crosby (Eds.). *Chirality in Industry II. Developments in the Manufacture of Optically Active Compounds*. John Wiley & Sons, Chichester, 1997.
- [23] J. Crosby. Introduction. In: A. Collins, G. Sheldrake, and J. Crosby (Eds.): *Chirality in Industry II. Developments in the Manufacture of Optically Active Compounds*. John Wiley & Sons, Chichester, 1997, 1–10.
- [24] K. M. Koeller and C. Wong. Enzymes for chemical synthesis. *Nature* 409 (2001) 232–240.
- [25] C. Walsh. Enabling the chemistry of life. *Nature* 409 (2001) 226–231.
- [26] E. García-Junceda, J. F. García-García, A. Bastida, and A. Fernández-Mayoralas. Enzymes in the synthesis of bioactive compounds: the prodigious decades. *Bioorganic & Medicinal Chemistry* 12 (2004) 1817–1834.
- [27] N. M. Maier, P. Franco, and W. Lindner. Separation of enantiomers: needs, challenges, perspectives. *Journal of Chromatography A* 906 (2001) 3–33.
- [28] A. Bruggink. Rational Design in Resolutions. In: A. Collins, G. Sheldrake, and J. Crosby (Eds.): *Chirality in Industry II. Developments in the Manufacture of Optically Active Compounds*. John Wiley & Sons, Chichester, 1997, 81–98.
- [29] C. Bayley and N. Vaidya. Resolution of Racemates by Diastereomeric Salt Formation. In: A. Collins, G. Sheldrake, and J. Crosby (Eds.): *Chirality in Industry. The Commercial Manufacture and Applications of Optically Active Compounds*. John Wiley & Sons, Chichester, 1992, 69–77.
- [30] G. Subramanian (Ed.). *Chiral Separation Techniques - A Practical Approach*. 2nd ed. Wiley-VCH, Weinheim, 2000.

- [31] E. R. Francotte. Enantioselective chromatography as a powerful alternative for the preparation of drug enantiomers. *Journal of Chromatography A* 906 (2001) 379–397.
- [32] L. Pasteur. Recherches sur les relations qui peuvent exister entre la forme cristalline et la composition chimique, et le sens de la polarisation rotatoire. *Annales de Chimie et de Physique* 3 (1848) 442–459.
- [33] A. A. Rodrigo, H. Lorenz, and A. Seidel-Morgenstern. Online monitoring of preferential crystallization of enantiomers. *Chirality* 16 (2004) 499–508.
- [34] A. Collet. Racematspaltung: Sagten Sie "klassisch" ? *Angewandte Chemie* 110 (1998) 3429–3431.
- [35] I. Markovits, G. Egri, and E. Fogassy. Nonlinearity in optical resolution via distillation applying mixtures of resolving agents. *Chirality* 14 (2002) 674–676.
- [36] J. Keurentjes and F. Voermans. Membrane Separations in the Production of Optically Pure Compounds. In: A. Collins, G. Sheldrake, and J. Crosby (Eds.): *Chirality in Industry II. Developments in the Manufacture of Optically Active Compounds*. John Wiley & Sons, Chichester, 1997, 157–180.
- [37] A. Blacker and R. Holt. Development of a Multi-stage Chemical and Biological Process for an Optically Active Intermediate for an Anti-glaucoma Drug. In: A. Collins, G. Sheldrake, and J. Crosby (Eds.): *Chirality in Industry II. Developments in the Manufacture of Optically Active Compounds*. John Wiley & Sons, Chichester, 1997, 245–261.
- [38] A. Bommarius, K. Drauy, U. Groeger, and C. Wandrey. Membrane Bioreactors for the Production of Enantiomerically Pure α -Amino Acids. In: A. Collins, G. Sheldrake, and J. Crosby (Eds.): *Chirality in Industry. The Commercial Manufacture and Applications of Optically Active Compounds*. John Wiley & Sons, Chichester, 1992, 371–397.
- [39] B. Sellergren. Enantiomer Separation Using Tailor-Made Phases Prepared by Molecular Imprinting. In: G. Subramanian (Ed.): *Chiral Separation Techniques - A Practical Approach*. 2nd ed. Wiley-VCH, Weinheim, 2000, 69–93.
- [40] C. Baudequin, J. Baudoux, J. Levillain, D. Cahard, A.-C. Gaumont, and J.-C. Plaquevent. Ionic liquids and chirality: opportunities and challenges. *Tetrahedron: Asymmetry* 14 (2003) 3081–3093.
- [41] B. Simandi, S. Keszei, E. Fogassy, S. Kemeny, and J. Sawinsky. Separation of enantiomers by supercritical fluid extraction. *Journal of Supercritical Fluids* 13 (1998) 331–336.
- [42] G. Biressi, F. Quattrini, M. Juza, M. Mazzotti, V. Schurig, and M. Morbidelli. Gas chromatographic simulated moving bed separation of the enantiomers of the inhalation anesthetic enflurane. *Chemical Engineering Science* 55 (2000) 4537–4547.
- [43] A. Stankiewicz. Reactive separations for process intensification: an industrial perspective. *Chemical Engineering and Processing* 42 (2003) 137–144.

- [44] D. W. Agar. Prozessintegration. *Chemie Ingenier Technik* 75 (2003) 1408–1410.
- [45] R. F. Dunn and M. M. El-Halwagi. Process integration technology review: background and applications in the chemical process industry. *Journal of Chemical Technology and Biotechnology* 78 (2003) 1011–1021.
- [46] F. M. Dautzenberg and M. Mukherjee. Process intensification using multifunctional reactors. *Chemical Engineering Science* 56 (2001) 251–267.
- [47] N. Hallale. Trends in Process Integration. *Chemical Engineering Progress* 97 (2001) 30–41.
- [48] K. Sundmacher, A. Kienle, and A. Seidel-Morgenstern (Eds.). *Integrated Chemical Processes*. Wiley-VCH, 2005.
- [49] R. Waschler. *Nonlinear Analysis of Chemical Processes with Material and Energy Recycles*. Ph.D. thesis. Otto-von-Guericke Universität Magdeburg (2005).
- [50] J. Blehaut and R.-M. Nicoud. Recent aspects in simulated moving bed. *Analysis Magazine* 26 (1998) M60–M70.
- [51] S. Datta and D. J. W. Grant. Crystal structures of drugs: Advances in determination, prediction and engineering. *Nature Reviews Drug Discovery* 3 (2004) 42–57.
- [52] B.-G. Lim, C.-B. Ching, R. B. H. Tan, and S.-C. Ng. Recovery of (–)-praziquantel from racemic mixtures by continuous chromatography and crystallisation. *Chemical Engineering Science* 50 (1995) 2289–2298.
- [53] B.-G. Lim, R. B. H. Tan, S.-C. Ng, and C.-B. Ching. Solubility phase diagram of praziquantel enantiomeric system. *Chirality* 7 (1995) 74–81.
- [54] M. Kearney and D. Rearick. Raw Juice Chromatographic Separation Process. *International Sugar Journal* 98 (1996) 144–148.
- [55] G. Vaccari, G. Mantovani, G. Sgualdino, and W. J. Colonna. Cooling Crystallization Applied to the "Extract" of a Chromatographic Separation Process (SMB) of Molasses In: *Proceedings of the Conference on Sugar Processing Research*. Savannah, GA (USA), 1998 93–108.
- [56] H. Lorenz, P. Sheehan, and A. Seidel-Morgenstern. Coupling of simulated moving bed chromatography and fractional crystallisation for efficient enantioseparation. *Journal of Chromatography A* 908 (2001) 201–14.
- [57] M. Kaspereit, P. Jandera, M. Skavrada, and A. Seidel-Morgenstern. Impact of adsorption isotherm parameters on the performance of enantioseparation using simulated moving bed chromatography. *Journal of Chromatography A* 944 (2002) 249–262.
- [58] M. Kaspereit, H. Lorenz, and A. Seidel-Morgenstern. Coupling of simulated moving bed technology and crystallization to separate enantiomers. In: K. Kaneko *et al.* (Eds.): *Fundamentals of adsorption*, vol. 7. IK International Ltd., Shinjuko, Japan, 2002, 101–108.

- [59] G. Ströhlein, M. Schulte, and J. Strube. Hybrid Processes: Design Method for Optimal Coupling of Chromatography and Crystallization Units. *Separation Science and Technology* 38 (2003) 3353–3383.
- [60] K. Gedicke, W. Beckmann, A. Brandt, D. Sapoundjiev, H. Lorenz, U. Budde, and A. Seidel-Morgenstern. Coupling of Chromatography and Crystallization for Efficient Separation of Enantiomers. *Adsorption* 11 (2005) 591–596.
- [61] M. Kaspereit, K. Gedicke, V. Zahn, A. W. Mahoney, and A. Seidel-Morgenstern. Shortcut method for evaluation and design of a hybrid process for enantioseparations. *Journal of Chromatography A* 1092 (2005) 43–54.
- [62] G. Ganetsos and P. Barker (Eds.). Preparative and production scale chromatography. Decker, New York, 1993.
- [63] G. Guiochon, S. G. Shirazi, and A. M. Katti. Fundamentals of preparative and nonlinear chromatography. Academic Press, Boston, 1994.
- [64] K. K. Unger. Handbuch der HPLC. Teil 2: Präparative Säulenflüssig-Chromatographie. GIT Verlag, Darmstadt, 1994.
- [65] G. Guiochon. Preparative liquid chromatography. *Journal of Chromatography A* 965 (2002) 129–161.
- [66] H. Schmidt-Traub (Ed.). Preparative chromatography of fine chemical and pharmaceutical agents. Wiley-VCH, Weinheim, 2005.
- [67] D. B. Broughton and C. G. Gerhold. Continuous Sorption Process Employing Fixed Bed of Sorbent and Moving Inlets and Outlets. U.S. Patent 2 985 589 (1961).
- [68] S. Franzen, M. Grünewald, and H. Schmidt-Traub. Stoffaustausch in kontinuierlich betriebenen Flüssig/Fest-Wirbelschichtprozessen mit Gegenstromführung. *Chemie-Ingenieur-Technik* 74 (2002) 1322–1326.
- [69] M. Schulte and J. Strube. Preparative enantioseparation by simulated moving bed chromatography. *Journal of Chromatography A* 906 (2001) 399–416.
- [70] S. Imamoglu. Simulated moving bed chromatography (SMB) for application in bioseparation. *Advances in Biochemical Engineering/Biotechnology* 76 (2002) 211–231.
- [71] D. Wu, Z. Ma, and N.-H. L. Wang. Optimization of throughput and desorbent consumption in simulated moving-bed chromatography for paclitaxel purification. *Journal of Chromatography A* 855 (1999) 71–89.
- [72] H. Schramm, A. Kienle, M. Kaspereit, and A. Seidel-Morgenstern. Improved operation of simulated moving bed processes through cyclic modulation of feed flow and feed concentration. *Chemical Engineering Science* 58 (2003) 5217–5227.

- [73] H. Schramm, M. Kaspereit, A. Kienle, and A. Seidel-Morgenstern. Simulated moving bed process with cyclic modulation of the feed concentration. *Journal of Chromatography A* 1006 (2003) 77–86.
- [74] O. Ludemann-Hombourger, G. Pigorini, R.-M. Nicoud, D. Ross, and G. Terfloth. Application of the "VariCol" process to the separation of the isomers of the SB-553261 racemate. *Journal of Chromatography A* 947 (2002) 59–68.
- [75] O. Ludemann-Hombourger, R.-M. Nicoud, and M. Bailly. The "VariCol" process: a new multicolumn continuous chromatographic process. *Separation Science and Technology* 35 (2000) 1829–1862.
- [76] M. Kearney and K. Hieb. Time variable simulated moving bed process. US patent 5 102 553 (1992).
- [77] E. Kloppenburg and E. Gilles. A new concept for operating simulated moving-bed processes. *Chemical Engineering Technology* 22 (1999) 813–817.
- [78] Y. Zang and P. C. Wankat. SMB operation strategy – partial feed. *Industrial and Engineering Chemistry Research* 41 (2002) 2504–2511.
- [79] Z. Zhang, M. Mazzotti, and M. Morbidelli. PowerFeed operation of simulated moving bed units: changing flow-rates during the switching interval. *Journal of Chromatography A* 1006 (2003) 87–99.
- [80] Z. Zhang, M. Mazzotti, and M. Morbidelli. Continuous Chromatographic Processes with a Small Number of Columns: Comparison of Simulated Moving Bed with Varicol, Power-Feed, and ModiCon. *Korean Journal of Chemical Engineering* 21 (2004) 454–464.
- [81] A. Seidel-Morgenstern. Experimental determination of single solute and competitive adsorption isotherms. *Journal of Chromatography A* 1037 (2004) 255–272.
- [82] F. Charton and R.-M. Nicoud. Complete design of a simulated moving bed. *Journal of Chromatography A* 702 (1995) 97–112.
- [83] D. B. Broughton. Adsorption isotherms for binary gas mixtures. *Industrial Engineering Chemistry* 8 (1948) 1506–1508.
- [84] A. Gentilini, C. Migliorini, M. Mazzotti, and M. Morbidelli. Optimal operation of simulated moving-bed units for non-linear chromatographic separations: II. Bi-Langmuir isotherm. *Journal of Chromatography A* 805 (1998) 37–44.
- [85] A. Myers and J. M. Prausnitz. Thermodynamics of mixed-gas adsorption. *AIChE Journal* 11 (1965) 121–127.
- [86] C. J. Radke and J. M. Prausnitz. Thermodynamics of multi-solute adsorption from dilute liquid solutions. *AIChE Journal* 18 (1972) 761–768.
- [87] A. L. Myers. Activity Coefficients of Mixtures Adsorbed on Heterogeneous Surfaces. *AIChE Journal* 29 (1983) 691–693.

- [88] D. M. Ruthven. Principles of Adsorption and Adsorption Processes. John Wiley, NY, 1984.
- [89] A. Seidel-Morgenstern. Mathematische Modellierung der präparativen Flüssigchromatographie. Deutscher Universitätsverlag, Wiesbaden, 1995.
- [90] D. D. Do. Adsorption Analysis: Equilibria and Kinetics. Imperial College Press, London, 1998.
- [91] J. J. van Deemter, F. J. Zuiderweg, and A. Klinkenberg. Longitudinal Diffusion and Resistance to Mass Transfer as Causes of Nonideality in Chromatography. *Chemical Engineering Science* 5 (1956) 271–289.
- [92] A. Seidel-Morgenstern. Analysis of boundary conditions in the axial dispersion model by application of numerical laplace inversion. *Chemical Engineering Science* 46 (1991) 2567–2571.
- [93] S. K. Godunov. A finite difference method for the numerical computation of discontinuous solutions of the equations of fluid dynamics. *Mat Sb* 47 (1959) 271–290.
- [94] P. Rouchon, M. Schonauer, P. Valentin, and G. Guiochon. Numerical Solution of Band Propagation in Nonlinear Chromatography. *Separation Science and Technology* 22 (1987) 1793–1833.
- [95] H. Kniep. Vergleich verschiedener verfahrenstechnischer Konzepte zur Durchführung der präparativen Flüssigchromatographie. Ph.D. thesis. Otto-von-Guericke Universität Magdeburg (1998).
- [96] M. Ginkel, A. Kremling, T. Nutsch, R. Rehner, and E. Gilles. Modular modeling of cellular systems with PROMOT/Diva. *Bioinformatics* 19 (2003) 1169–1176.
- [97] H. Schramm. Neue Betriebsweisen und Prozessführungskonzepte für chromatographische Prozesse mit simuliertem Gegenstrom. Ph.D. thesis. Otto-von-Guericke Universität Magdeburg (2005).
- [98] F. Tränkle, M. Zeitz, M. Ginkel, and E. Gilles. PROMOT: A modeling tool for chemical processes. *Mathematical and computer modelling of dynamical systems* 6 (2000) 283–307.
- [99] A. Jupke, A. Epping, and H. Schmidt-Traub. Optimal design of batch and simulated moving bed chromatographic separation processes. *Journal of Chromatography A* 944 (2002) 93–117.
- [100] Z. Zhang, M. Mazzotti, and M. Morbidelli. Multiobjective optimization of simulated moving bed and Varicol processes using a genetic algorithm. *Journal of Chromatography A* 989 (2003) 95–108.
- [101] Z. Ma and N.-H. L. Wang. Standing Wave Analysis of SMB Chromatography: Linear Systems. *AIChE Journal* 43 (1997) 2488–2508.
- [102] T. Mallmann, B. D. Burris, Z. Ma, and N.-H. L. Wang. Standing Wave Design of Nonlinear SMB Systems for Fructose Purification. *AIChE Journal* 44 (1998) 2628–2646.

- [103] M. Mazzotti, G. Storti, and M. Morbidelli. Optimal operation of simulated moving bed units for nonlinear chromatographic separations. *Journal of Chromatography A* 769 (1997) 3–24.
- [104] R. Perry and D. Green (Eds.). *Perry's Chemical Engineers' Handbook*. 6 ed. McGraw-Hill, 1984.
- [105] H. W. Bakhuis Roozeboom. Über die Löslichkeit von Mischkrystallen, speziell zweier isomorphen Körper. *Zeitschrift für Physikalische Chemie* 8 (1891) 504–530.
- [106] H. W. Bakhuis Roozeboom. Löslichkeit und Schmelzpunkt als Kriterien für racemische Verbindungen, pseudoracemische Mischkrystalle und inaktive Konglomerate. *Zeitschrift für Physikalische Chemie* 28 (1899) 494–517.
- [107] P. Marchand, L. Lefe'uvre, F. Querniard, P. Cardinaël, G. Perez, J.-J. Couniouxc, and G. Coquerel. Diastereomeric resolution rationalized by phase diagrams under the actual conditions of the experimental process. *Tetrahedron: Asymmetry* 15 (2004) 2455–2465.
- [108] C. Wibowo, L. O'Young, and K. M. Ng. Streamlining Crystallization Process Design. *Chemical Engineering Progress* 100 (2004) 30–42.
- [109] D. W. Slaughter and M. F. Doherty. Calculation of Solid-Liquid Equilibrium and Crystallization Paths for Melt Crystallization Processes. *Chemical Engineering Science* 50 (1995) 1679–1694.
- [110] V. N. Kiva, E. K. Hilmen, and S. Skogestad. Azeotropic Phase Equilibrium Diagrams: A Survey. *Chemical Engineering Science* 58 (2003) 1903–1953.
- [111] A. Mersmann (Ed.). *Crystallization technology handbook*. Dekker, New York, 2001.
- [112] M. J. Hounslow and E. J. W. Wynn. Short-cut models for particulate processes. *Computers & Chemical Engineering* 17 (1993) 505–516.
- [113] A. D. Randolph and M. A. Larson. *Theory of Particulate Processes*. Academic Press, 1988.
- [114] M. J. O. *et al.* (Ed.). *The Merck index: an encyclopedia of chemicals, drugs, and biologicals*. 13th ed. Whitehouse Station, NJ, 2001.
- [115] *Ullmann's encyclopedia of industrial chemistry*. 6th Ed. (CD-ROM). Wiley-VCH, Weinheim, 2003.
- [116] P. Jandera, M. Skavrada, K. Klemmova, V. Backovska, and G. Guiochon. Effect of the mobile phase on the retention behaviour of optical isomers of carboxylic acids and amino acids in liquid chromatography on bonded Teicoplanin columns. *Journal of Chromatography A* 917 (2001) 123–133.
- [117] C. Blümel, P. Hugo, and A. Seidel-Morgenstern. Quantification of single solute and competitive adsorption isotherms using a closed-loop perturbation method. *Journal of Chromatography A* 865 (1999) 51–71.

- [118] H. Lorenz, D. Sapoundjiev, and A. Seidel-Morgenstern. Solubility Equilibria in Chiral Systems and Their Importance for Enantioseparation. *Engineering in Life Sciences* 3 (2003) 132–136.
- [119] D. Sapoundjiev. Ph.D. thesis (in preparation). Otto-von-Guericke Universität Magdeburg.
- [120] H. Lorenz, D. Sapoundjiev, and A. Seidel-Morgenstern. Enantiomeric Mandelic Acid Systems – Melting Point Phase Diagram and Solubility in Water. *J Chem Eng Data* 47 (2002) 1280–1284.
- [121] K. Okamoto and M. Ikeda. Development of an Industrially Stable Process for *L*-Threonine Fermentation by an *L*-Methionine -Auxotrophic Mutant of *Escherichia coli*. *Journal of Bioscience and Bioengineering* 89 (1999) 87–89.
- [122] P. Forssén, J. Lindholm, and T. Fornstedt. Theoretical and experimental study of binary perturbation peaks with focus on peculiar retention behaviour and vanishing peaks in chiral liquid chromatography. *Journal of Chromatography A* 991 (2003) 31–45.
- [123] H. Kniep, G. Mann, C. Vogel, and A. Seidel-Morgenstern. Separation of Enantiomers through Simulated Moving-Bed Chromatography. *Chemical Engineering Technology* 23 (2000) 853–857.
- [124] G. Storti, R. Baciocchi, M. Mazzotti, and M. Morbidelli. Design of Optimal Operating Conditions of Simulated Moving Bed Adsorptive Separation Units. *Industrial and Engineering Chemistry Research* 34 (1995) 288–301.
- [125] C. Migliorini, M. Mazzotti, and M. Morbidelli. Continuous chromatographic separation through simulated moving beds under linear and nonlinear conditions. *Journal of Chromatography A* 827 (1998) 161–173.
- [126] J. W. Priegnitz and B. McCulloch. Chiral separations by simulated moving bed chromatography operating at low k' values. US patent 5 518 625 (1996).
- [127] G. Biressi, O. Ludemann-Hombourger, M. Mazzotti, R. Nicoud, and M. Morbidelli. Design and optimisation of a simulated moving bed unit: role of deviations from equilibrium theory. *Journal of Chromatography A* 876 (2000) 3–15.
- [128] D. Antos and A. Seidel-Morgenstern. Two-step solvent gradients in simulated moving bed chromatography. Numerical study for linear equilibria. *Journal of Chromatography A* 944 (2002) 77–91.
- [129] H. Schramm, S. Grüner, and A. Kienle. Optimal operation of simulated moving bed chromatographic processes by means of simple feedback control. *Journal of Chromatography A* 1006 (2003) 3–13.
- [130] S. Natarajan and J. Lee. Repetitive model predictive control applied to a simulated moving bed chromatography system. *Computers & Chemical Engineering* 24 (2000) 1127–1133.

- [131] E. Kloppenburg and E. Gilles. Automatic control of the simulated moving bed process for C8 aromatics separation. *Journal of Process Control* 9 (1999) 41–50.
- [132] K.-U. Klatt, F. Hanisch, G. Dünnebier, and S. Engell. Model-based optimization and control of chromatographic processes. *Computers & Chemical Engineering* 24 (2000) 1119–1126.
- [133] K.-U. Klatt, F. Hanisch, and G. Dünnebier. Model-based control of a simulated moving bed chromatographic process for the separation of fructose and glucose. *Journal of Process Control* 12 (2002) 203–219.
- [134] Z. Zhang, K. Hidajat, A. Ray, and M. Morbidelli. Multiobjective Optimization of SMB and Varicol Process for Chiral Separation. *AIChE Journal* 48 (2002) 2800–2816.
- [135] H. Subramani, K. Hidajat, and A. Ray. Optimization of reactive SMB and Varicol systems. *Computers & Chemical Engineering* 27 (2003) 1883–1901.
- [136] D. Azevedo and A. Rodrigues. Fructose-Glucose Separation in a SMB Pilot Unit: Modeling, Simulation, Design, and Operation. *AIChE Journal* 47 (2001) 2042–2051.
- [137] The NAG Library, Mark 15, Vols. 1-10, NAG Ltd, Oxford (1991).
- [138] R.-M. Nicoud. in: G. Subramanian (Ed.): *Bioseparation and Bioprocessing*. Wiley-VCH, 1998.
- [139] F. Helfferich. Non-linear waves in chromatography III. Multicomponent Langmuir and Langmuir-like systems. *Journal of Chromatography A* 768 (1997) 169–205.
- [140] J. M. Prausnitz, R. N. Lichtenthaler, and E. G. de Azevedo. *Molecular thermodynamics of fluid-phase equilibria*. Prentice-Hall, Upper Saddle River, NJ, 1999.
- [141] I. Prigogine and R. Defay. *Chemische Thermodynamik*. VEB Deutscher Verlag für Grundstoffindustrie, Leipzig, 1962.
- [142] K. Stephan and F. Mayinger. *Thermodynamik: Grundlagen und technische Anwendungen*. Bd. 2: Mehrstoffsysteme und chemische Reaktionen. Springer, Berlin, 1999.
- [143] P. R. Rony. The Degree of Separation – A Universal Separation Index. *Separation Science* 3 (1968) 239–248.
- [144] M. Doherty and M. Malone. *Conceptual Design of Distillation Systems*. McGraw-Hill, New York, 2001.
- [145] S. K. Mallik. Synthesis of Separation Processes with Nonsharp Separators. *Chemical Engineering Science* 46 (1991) 2729–2737.
- [146] S. K. Mallick. Synthesis of stagewise separation processes. *Computers & Chemical Engineering* 15 (1991) 427–436.
- [147] K. J. Bombaugh, W. A. Dark, and R. F. Levangie. High Resolution Steric Chromatography. *Journal of Chromatographic Science* 7 (1969) 42–47.